HI 21CM ABSORBERS AT MODERATE REDSHIFTS

RIJKSUNIVERSITEIT GRONINGEN

HI 21cm Absorbers at Moderate Redshifts

PROEFSCHRIFT

ter verkrijging van het doctoraat in de
Wiskunde en Natuurwetenschappen
aan de Rijksuniversiteit Groningen
op gezag van de
Rector Magnificus, dr. D.F.J. Bosscher
in het openbaar te verdedigen op
maandag 9 oktober 2000
om 14.15 uur

door
Wendy Meredith Lane

geboren op 23 augustus 1974
te Winchester, MA, USA

Promotor: prof. dr. F.H. Briggs

Beoordelingscomissie: prof. dr. A.G. de Bruyn
                                       prof. dr. R. Sancisi
                                       prof. dr. R.H. Sanders

"To see a world in a grain of sand
And a heaven in a wildflower
Hold infinity in the palm of your hand
And eternity in an hour...."

—William Blake
Auguries of Innocence

Contents

CONTENTS

1

Introduction

The H I 21cm line has proved to be a powerful tool for tracing the neutral H I in our own and other galaxies, providing information on the distribution, amount, kinematics, and temperature of the gas. In this thesis we describe a study of H I 21cm absorbers at moderate redshifts including both a large survey to identify new absorbers and detailed study of a few individual systems. Here we give some background for this work and provide a brief outline of the thesis.

1.1 H I Gas in Galaxies

The theoretical detectability of interstellar neutral hydrogen (H I) via the $\lambda = 21$cm radio line was first discussed by van de Hulst (Bakker and van de Hulst 1945); the first Galactic detections of 21cm emission (Ewen and Purcell 1951, Muller and Oort 1951) and absorption (Hagen et al. 1954, Hagen and McClain 1954, Hagen et al. 1955) were reported less than 10 years later. In the nearly 50 years since that time, the H I 21cm line has proved to be a powerful tool for tracing the neutral H I in our own and other galaxies, providing information on the distribution, amount, kinematics, and temperature of the gas. H I emission maps reveal that many galaxies extend to radii far beyond their optical disks and may indicate interactions between galaxies which appear undisturbed in optical images. Rotation curves derived from 21cm emission measurements can provide evidence for the existence of dark matter halos. Surveys for 21cm emission in nearby galaxies can be used to derive the H I mass function of galaxies and the cosmic mass density of H I gas at $z \approx 0$.

H I within our galaxy is found in two main temperature phases (eg. Kulkarni and Heiles 1988). Widespread diffuse gas, with temperatures in the range $5000 < T < 8000$ K makes up the warm neutral medium (WNM). Roughly half of all neutral hydrogen atoms are in this warm, diffuse phase which is distributed throughout

the galaxy. By contrast, the cold neutral medium (CNM) is composed of relatively dense clouds which do not fill a significant fraction of the interstellar volume. Gas in the CNM has typical temperatures of about $20 < T < 250$ K, and the temperature increases with distance from the Galactic plane. In fact the CNM is more tightly confined to a thin layer than the WNM, which has a vertical scale height of order 1.5 times that of the CNM (Dickey and Lockman 1990). Observations of nearby dwarf galaxies have found warm and cold phase H I gas with similar temperatures and distributions (eg. Young and Lo 1997a, 1997b).

The flux of an H I emission signal is inversely proportional to the square of the distance to the unresolved emitting cloud. With existing telescopes we are able to detect massive H I systems at redshifts out to only $z \approx 0.2$. Radio studies at higher redshifts presently rely on 21cm absorption measurements against bright background radio sources. Observations of H I 21cm absorption are most sensitive to the CNM, although the WNM is occasionally detected when the background source is sufficiently bright (Carilli et al. 1998, Lane et al. 2000). In general, this limits study of the neutral gas at higher redshifts to sight lines that pass through the CNM clouds of the intervening galaxy. Due to the low filling factor of the CNM gas, a sight line passing through a galaxy that is rich in H I may fail to intercept any gas which produces a detectable 21cm absorption feature.

1.2 QSO Absorption Lines

Absorption lines seen in the spectra of QSOs provide us with much of our knowledge about the gaseous components of the high redshift universe. The apparent surface brightness of the emission from a galaxy is diminished by the cosmological factor $(1 + z)^{-4}$. As a result the detection of high redshift galaxies through optical imaging is difficult and biased towards high surface brightness and lensed objects. QSOs are more common at high redshifts and their luminosity makes them ideal background sources for the study of absorption caused by gas in systems which fall along their sight lines (eg. Wagoner 1967, Bahcall and Spitzer 1969).

The first searches for redshifted H I 21cm absorption lines were made in the late 1960's (Shuter and Gower 1969, Heiles and Miley 1970), and the first detection was made against the bright radio source 3C286 at a redshift $z = 0.692$ (Brown and Roberts 1973). Subsequently several more absorbers were identified, but a low detection rate hampered the work. Due to limitations on the radio spectrometers and receivers then available, it was difficult to survey large amounts of redshift space in a timely fashion. Radio astronomers increasingly focussed on observing redshifts and sight lines with known optical absorption systems.

Large spectroscopic surveys have identified a plethora of optical absorption line systems, largely through the identification of metal-lines (eg. Junkarinnen et al. 1991). Among the most common absorption lines is the C IV $\lambda\lambda1548, 1550$ Å resonance doublet (eg. Foltz et al. 1986). Also easily recognized is the low ionization Mg II $\lambda\lambda2796, 2803$ Å resonance doublet, which can be observed in ground-based optical spectra at redshifts $z \geq 0.2$ (Lanzetta et al. 1987, Steidel and Sargent 1992). A

third distinctive line is the saturated profile of a Lyα λ1216 Å absorption line which arises in H I gas with a column density $N_{HI} \geq 2 \times 10^{20}$ cm^{-2}. It is called a damped Lyα (DLA) absorption line due to the broad damping wings of the absorption profile. At redshifts $z > 1.65$ it can be studied using ground-based instruments (eg. Wolfe et al. 1986, Storrie-Lombardi et al. 1996), while at redshifts $z < 1.65$, observations of this line are made using spaced based-telescopes (eg. Lanzetta et al. 1995, Rao and Turnshek 2000).

Because they have high column densities of neutral gas, DLA absorption systems make ideal candidates for H I 21cm absorption measurement. Unfortunately, there are relatively few which have been identified (roughly 100, eg. Lanzetta et al. 1995) and only about a third of these fall in front of QSOs which are bright at radio wavelengths. The Mg II absorption line systems, on the other hand, have been identified in large numbers (eg. Steidel and Sargent 1992), and it is possible to assemble a reasonably sized sample of Mg II absorbers which lie in front of bright radio QSOs. All known H I 21cm/DLA absorbers have associated Mg II absorption.

The cross-section for Mg II-absorption in a galaxy is much larger than that for DLA/21cm absorption (for an illustration, see Briggs 1999). In early studies about 1 in 10 Mg II-absorbers showed associated H I 21cm absorption (Briggs and Wolfe 1983). In other words, a sight line passing through a galaxy is about 10 times more likely to encounter Mg II absorbing gas than H I 21cm absorbing gas. A recent study by Rao and Turnshek (2000) indicates that the detection probability for finding DLA absorbers in Mg II-selected systems increases to nearly 50% if a minimum rest equivalent width selection criteria of Mg II $W_o^{\lambda 2796} > 0.5$ Å and Fe II $W_o^{\lambda 2600} > 0.5$ Å are imposed.

1.3   Tracing the Gas

The power of the QSO absorption line studies, and in particular H I 21cm and DLA absorption lines studies, lies in the identification and characterization of redshifted gas-rich galaxies. At redshifts $z \approx 0$ the bulk of the neutral H I gas is found in luminous spiral disks (Rao and Briggs 1993, Zwaan et al. 1999). Early surveys which targeted DLA absorption were expecting to find high-redshift analogues or predecessors of the local gas-rich disks (Wolfe et al. 1986). However the association of the neutral gas responsible for DLA absorption with any particular class of absorber remains an open question (Wolfe et al. 1995). This is partly due to the difficulty of visual and spectroscopic identifications of faint high-redshift galaxies.

Studies of the metal-line absorption associated with high- and moderate-redshift DLA/21cm absorbers have helped to characterize these systems. The column densities of these systems, $N_{HI} \geq 2 \times 10^{20}$ cm^{-2}, are typical of the inner regions of gas rich $z \approx 0$ spirals. High-redshift DLA systems have low metallicities (Pettini et al. 1994, Pettini et al. 1997, Centurión et al. 2000). They are probably not a part of the population of galaxies responsible for the bulk of the star formation density that is associated with the Lyman break galaxies (LBGs) which are identified by their optical colors (Pettini et al. 1999). DLA/21cm absorbers have a low dust to gas ratio

(Pei et al. 1991), and are rarely observed to contain molecular gas (eg. Lanzetta et al. 1989, Levshakov et al. 1992; cf. Srianand and Petitjean 1998). Comparisons between radio observations of the 21cm line and optical observations of the DLA line show that the mean spin temperature, $< T_s >$, of the neutral gas is usually ~ 1000 K, which is much higher than values found for discrete clouds in our Galaxy (Carilli et al. 1996).

Prochaska and Wolfe (1997, 1998) argue that the profiles of associated metal lines in DLA systems are consistent with the hypothesis that they arise in large, rapidly-rotating disks with substantial vertical scale heights. Studies of several H I 21cm absorbers at spatial resolutions that resolve the extended radio QSOs have also found that the absorption is consistent with a large rotating disk galaxy which is intercepted in several places by sight lines to the extended background quasar (Brown and Mitchell 1983, Briggs 1999). However, the metal-line profiles are also consistent with those produced in models based on cold dark matter (CDM) simulations of small interacting systems (Rauch et al. 1997, Haehnelt et al. 1998). When statistics for the DLA absorbers are computed, it is found that at high redshifts they are the dominant contributors to $\Omega_{H\,I}(z)$, the cosmic mass density of H I (Wolfe et al. 1995, Storrie-Lombardi et al. 1996). This leads both Prochaska and Wolfe (1997, 1998), and Haehnalt et al. (1998) to conclude that the high-redshift DLA systems do represent the progenitors of "normal" $z \approx 0$ galaxies, despite the two groups' difference of opinion on what exactly the DLA objects are.

At relatively low redshifts, $z \sim 0.5$ and lower, we have a greater ability to identify the host galaxy optically and spectroscopically. Until recently, only a few DLA absorbers had been identified at $z < 1.65$. A recently completed *Hubble Space Telescope* survey for low redshift DLA absorption (Rao and Turnshek 2000) and the H I 21cm survey presented in this thesis have greatly improved this situation. Imaging of these and few previously known DLA/21cm absorbers at low redshifts identify a variety of host and candidate-host galaxies for the absorbing gas. Although the host system is a disk galaxy on some sight lines (3C 196; Le Brun et al. 1997), on many it is either a compact galaxy (0302-223, 0454+039) or or an amorphous low surface brightness object (1229-021, 3C286, 3C336; Steidel et al. 1994, Le Brun et al. 1997, Steidel et al. 1997). For a few of the absorbers, the host galaxy falls mostly under the QSO point-spread function (PSF) in groundbased images and its morphology is not known (eg. 0738+313; Turnshek et al. 2000). In the case of AO 0235+164 it is entirely unclear what sort of object is responsible for the absorption, even in observations made with the *HST* (Burbidge et al. 1996). Finally, there is evidence that 21cm absorption may arise in a small group of interacting galaxies (1127-145; this thesis).

The range of morphologies identified in images of the low and intermediate redshift DLA/21cm absorbers indicate the importance of host galaxy identification in our attempts to understand how the QSO absorption lines are related to the galaxies in which they arise. It is necessary to continue adding to the sample of identified low and moderate redshift DLA/21cm absorbers and to study their host galaxies by as many methods as possible. Only by building a clear picture of these systems can we hope to understand how high redshift DLA/21cm absorbers evolve into our local $z \approx 0$ gas-rich galaxies.

1.4   A Brief Outline of This Thesis

When this thesis was started, an on-going upgrade at the Westerbork Synthesis Radio Telescope (WSRT) had resulted in the availability of new UHF-high receivers operating in the frequency range 700-1200 MHz, which corresponds to redshifts $0.2 < z < 1.0$ for the H I 21cm line (rest frequency 1420.4057 MHz). At that time, there were no other radio telescopes observing effectively at these frequencies, and only a small handful of H I 21cm and DLA absorbers were known in this redshift interval.

The WSRT has more collecting area than most single dish telescopes such as the Green Bank 140 ft., and it has more frequency agility than Arecibo. Most importantly for observations in the UHF-high band where telecommunications, radio, and television signals all contribute significant amounts of radio frequency interference (rfi), the cross-correlation spectrometer of the WSRT has a greater immunity to rfi than any of the single-dish telescopes.

The goal of the research was to make use of the "new" WSRT to find 21cm absorbers which would be suitable for optical and radio followups, thus adding to our understanding of the galaxies in which high neutral column density absorbers arise.

In the first part of the thesis we discuss our efforts to find moderate redshift 21cm absorbers. In Chapter 2 we present the spectra from a WSRT survey for 21cm absorption in 62 Mg II-selected absorbers, spread over the entire redshift range of the receivers. In Chapter 3 we combine the 62 WSRT systems with 10 Mg II-selected systems from the literature (Briggs and Wolfe 1983, Peterson and Foltz 1980). The combined sample of 72 Mg II absorbers includes 5 H I absorbers and at least 1 strong candidate. We look for correlations between the metal-line equivalent widths and the 21cm detections/non-detections, and use our detection rate and the statistics of Mg II absorbers to estimate a value for the cosmic mass density of H I gas at the average redshift of our sample.

In the latter part of the thesis we present observations intended to characterize the host galaxies of the 21cm absorbers. In Chapter 4 we present high velocity resolution 21cm spectra for the three H I absorbers identified in the WSRT survey, and discuss the temperature of redshifted 21cm absorbers. In Chapter 5, 21cm absorption and emission measurements of a $z = 0.09$ DLA absorber are presented, and we show that a significant fraction of the H I gas in this system is warm-phase H I. In Chapter 6 we present near infrared images of two DLA/21cm absorption fields and discuss possible host galaxies for the absorbing gas.

References

Bahcall, J. N. and Spitzer, L. J. 1969, ApJ, 156, L63

Bakker, C. J. and van de Hulst, H. C. 1945, Ned. Tijdschr. Natuurk., 11, 201

Briggs, F. H. 1999, in *ASP Conf. Ser. 156: Highly Redshifted Radio Lines*, ed. C. Carilli et al., (San Francisco: Astronomical Society of the Pacific), 16

Briggs, F. H. and Wolfe, A. M. 1983, ApJ, 268, 76

Brown, R. L. and Mitchell, K. J. 1983, ApJ, 264, 87

Brown, R. L. and Roberts, M. S. 1973, ApJ, 184, L7

Burbidge, E. M., Beaver, E. A., Cohen, R. D., Junkkarinen, V. T., and Lyons, R. W. 1996, AJ, 112, 2533

Carilli, C. L., Dwarakanath, K. S., and Goss, W. M. 1998, ApJ, 502, L79

Carilli, C. L., Lane, W., de Bruyn, A. G., Braun, R., and Miley, G. K. 1996, AJ, 111, 1830

Centurión, M., Bonifacio, P., Molaro, P., and Vladilo, G. 2000, ApJ, 536, 540

Dickey, J. M. and Lockman, F. J. 1990, ARA&A, 28, 215

Ewen, H. I. and Purcell, E. M. 1951, Nature, 168, 356

Foltz, C. B., Weymann, R. J., Peterson, B. M., Sun, L., Malkan, M. A., and Chaffee, F. H., J. 1986, ApJ, 307, 504

Haehnelt, M. G., Steinmetz, M., and Rauch, M. 1998, ApJ, 495, 647

Hagen, J. P., Lilley, A. E., and McClain, E. F. 1955, ApJ, 122, 361

Hagen, J. P. and McClain, E. F. 1954, ApJ, 120, 368

Hagen, J. P., McClain, E. F., and Hepburn, N. 1954, AJ, 59, 323

Heiles, C. and Miley, G. K. 1970, ApJ, 160, L83

Junkkarinen, V., Hewitt, A., and Burbidge, G. 1991, ApJS, 77, 203

Kulkarni, S. R. and Heiles, C. 1988, in *Galactic and Extragalactic Radio Astronomy*, ed. G. Verschuur and K. Kellerman, (New York: Springer-Verlag), 95

Lane, W., Briggs, F., and Smette, A. 2000, ApJ, 532, 146

Lanzetta, K. M., Wolfe, A. M., and Turnshek, D. A. 1987, ApJ, 322, 739

Lanzetta, K. M., Wolfe, A. M., and Turnshek, D. A. 1989, ApJ, 344, 277

Lanzetta, K. M., Wolfe, A. M., and Turnshek, D. A. 1995, ApJ, 440, 435

Le Brun, V., Bergeron, J., Boisse, P., and Deharveng, J. M. 1997, A&A, 321, 733

Levshakov, S. A., Chaffee, F. H., Foltz, C. B., and Black, J. H. 1992, A&A, 262, 385

Muller, C. A. and Oort, J. H. 1951, Nature, 168, 357

Pei, Y. C., Fall, S. M., and Bechtold, J. 1991, ApJ, 378, 6

Peterson, B. M. and Foltz, C. B. 1980, ApJ, 242, 879

Pettini, M., Ellison, S. L., Steidel, C. C., and Bowen, D. V. 1999, ApJ, 510, 576

Pettini, M., Smith, L. J., Hunstead, R. W., and King, D. L. 1994, ApJ, 426, 79

Pettini, M., Smith, L. J., King, D. L., and Hunstead, R. W. 1997, ApJ, 486, 665

Prochaska, J. X. and Wolfe, A. M. 1997, ApJ, 487, 73

Prochaska, J. X. and Wolfe, A. M. 1998, ApJ, 507, 113

Rao, S. and Briggs, F. 1993, ApJ, 419, 515

Rao, S. and Turnshek, D. 2000, astro-ph/9909164

Rauch, M., Haehnelt, M. G., and Steinmetz, M. 1997, ApJ, 481, 601

Shuter, W. and Gower, J. 1969, Nature, 223, 1046

Srianand, R. and Petitjean, P. 1998, A&A, 335, 33

Steidel, C. C., Dickinson, M., Meyer, D. M., Adelberger, K. L., and Sembach, K. R. 1997, ApJ, 480, 568

Steidel, C. C., Pettini, M., Dickinson, M., and Persson, S. E. 1994, AJ, 108, 2046

Steidel, C. C. and Sargent, W. L. W. 1992, ApJS, 80, 1

Storrie-Lombardi, L. J., McMahon, R. G., and Irwin, M. J. 1996a, MNRAS, 283, L79

Storrie-Lombardi, L. J., McMahon, R. G., Irwin, M. J., and Hazard, C. 1996b, ApJ,

468, 121

Turnshek, D., Rao, S., Nestor, D., Lane, W., Monier, E., Bergeron, J., Briggs, F., and Smette, A. 2000, in prep.

Wagoner, R. V. 1967, ApJ, 149, 465

Wolfe, A. M., Lanzetta, K. M., Foltz, C. B., and Chaffee, F. H. 1995, ApJ, 454, 698

Wolfe, A. M., Turnshek, D. A., Smith, H. E., and Cohen, R. D. 1986, ApJS, 61, 249

Young, L. M. and Lo, K. Y. 1997a, ApJ, 476, 127

Young, L. M. and Lo, K. Y. 1997b, ApJ, 490, 710

Zwaan, M. A., Verheijen, M. A. W., and Briggs, F. H. 1999, PASAu, 16, 100

2

The 21cm Survey: Data

We present the data from a Westerbork Synthesis Radio Telescope survey for H I 21cm absorption in 62 Mg II-selected absorbers at redshifts $0.2 < z < 1.0$. Three new H I 21cm absorbers and one strong candidate absorber have been identified.

2.1 Introduction

Damped Lyα (DLA) and H I 21cm absorption lines are the spectral signatures of systems with high neutral hydrogen column densities. Such systems are the major contributors to the cosmic mass density of neutral gas at high redshifts ($z \approx 3$). The study of low redshift examples of the quasar absorption line systems responsible for the DLA/21cm absorption lines is important to help bridge our understanding of neutral gas-rich systems between those at redshift $z = 0$ and those at high z. Our knowledge of the neutral gas in nearby spiral galaxies is mainly based on observations of the H I 21cm line in emission. At high redshift, however, we observe the H I 21cm line in absorption, which can only be seen along a limited number of lines of sight through the intervening absorber, making detailed knowledge of the gas characteristics difficult to obtain. The low redshift ($z < 1$) neutral absorbers are still close enough that both optical and radio data of reasonable quality can be used to investigate their kinematics, morphologies, and physical gas characteristics. Such information is necessary to build a framework for a correct interpretation of the higher z counterparts to these systems.

Searches for redshifted H I 21cm absorption can be time-consuming because radio spectrometers are typically capable of observing only relatively narrow instantaneous bandwidths and only a few of the coldest high neutral column density QSO absorption line systems have measurable optical depths in the 21cm line. DLA systems have very high column densities of neutral H I (canonically, $N_{HI} \geq 2 \times 10^{20}$ cm^{-2}; Wolfe et al. 1986) so they are the best selectors for systems likely to have H I 21cm

absorption. Unfortunately the Lyα line is not shifted into the optical window until redshifts $z \geq 1.65$, so finding these lines at low redshift requires UV spectra taken with space telescopes. This, combined with the small cross section for DLA absorption, means that only a small number of DLA systems have been identified at low redshift. In turn, only a fraction of these fall in front of radio-bright QSOs. Alternative selection criteria which are reasonably effective at finding H I 21cm absorbers must be used.

All known DLA and H I 21cm absorbers have associated low-ionization metal lines such as the Mg II $\lambda\lambda2796, 2803$ doublet, which can be observed easily in ground-based spectra at redshifts $z > 0.1$ (Lu and Wolfe 1994). This suggests that Mg II can be used to optically select low-redshift systems likely to have high column densities of neutral gas observable as either DLA or H I 21cm absorption. Statistics on the number of Mg II absorbers and their evolution with redshift have been established from the Mg II-surveys (Steidel and Sargent 1992). These numbers along with the fraction of H I absorbers in an Mg II-selected sample can be used to estimate similar statistics for the 21cm absorbers. A study of Mg II-selected systems using previously existing UV data yielded about 1 DLA system per 10 Mg II systems observed (Rao et al. 1995). A similar statistic exists for H I 21cm absorption in a small number of Mg II-selected systems (Briggs and Wolfe 1983).

In this chapter we discuss a large survey for H I 21cm absorption in Mg II-selected systems at redshifts $0.2 < z < 1.0$. Individual spectra for each system are presented. In subsequent chapters we will discuss some of the statistical results of the survey and present the newly identified 21cm absorbers in more detail.

2.2 The Data

2.2.1 Sample Selection

The survey was designed for the Westerbork Synthesis Radio Telescope (WSRT)[1] UHF-High receivers which can observe HI 21cm absorption at redshifts $0.2 < z < 1.0$ (700 - 1200 MHz). A sample of Mg II $\lambda\lambda2796, 2803$ doublet absorbers over this redshift range was compiled in 1996 from then available catalogues and surveys in the literature, including Junkkarinen, Hewitt, & Burbidge (1991), Rao (1994), Aldcroft, Bechtold, & Elvis (1994), Aldcroft, Elvis, and Bechtold (1993), and Steidel & Sargent (1992). Those absorbers on sight lines to QSOs at declinations $\delta < -30°$ (where sources are no longer visible at the WSRT) were removed. The background QSOs were also required to have a minimum measured or extrapolated flux density at 1400 MHz of $S_\nu \approx 0.5$ Jy. Known 21cm absorbers were removed, as were systems which fell at frequencies with known radio frequency interference (rfi), resulting in a sample of 62 systems, which we refer to as the WSRT-sample.

---

[1]The Westerbork Synthesis Radio Telescope is operated by the Netherlands Foundation for Research in Astronomy (NFRA/ASTRON) with support from the Netherlands Foundation for Scientific Research(NWO).
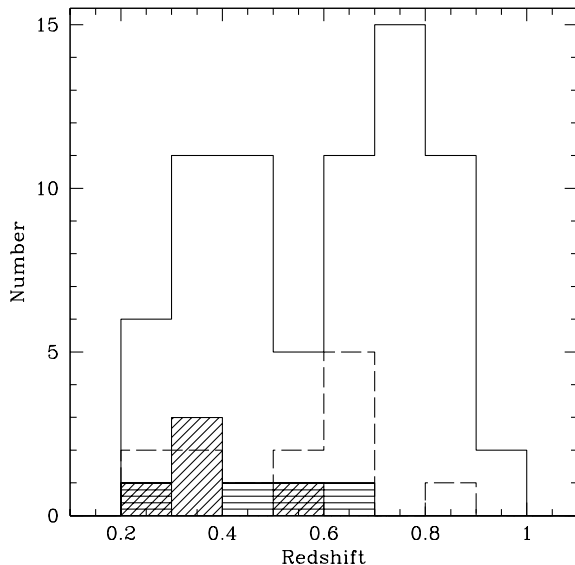
Figure 2.1: A histogram showing the redshift distribution of the Mg II sample observed in the survey. The Mg II-selected 21cm absorbers are shaded diagonally, while other 21cm absorbers are marked with horizontal lines. The distribution of known DLA absorbers over this redshift range is indicated by the dashed histogram.

No Mg II equivalent width constraints were placed on the sample, because the requirement of a strong QSO radio flux density is more limiting. However, although there are 12 systems for which no measured widths are reported in the literature, only 3 systems with Mg II rest equivalent widths $W_o^{\lambda 2796} < 0.3$ Å are included. Figure 2.1 is a histogram showing the redshift distribution of the WSRT-sample. For comparison, the distribution of H I 21cm absorbers (some found in this study) and DLA absorbers is also indicated.

2.2.2   Data Acquisition

The WSRT is an array of 14 25-m diameter radio telescopes spread out on a straight line running nearly east-west. Observations were made between 12/96 and 12/98 using the UHF-high receivers which operate at 700-1200 MHz. After a full 12-hour observation, the WSRT synthesizes an elliptically shaped beam with an angular resolution:

$$\Theta_{min} = 0.8\frac{\lambda}{D} \tag{2.1}$$

$$\Theta_{maj} = 0.8\frac{\lambda}{D\sin(\delta)} \tag{2.2}$$

for the major and minor axes respectively, where δ is the declination of the source being observed and the standard taper has been applied. $D \approx 2.7$ km is the length of the longest baseline at the WSRT. The position angle of the ellipse is actually very close to zero, so the minor axis is the x-axis and the major axis is the y-axis in a given

map, while the factor of $\sin(\delta)$ determines the elongation. Using these equations we find that the best spatial resolution attained in our survey should be $\Theta_{min} \approx 15''$ at 1200 MHz and $\Theta_{min} \approx 26''$ at 700 MHz.

Most of the data were taken with the DXB correlator (Bos et al. 1981). When the new DZB correlator (http://www.nfra.nl/ morganti/wsrt/index.html) became partially operational some data were obtained with it as well. Details of the DXB observations are summarized in Table 2.1 and Table 2.2 summarizes the DZB observations.

Using the DXB correlator, the instrumental setup gave a maximum of 40 baselines in each of two linear polarizations (XX and YY), for a combined maximum of 80 baselines. The objects were observed with a 2.5 MHz bandwidth divided into 128 channels. This gives a channel spacing of 19.5 kHz, which corresponds to a velocity spacing of 4.9 km s^{-1} at 1200 MHz, and 8.4 km s^{-1} at 700 MHz. Most of the data were taken with no online smoothing, and the applied uniform taper gives a spectral resolution of 1.2 times the channel width. Hanning smoothing was inadvertently applied on-line at the telescope to a few of the datasets (all noted in Section 2.4.1), creating a spectral resolution of twice the channel width.

The DZB correlator provides better frequency resolution and also allows more baselines to be correlated. When complete it will allow all 91 possible telescope combinations as well as the 14 autocorrelation spectra to be recorded in each polarization. During this survey period, it was only able to provide a maximum of 64 baselines in each of the two polarizations (128 baselines total) when the spectrometer was configured to observe 256 channels over a 2.5 MHz bandwidth. This provides double the resolution of the DXB data. The increased number of baselines allowed us to reach the same sensitivity levels (measured in mJy per beam per channel) in about the same amount of time.

The observations were intended to maximize the spectral signal to noise ratio while minimizing observing time. For this reason, few but the weakest quasars were observed for the full 12-hours necessary to fill the U-V plane with an East-West array. This observing technique was justified by the fact that most of the radio quasars in this survey are much smaller than the synthesized beam, and can thus be treated as unresolved point sources. The length of each observation was chosen to give a theoretical spectral channel noise at the 3σ level equivalent to about one percent of the background radio continuum. In practice the sensitivity limits achieved were somewhat higher.

The total integration time of the data included in each final spectrum is difficult to estimate as radio frequency interference (rfi) often made it necessary to edit the data unevenly between polarizations and baselines. For this reason, the total observation time listed in column 3 of Tables 2.1 and 2.2 will usually overestimate the amount of data included in the final spectra. Due to the ongoing upgrades to the WSRT receivers there were seldom, if ever, 14 telescopes operating for a given observation. Because the number of baselines left in each polarization after editing and removing non-operational antennae might be different, we list the combined number of baselines for both polarizations in column 5 of these tables.

Table 2.1: DXB Observation Log

Object	Date (DD/MM/YY)	Int. (hrs)	Obs. Freq. (MHz)	# of Ifrs
0051+291	27/12/97	6	769.174	54
0109+176	30/12/97	7	771.634	66
0109+200	28/12/97	12	925.499	66
0119−046	29/12/97	6	825.785	66
0119−046	26/12/97	6	856.771	62
	10/1/98	5.5	856.769	66
	17/1/98	5	856.769	65
0141+339	23/3/97	2	1001.856	49
0229+131	14/1/97	2	1001.811	71
	22/3/97	2	1001.846	49
0229+341	17/1/97	1	799.976	28
0248+430	4/1/98	6	978.510	48
0248+430	14/3/97	2	1018.789	40
	18/1/97	2.5	1018.786	44
0454−234	18/1/98	5	810.690	54
0454−234	3/1/98	6	871.434	62
0454−234	2/1/98	4	884.458	66
0454+039	23/12/96	2	763.798	56
	27/12/96	5.5	763.795	42
0710+118	15/1/97	1	970.873	72
0738+313	27/4/97	1.5	1162.918	48
0805+046	14/12/97	11	834.162	42
	18/12/97	4	834.158	66
0827+243	11/12/97	6	932.090	64
0843+136	31/12/97	4.5	884.812	66
0855−196	22/4/97	2	862.722	52
0941+261	15/12/97	6	765.945	50
	3/1/98	6	765.928	50
0941+261	18/03/97	4.5	829.967	28
0952+179	28/1/97	2	1147.651	40
0957+003	16/4/97	4	849.458	48
1011+250	12/3/97	9	1128.692	64
1019+309	20/1/97	12	1055.244	48
1049+616	7/3/97	12	1019.418	64
1049+616	23/3/97	12	1159.363	49
1127−145	16/3/97	1	1081.810	49
1137+660	14/3/97	.75	868.188	49
1148+387	17/1/98	7	1171.053	50
1206+439	16/3/97	1.25	1005.650	56
1218+339	16/3/97	1.5	815.241	56

DXB Observation Log *(cont'd)*

Object	Date (DD/MM/YY)	Int. (hrs)	Obs. Freq. (MHz)	# of Ifrs
1243−072	19/1/98	6.5	989.236	52
1308+326	28/1/97	2	755.986	36
1327−206	4/1/97	8	766.700	64
1327−214	18/3/97	1	1091.836	34
1331+170	13/3/97	12	814.201	64
1354+258	27/3/97	11.5	753.301	48
1354+258	4/1/98	3	764.338	50
1437+623	3/4/97	1.25	758.630	56
1510−089	2/4/97	1	1051.436	48
1540+180	29/12/97	6	821.3792	66
1540+180	16/1/98	6	821.3907	64
1556−245	2/1/98	4	801.951	64
	3/1/98	4	801.952	66
1622+239	19/3/97	2	790.349	49
1622+239	20/3/97	2	855.616	42
1622+239	19/3/97	1	857.787	42
1622+239	20/3/97	1.5	1038.751	42
1622+239	19/3/97	1	1077.683	42
1629+120	18/3/97	1.5	747.482	32
1629+120	11/3/97	2	927.656	49
1704+608	1/1/98	2	1162.4720	57
1756+237	21/12/97	6	1035.810	58
1821+107	24/12/97	5.5	904.596	62
	25/12/97	6	904.597	58
1857+566	10/3/97	12	828.187	63
1901+319	2/4/97	1	1021.860	48
2128−123	1/1/98	2	993.296	66
2145+067	3/1/98	2	793.200	48
2212−299	12/03/97	3	869.904	54
2249+185	29/3/97	1	797.105	58

Channel spacing is 19.5 kHz

Columns are: IAU (B1950) Designation, Date of observation, length of integration, observed (not heliocentric) frequency at the center of the band, and the combined number of baselines for both pols.

Table 2.2: DZB Observation Log

Object	Date DD/MM/YY	Int. (hrs)	Sky Freq. (MHz)	# of Ifrs
0051+291	24/10/98	8	769.237	128
0109+200	15/2/98	1	925.505	101
	15/2/98	5	925.505	101
0119−046	20/2/98	4	825.759	92
0248+430	28/2/98	6	978.487	92
0454−234	23/2/98	6	884.370	100
0735+178	14/2/98	1	996.998	110
0805+046	21/2/98	1	724.263	106
0827+243	13/3/98	11	931.961	72
1040+123	20/2/98	1.25	856.140	61
1137+660[a]	20/11/99	7	867.746	126
1229−021	23/2/98	1.5	808.422	110
1243−072	25/5/98	3	989.061	110
1354+195	19/2/98	3	975.423	110
1704+608	11/2/98	2	1162.468	110
1901+319	9/10/99	7.5	1021.275	117
2128−123	23/2/98	2	993.377	92

Two values for the 1σ noise limit indicate a resolved source
Channel spacing is 9.765 kHz
[a]Channel spacing is 19.5 kHz
Columns are: IAU (B1950) Designation, Date of observation,
    length of integration, observed (not heliocentric)
    frequency at the center of the band, and the
    combined number of baselines for both pols.

2.2.3 Data Reduction

Radio frequency interference (rfi) is very common in the UHF-high band. In addition to communications bands and cell phone signals, mixing products from lower frequency television signals are a significant contributor to this problem. The rfi-environment at the telescope became worse during the second year of observations when a number of new regional television antennae started to broadcast. Most of the interference is time variable, occurring either near HA∼ 0, or when the telescopes are pointing towards a source near the horizon. The interference is usually stronger in one polarization and appears most strongly in the data from short baselines.

After editing the rfi-contaminated data, all objects were flux and passband calibrated using observations of one of the standard calibrator sources 3C48, 3C147, 3C286, or 3C295. Because almost no models of these sources exist over the frequency

range of the UHF-high band, flux densities were calculated using the VLA 1995.2 co-efficients which are tied to flux density of 3C295 as determined by Baars et al. (1977). The calibrations were performed using either the standard CALIB and BPASS routines in AIPS, or using the routine NCALIB in the data reduction package NEWSTAR which has been developed for use with WSRT data. Corrections for the telescope temperature, T_{sys}, were applied to the DXB observations but were unavailable for the DZB datasets. After initial calibration, any further data reduction and the spectrum extraction were performed in AIPS.

Due to the lack of U-V coverage, the spatial information in these data sets is often very poor. Many of the spectra were created by using the task POSSM to extract a vector-averaged point source spectrum from the calibrated data. For those data which showed evidence of poor calibration, were observed with the QSO not at phase center, or were partially resolved by the observations, further processing was necessary. An iterative process of clean mapping (using IMAGR), and phase self-calibration to the resulting clean components (CALIB) was applied, ending with an amplitude self-calibration. At this point, spectra for the unresolved sources in un-crowded fields were extracted using POSSM. The continuum emission from resolved sources and sources in crowded fields was subtracted using UVSUB and UVLIN. Map cubes were then synthesized, and spectra were extracted using ISPEC at the location(s) of the continuum.

Multiple observations of the same source were combined using DBCON in AIPS when possible, allowing one composite spectrum to be extracted from the data. In a few cases, previously extracted spectra were combined outside of AIPS, using the number of visibilities for weights. DXB and DZB spectra of the same object were never combined due to the difference in velocity resolution. During the early months of commissioning the DZB correlator, DXB backups were made for all observations, so only five of the objects observed with the DZB lack a DXB spectrum.

2.3 Noise Properties

The noise in an interferometric radio observation can be expressed as:

$$\Delta S(Jy) = \frac{1}{Const} \frac{T_{sys}}{\sqrt{N_{ifrs}N_{pol}\Delta\nu(Hz)\Delta t(s)}} \qquad (2.3)$$

where the $Const \approx 0.1$ K Jy^{-1} depends on spectrometer and telescope parameters for the WSRT, $T_{sys} = 120 - 180$ K is the system temperature, N_{ifrs} is the number of baselines or interferometric pairs, N_{pol} is the number of polarizations, $\Delta\nu$ is the band- or channel width in Hz, and Δt is the integration time in seconds. In order to assess how close to this theoretical noise value our data came, and also to characterize the noise across the entire UHF-band, we use Eq. 2.3 to normalize the noise in our spectra to a standard configuration with 91 baselines, 2 polarizations, channel widths of 19.5 kHz, and an integration time of 12 hours. We assume that the integration time is equal to the observation length, and take this value and the actual number
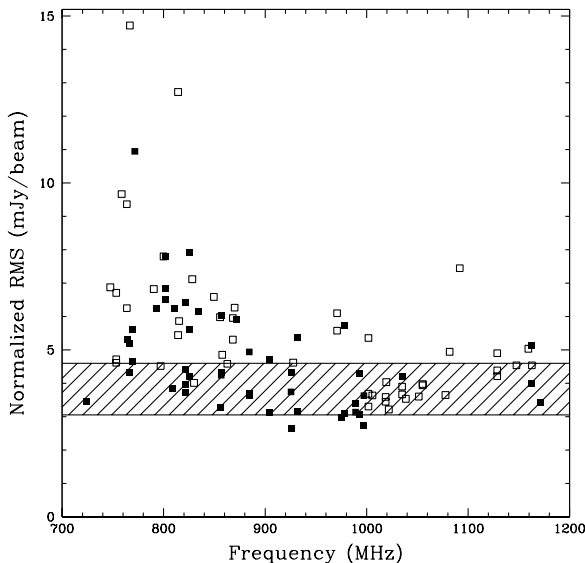
Figure 2.2: The points in this plot show the measured spectral channel noise, ΔS, normalized to 91 baselines, 2 polarizations, 19.5 kHz channel width and 12 hours of integration, from our survey spectra. Open symbols are from data taken during the first year of observations while filled symbols are from the second year. The shaded band indicates the theoretical noise values for $120 < T_{sys} < 180$ K, which are the measured system temperature limits across the band. The average value of the measured noise is 5.0 mJy/beam.

of baselines from Tables 2.1 and 2.2. The observed noise was measured as the RMS noise per channel of each spectrum. Small, $3-4\sigma$ noise spikes were included in the measurement of the observed RMS noise values. For spectra with large rfi features, the RMS noise was measured from the clean part of the spectrum.

The normalized observed noise is plotted against observation frequency in Figure 2.2. The shaded horizontal band shows the theoretical noise limits across the band calculated with Eq. 2.3. The average value of the normalized noise across the band is 5 mJy/beam. The increase in noise near the band edges, caused by higher system temperatures on both ends, and increased rfi near 700 MHz, is clearly visible. At frequencies above 900 MHz, most of the datasets are close to the expected theoretical noise level. For many of the systems, the assumption that the total length of the observation is equal to the integration time is not very valid due to extensive editing of time-dependent rfi. This would cause us to overestimate the normalized noise, and accounts for many of the systems which fall above the theoretical noise in Figure 2.2. The few systems which fall slightly below the theoretical noise appear to be the result of calibration errors.

2.4 The Data

In Figure 2.3 we show the distribution of limiting optical depths, $\tau_{3\sigma}$, for the complete WSRT-sample. Data obtained with the DXB and the DZB are indicated separately. Very few of the WSRT spectra actually reached our survey target of $\tau_{3\sigma} \approx 0.01$. In fact, the average optical depth reached for both the DXB and the DZB data is $\tau_{3\sigma} = 0.048$. There are two apparent reasons for this low sensitivity. First, when we
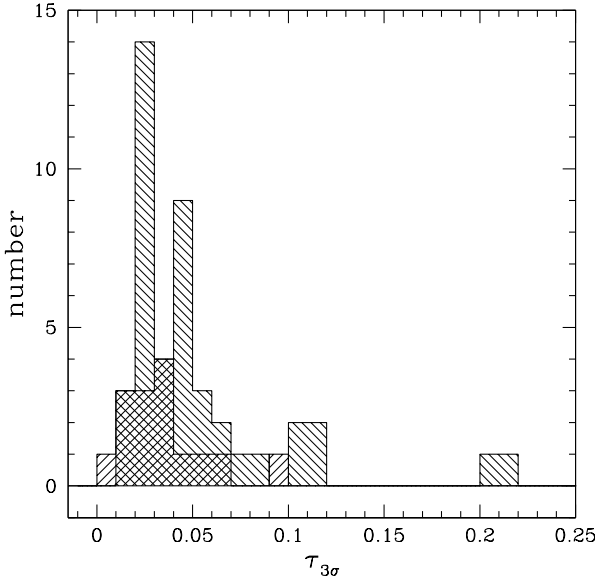
Figure 2.3: Histogram showing the measured values of $\tau_{3\sigma}$ for the WSRT-sample. For extended sources, only information from the sight line to the brightest part of the continuum was included. The DXB data histogram is hatched diagonally from upper left to lower right, and the DZB data is hatched from lower left to upper right. The mean values are $\tau_{3\sigma} = 0.053, 0.036$, & 0.048 for the DXB, DZB, and combined datasets respectively.

designed the survey we assumed a fully operational telescope array with 14 telescopes and the maximum number of baselines. Due to the ongoing upgrade, there were typically ~ 11 operational telescopes during the observations. In addition, these were not always operating with both polarizations, further reducing the number of functional baselines. Second, the prevalence of time-dependent rfi meant that we often lost substantial portions of the data after the observations were finished. More careful scheduling to maximize the time spent observing at hour angles when the rfi was absent could have alleviated this problem, however the rfi-environment was poorly known at the time the data were taken.

The final survey spectra are shown in Figures 2.4 and 2.5. For systems which have been observed with the DXB and the DZB correlators, both spectra are shown. The horizontal lines on the spectra indicate the mean flux density. For those objects where it was necessary to do a continuum subtraction this is roughly zero. Non-zero mean flux densities indicate spectra extracted directly from the UV dataset using POSSM. Sources are labeled with their B1950 IAU designations. When an A,B, or C appears after the IAU name of the object it indicates a multi-lobe source which is resolved by the observations. In general the spectra presented here are centered at the redshift of a given Mg II absorber. Most of the significant spikes in these spectra are the result of rfi.

The spectra in Figures 2.4 and 2.5 are presented at the highest spectral resolution available. When searching for significant features, we studied spectra which were Hanning smoothed to half of the full resolution in addition to the full resolution spectra. All features at greater than 3σ significance were investigated in more detail.

Each candidate absorption feature was tested using the following criteria. It must appear in both polarizations. There must be no indication of a problem with the cal-

ibrator source in either amplitude or phase at the channel(s) in question. When the observation is divided into several shorter time segments, the feature must appear in all of them. Finally the source observation must not have any rfi, time-dependent or otherwise, affecting the candidate absorption channel(s). Several candidate absorption features pass all of these tests, but are non-existent in subsequently obtained confirmation spectra, and these are assumed to be noise or rfi features as well.

Using these criteria, we identify three new H I 21cm absorbers in the WSRT-survey. These are the $z = 0.212$ absorber toward B 0738+313, the $z = 0.313$ absorber toward B 1127-145, and the $z = 0.394$ absorber toward B 0248+430. More detailed observations of these systems will be presented in Chapter 4. In addition we identify a strong candidate absorber at $z = 0.436$ in B 1243-072, but we have been unable to obtain a suitable confirming spectrum. The original survey spectra for all four of these systems are included in Figures 2.4 and 2.5.

2.4.1 Notes on Selected Individual Sight Lines

In this section, we discuss selected spectra in more detail. In particular we address significant noise and rfi features and other complications. The new H I 21cm absorbers are not mentioned here as they will be discussed in detail in Chapter 4.

B 0051+291, 769.242 MHz

The Mg II-absorber in this system lies at a redshift of $z_{abs} = 0.8465$ (Foltz et al. 1986, Burbidge et al. 1977). The feature near 769.5 MHz in the DXB spectrum is only one channel wide and slightly less than 3σ in significance. It does not appear in the more sensitive DZB spectrum.

B 0109+200, 925.587

This sight line has an Mg II-absorber at a redshift of $z = 0.5346$ (Bergeron and Boissé 1984). The DZB spectrum contains a deep narrow rfi spike at 925.9 MHz which is completely absent in the DXB spectrum.

B 0454-234, 810.734 MHz

One of the Mg II-absorbers on this sight line lies at $z = 0.752$ (Stickel et al. 1989). Its DXB spectrum has been Hanning smoothed online at the telescope but not resampled.

B 0454-234, 871.415 MHz

The DXB spectrum for this $z = 0.630$ Mg II-absorber (Stickel et al. 1989) has a one-channel 3.5σ spike at about 871.48 MHz. This is a very weak candidate 21cm absorption line.

B 0710+118, 970.886 MHz

This double-lobed radio quasar has an Mg II-absorption system at $z = 0.463$ on the optical sight line (Aldcroft et al. 1994). The two radio lobes have continuum flux densities of $S_A = 1.83$ Jy and $S_B = 1.25$ Jy.

B 0735+178, 997.056 MHz

We obtained a DZB spectrum for this $z = 0.424$ Mg II-absorber (Boksenberg et al. 1979). B 0735+178 is a highly variable BL-Lacertae Object, with no known emission redshift, and just the one absorption system which is assumed to be intervening. Previous attempts to find an associated H I 21cm absorber at about the same sensitivity limits were reported by Galt (1977). Slightly more sensitive constraints have been reported by Wolfe in private communication with the authors of Boksenberg, Carswell & Sargent (1979), but remain unpublished.

B 0805+046, 724.771 MHz

Although the DZB spectrum of this $z = 0.9598$ Mg II-absorber (Chen et al. 1981, Sargent et al. 1989) is dominated by three strong rfi features at 723.8, 724.75, and 725.0 MHz, these have little effect on the intervening spectrum, so we have included it in our sample. The spectrum presented here has been Hanning smoothed, and the channels affected by rfi have been blanked out for display purposes.

B 0843+136, 881.767 MHz

There is an Mg II-absorption doublet at $z = 0.6054$ on the optical sight line towards this extended radio source (Foltz et al. 1986). The continuum flux densities for the two resolved components are $S_A = 0.59$ Jy, and $S_B = 0.11$ Jy respectively.

B 0957+003, 819.525 MHz

There is an Mg II-absorber at $z = 0.6720$ on the optical sight line towards this extended radio-QSO (Bergeron and Boissé 1984). The $\sim 4\sigma$ feature at 849.55 MHz in the spectrum of both lobes is rfi and appears in one polarization only. The two radio lobes have continuum flux densities $S_A = 0.70$ Jy and $S_B = 0.55$ Jy.

B 1137+660, 868.219 MHz

This double-lobed quasar has an Mg II-absorber at $z = 0.636$ (Aldcroft et al. 1994). The DXB A-lobe spectrum shows what might be a broad absorption feature near 867.7 MHz. The more sensitive DZB spectrum gives no indication that this is real. This is the only system observed by the DZB at the lower channel spacing of 19.5 kHz. For the DZB spectrum, $S_A = 3.49$ Jy and $S_B = 0.79$ Jy.

B 1148+387, 1170.986 MHz

The Mg II-absorber lies at $z = 0.2130$ (Boissé et al. 1992) on this sight line. The DXB spectrum has been Hanning smoothed on-line at the telescope. The feature near 1171.25 MHz is due to rfi.

B 1243-072, 989.140 MHz

The DXB spectrum of the $z = 0.436$ Mg II-absorber (Wright et al. 1979) has been smoothed online at the telescope. There is a 3.5σ feature near frequency 988.65 MHz and a somewhat weaker one near 989.5 MHz. Careful inspection shows no evidence for rfi in the data. The higher resolution DZB spectrum, which was obtained several months after the DXB spectrum, also shows the feature near 988.65 although the weaker feature does not appear. We consider this a candidate H I 21cm absorber.

B 1327-206, 766.544 MHz

Strong interference at 767.2 MHz dominates this unsmoothed H I spectrum. The Mg II-absorber lies at a redshift of $z = 0.853$ (Kunth and Bergeron 1984, Bergeron et al. 1986).

B 1331+170, 814.313 MHz

The sight line towards B 1331+170 which contains two Mg II-absorbers, one at $z = 0.7443$ and the second at $z = 0.7454$ (Sargent et al. 1988). The corresponding H I 21cm frequencies for both systems are covered by one spectrum. The separation in velocity for these two systems is $\Delta v \approx 350$ km s^{-1}. Traditionally, metal-line absorption systems this close in redshift are assumed to be components of one larger system, and they are not included in computed statistics. This sight line has been dropped from our statistical analysis in Chapter 3.

B 1354+258, 764.275 MHz

The sight line towards B 1354+258 has two Mg II-absorbers at redshifts $z = 0.8585$ & 0.8856 (Barthel et al. 1990). The spectrum of the lower redshift system has an isolated rfi feature near 764.7 MHz, which was present in the calibrators as well as in the object. The two affected channels have been blanked in Figure 2.4.

B 1437+623, 758.642 MHz

This spectrum shows the most severe rfi of any in our survey. The rfi saturates the spectrum for a few channels near 759.3 MHz, and those channels have been blanked. No smoothing has been applied to the remaining channels. The Mg II-absorber lies at a redshift $z = 0.8723$ (Aldcroft et al. 1994).

B 1556-245, 801.900 MHz

The Mg II absorption redshift is $z = 0.7713$ (Barthel et al. 1990). The 4σ feature at 801.05 MHz in the DXB spectrum is the result of weak rfi.

B 1622+239, 1077.798, 1039.068, 857.733, and 790.300 Mhz

The sight line towards B 1622+239, also called 3C336, contains multiple metal-line absorption systems. It has been studied extensively by Steidel et al. (1997). We have obtained H I 21cm spectra for four of the Mg II-absorbers at redshifts $z = 0.318, 0.367,$ 0.656, & 0.797. Although the quasar itself is a very strong radio source with two large extended lobes, we observed each frequency for barely an hour near zenith. As a result the lobes were never resolved by the WSRT, and we have only one spectrum at each frequency.

B 1629+120, 747.425 MHz

This sight line contains two Mg II-absorbers at redshifts $z = 0.5313$ & 0.9004 (Aldcroft et al. 1994, Barthel et al. 1990). The feature at 747.6 MHz in the 21cm spectrum of the low redshift object is caused by interference which affected the passband calibrator as well as the object.

B 1704+608, 1162.457 MHz

The Mg II-absorber towards B 1704+608 lies at a redshift of $z = 0.2219$ (Boissé et al. 1992) , making it one of the lowest redshift systems in this survey. The quasar itself is also very low redshift ($z_{em} = 0.371$), and is highly extended in the radio regime. In Figure 2.4 we show DXB spectra extracted at the position of three peaks in the radio emission. There is a clear rfi feature near 1162.9 MHz in all three. The continuum flux densities of the resolved components are $S_A = 2.5$ Jy, and $S_B \approx S_C \approx 0.66$ Jy. In Figure 2.5 we show an independent observation made with the DZB correlator. The rfi at 1162.9 MHz is visible in this spectrum as well. This much shorter observation did not have sufficient UV coverage to resolve the individual components.

2.5   Conclusions

We have used the ready availability of Mg II absorber redshifts and statistics to construct a database of 62 systems. These were searched for H I 21cm absorption using the WSRT. Most of the observations were taken with the older DXB correlator. Although there are significant sources of rfi throughout the UHF-high band, narrow-band observations and careful flagging make it possible to obtain useful observations at these frequencies. This survey will provide the basis for further study of the characteristics and redshift evolution of H I 21cm absorbing galaxies.

References

Aldcroft, T. L., Bechtold, J., and Elvis, M. 1994, ApJS, 93, 1

Aldcroft, T. L., Elvis, M., and Bechtold, J. 1993, AJ, 105, 2054

Baars, J. W. M., Genzel, R., Pauliny-Toth, I. I. K., and Witzel, A. 1977, A&A, 61, 99

Barthel, P. D., Tytler, D. R., and Thomson, B. 1990, A&AS, 82, 339

Bergeron, J. and Boissé, P. 1984, A&A, 133, 374

Bergeron, J., Kunth, D., and D'Odorico, S. 1987, A&A, 180, 1

Boissé, P., Boulade, O., Kunth, D., Tytler, D., and Vigroux, L. 1992, A&A, 262, 401

Boksenberg, A., Carswell, R. F., and Sargent, W. L. W. 1979, ApJ, 227, 370

Bos, A., Raimond, E., and van Someren Greve, H. W. 1981, A&A, 98, 251

Briggs, F. H. and Wolfe, A. M. 1983, ApJ, 268, 76

Burbidge, E. M., Smith, H. E., Weymann, R. J., and Williams, R. E. 1977, ApJ, 218, 1

Chen, J. S., Morton, D. C., Peterson, B. A., Wright, A. E., and Jauncey, D. L. 1981, MNRAS, 196, 715

Foltz, C. B., Weymann, R. J., Peterson, B. M., Sun, L., Malkan, M. A., and Chaffee, F. H., J. 1986, ApJ, 307, 504

Galt, G. A. 1977, ApJ, 214, L9

Junkkarinen, V., Hewitt, A., and Burbidge, G. 1991, ApJS, 77, 203

Kunth, D. and Bergeron, J. 1984, MNRAS, 210, 873

Lu, L. and Wolfe, A. M. 1994, AJ, 108, 44

Rao, S. M. 1994, *Ph.D. thesis*, AA(Pittsburgh Univ.)

Rao, S. M., Turnshek, D. A., and Briggs, F. H. 1995, ApJ, 449, 488

Sargent, W. L. W., Steidel, C. C., and Boksenberg, A. 1988, ApJS, 68, 539

Sargent, W. L. W., Steidel, C. C., and Boksenberg, A. 1989, ApJS, 69, 703

Steidel, C. C., Dickinson, M., Meyer, D. M., Adelberger, K. L., and Sembach, K. R. 1997, ApJ, 480, 568

Steidel, C. C. and Sargent, W. L. W. 1992, ApJS, 80, 1

Stickel, M., Fried, J. W., and Kuehr, H. 1989, A&AS, 80, 103

Wolfe, A. M., Turnshek, D. A., Smith, H. E., and Cohen, R. D. 1986, ApJS, 61, 249

Wright, A. E., Peterson, B. A., Jauncey, D. L., and Condon, J. J. 1979, ApJ, 229, 73

Figure 2.4: Spectra taken using the WSRT with the DXB correlator. A rough estimate of the mean continuum level is indicated with the horizontal line. B1950 IAU designations for the quasars are indicated above each plot, and the addition of A,B, or C indicates separate sight lines to a resolved source.

Figure 2.4: (cont'd)

Figure 2.4: (cont'd)

Figure 2.4: (cont'd)

Figure 2.4: (cont'd)

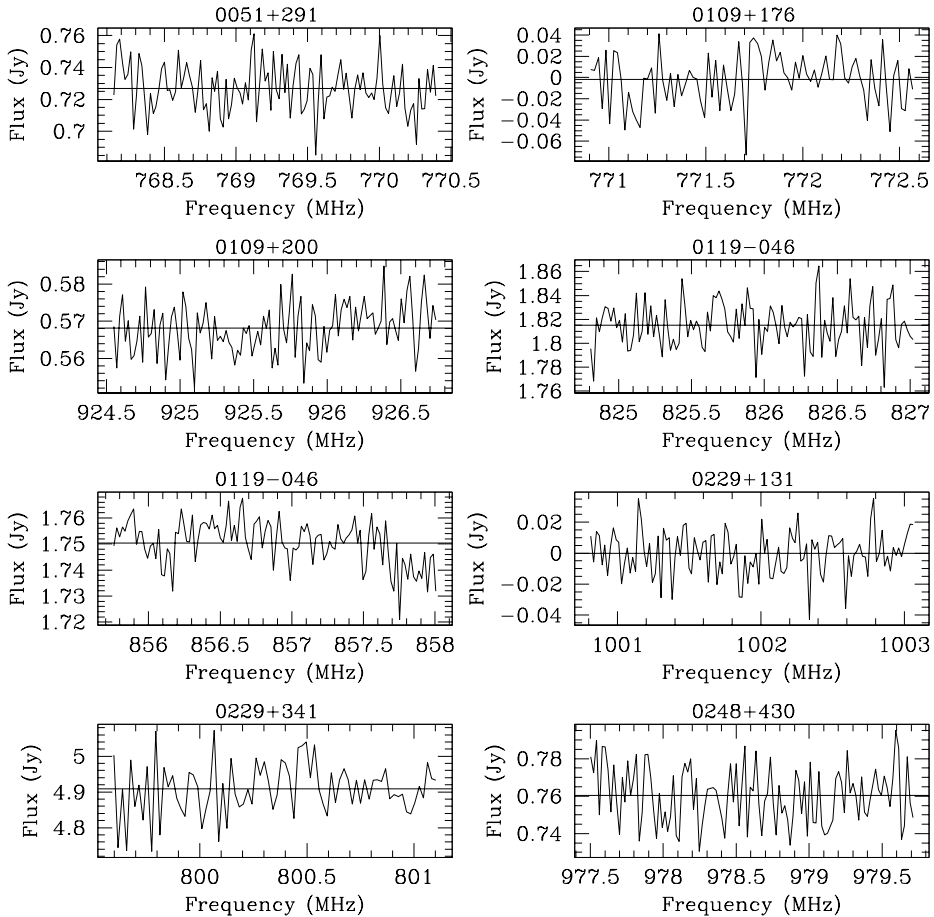Figure 2.4: (cont'd)

Figure 2.4: (cont'd)

Figure 2.4: (cont'd)

Figure 2.5: Spectra taken using the WSRT and the DZB Correlator. A rough estimate of the mean continuum level is indicated with the horizontal line. B1950 IAU designations for the quasars are indicated above each plot, and the addition of A,B, or C indicates separate sight lines to a resolved source.
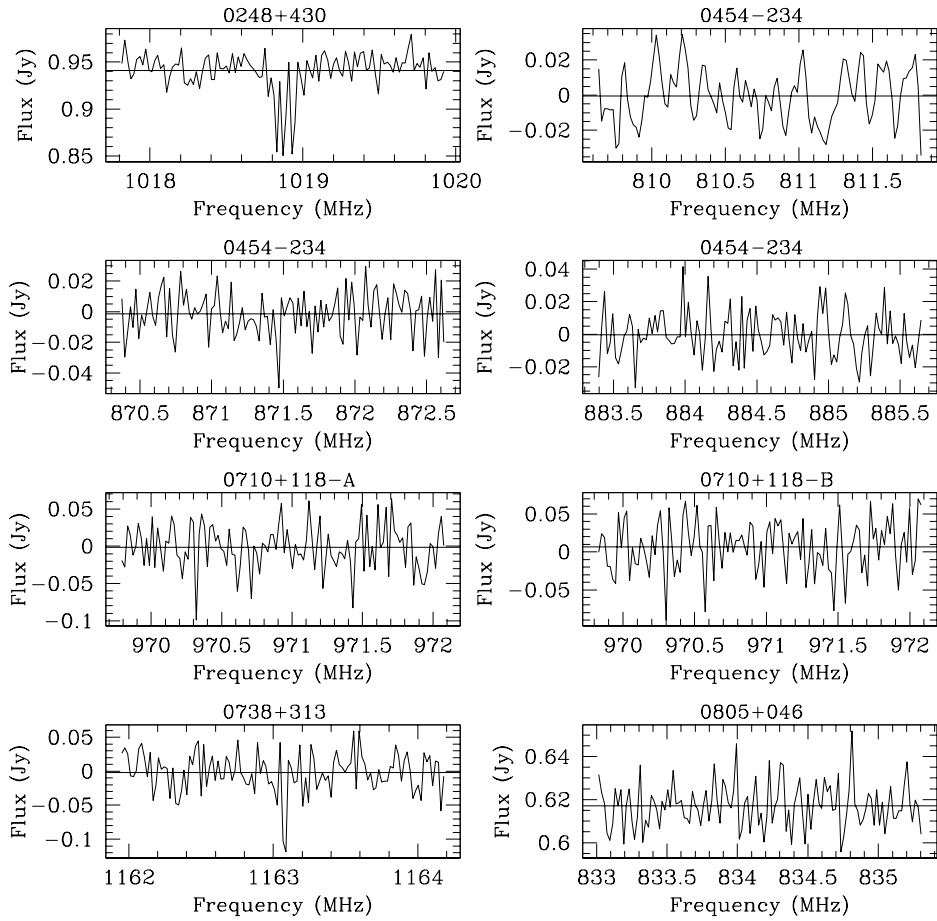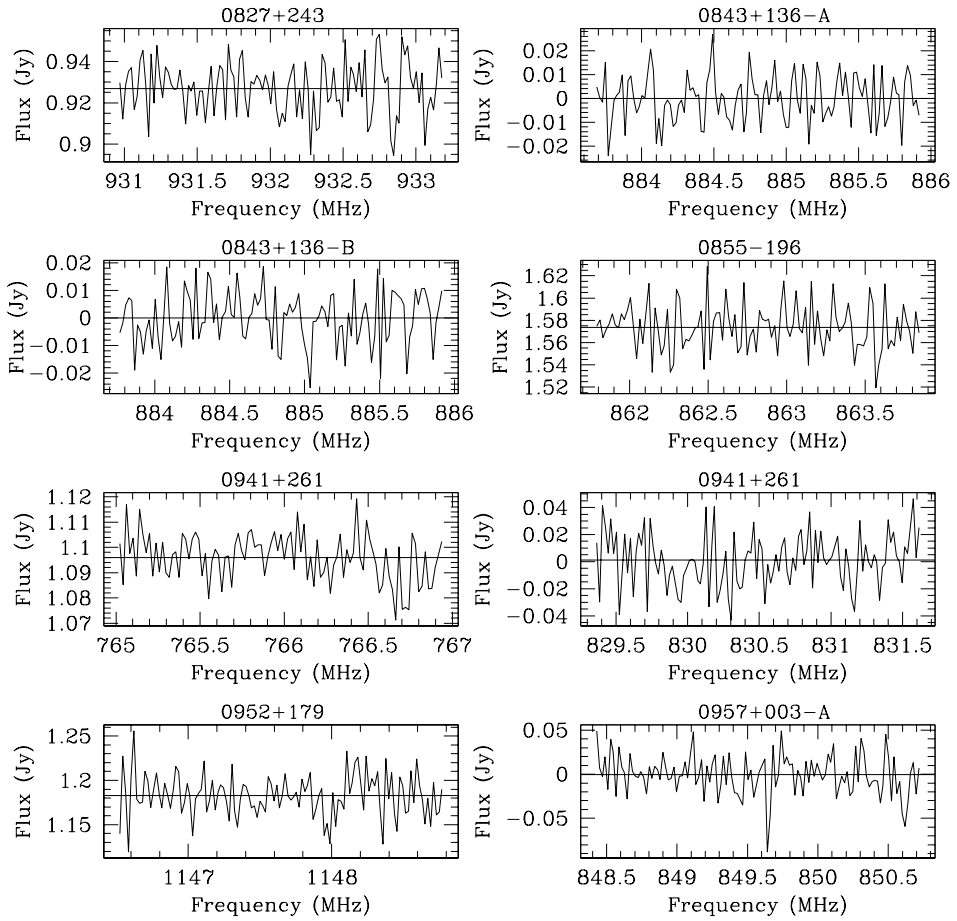
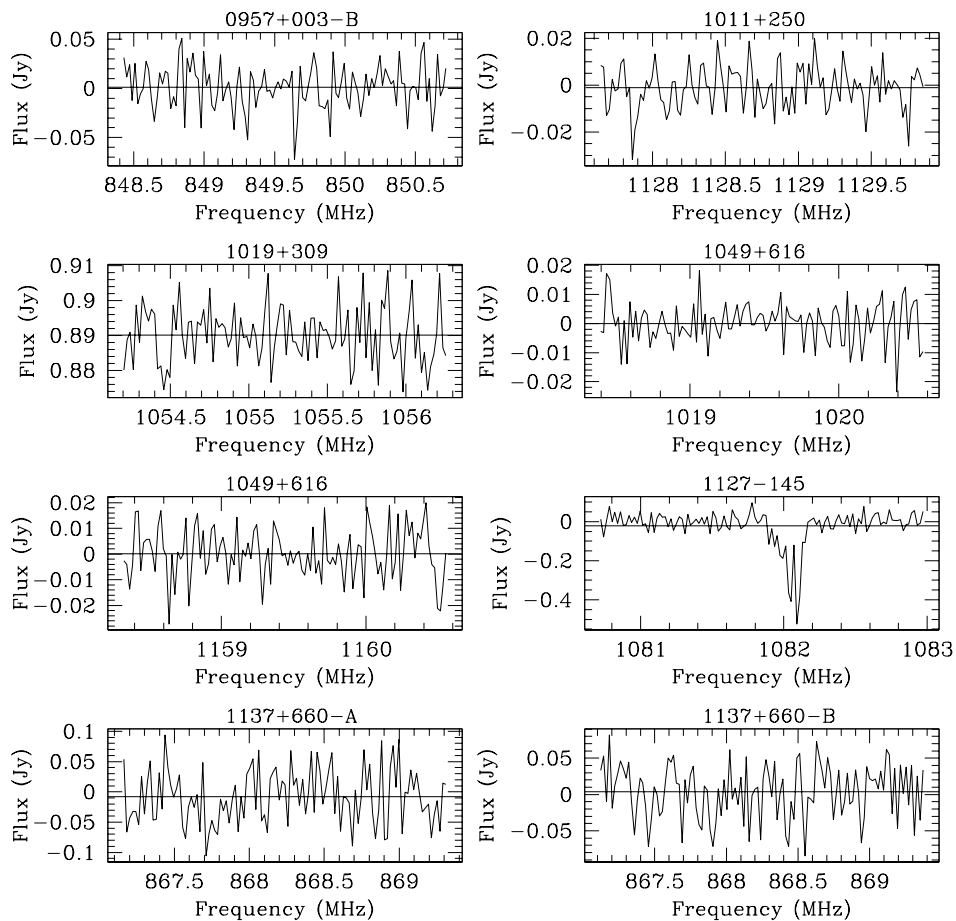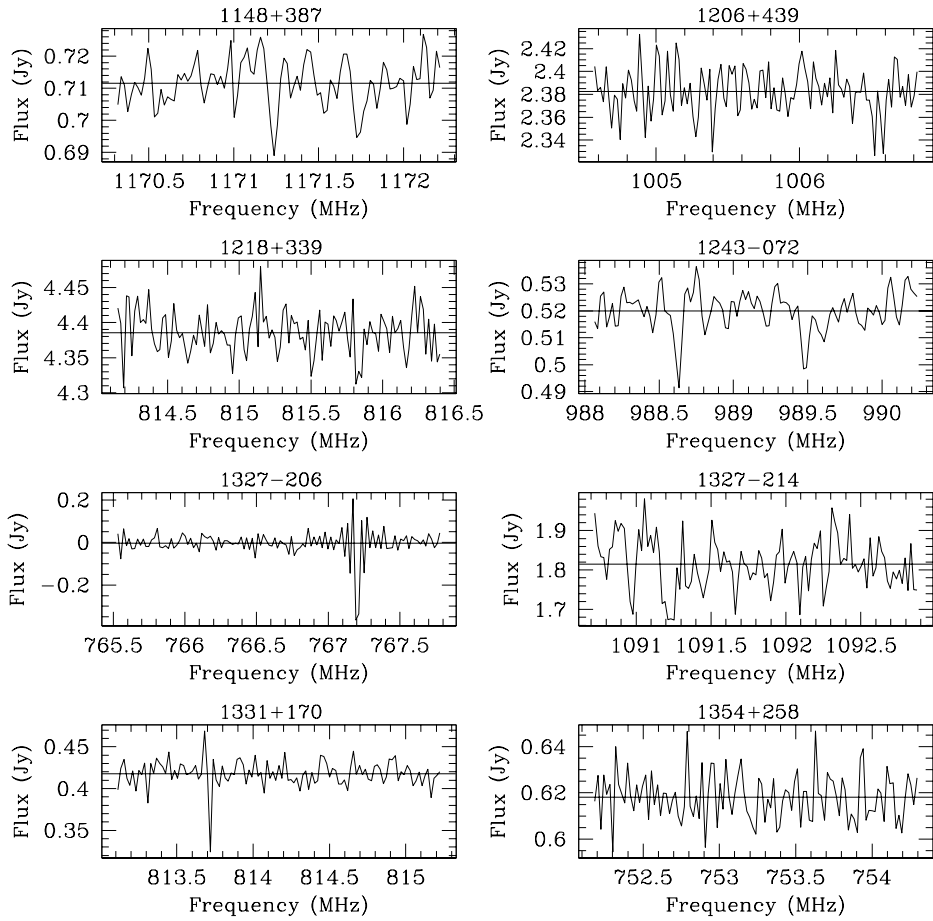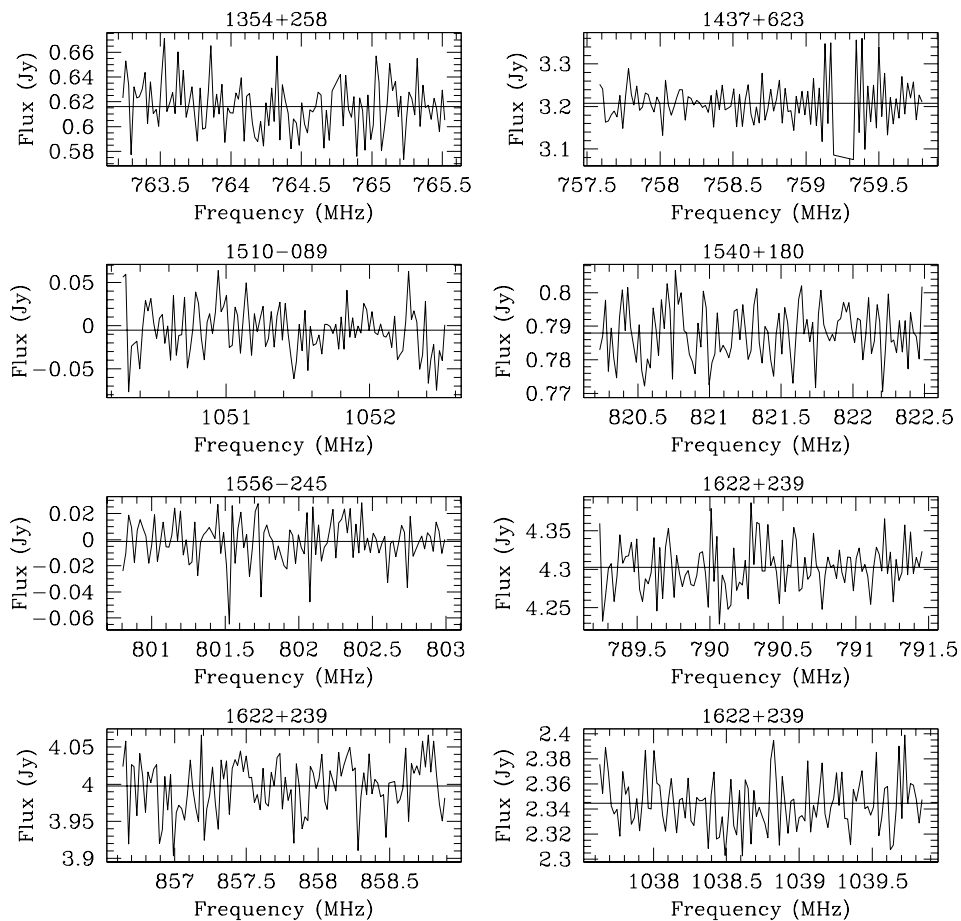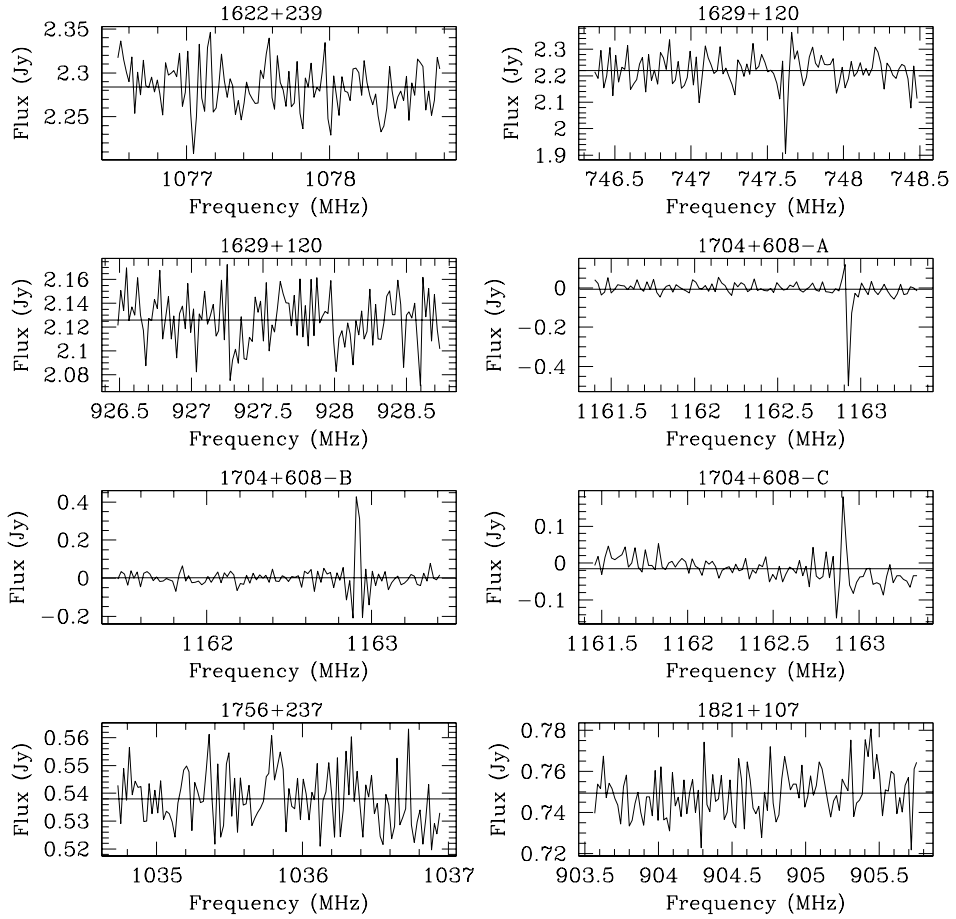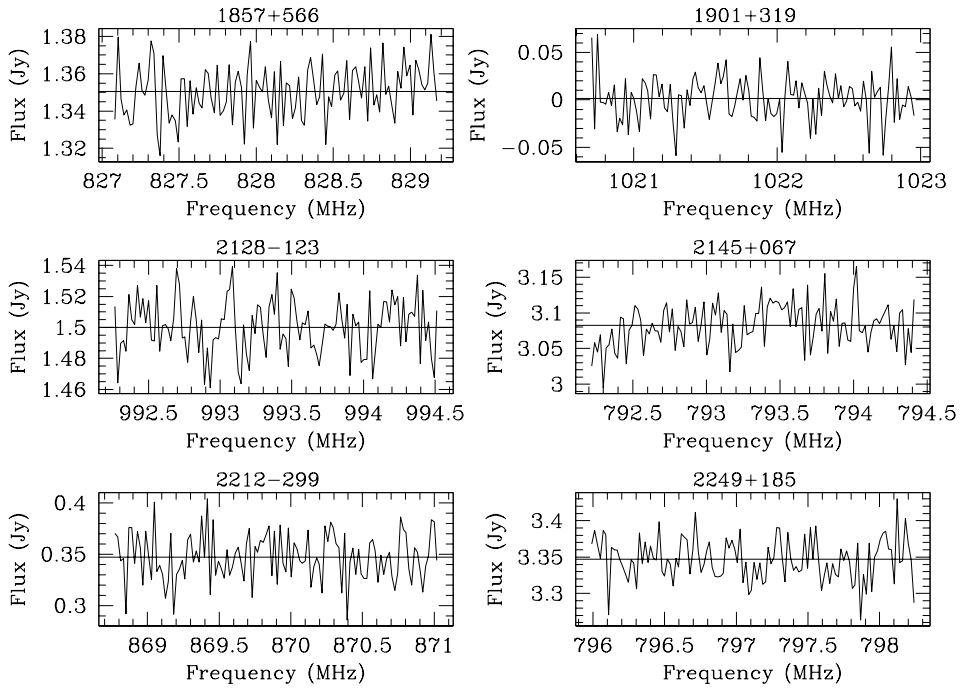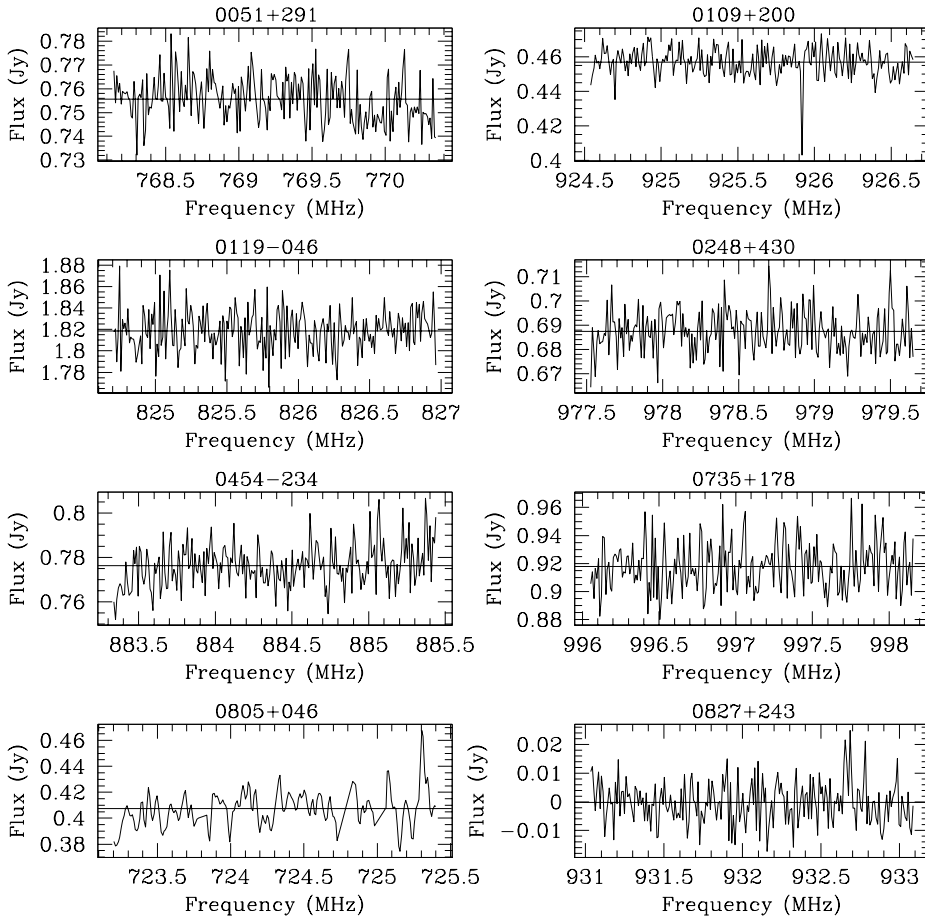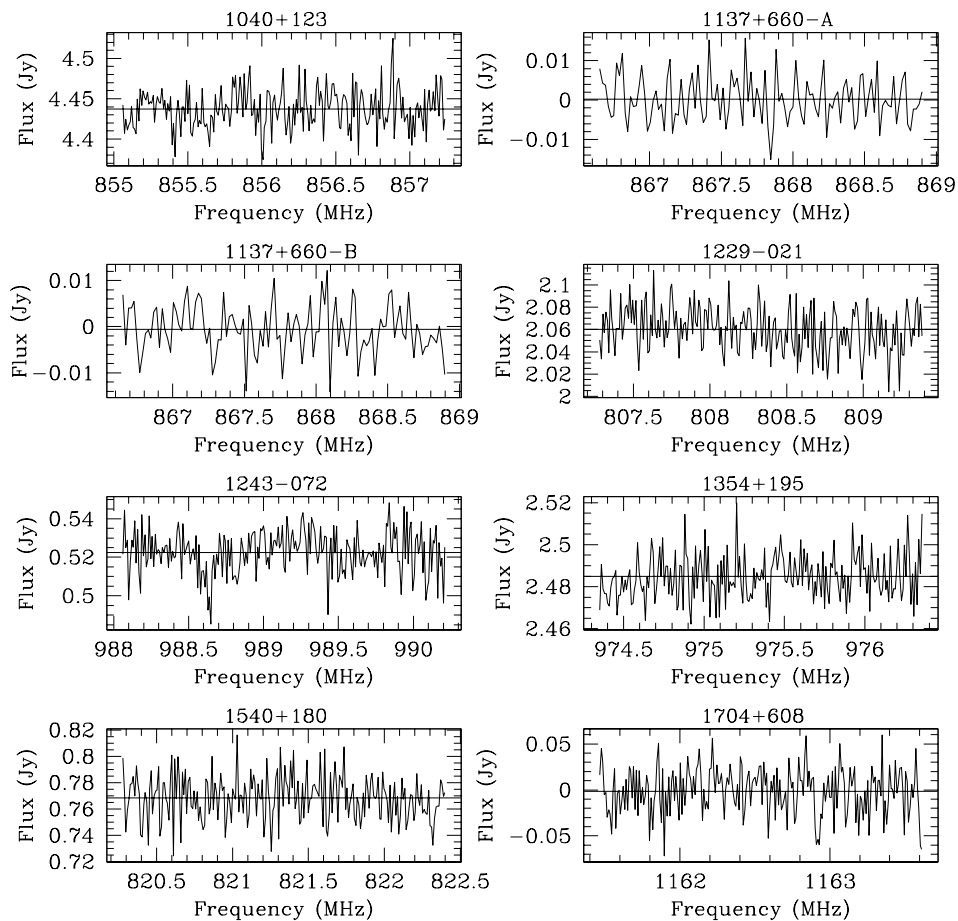Figure 2.5: (cont'd)
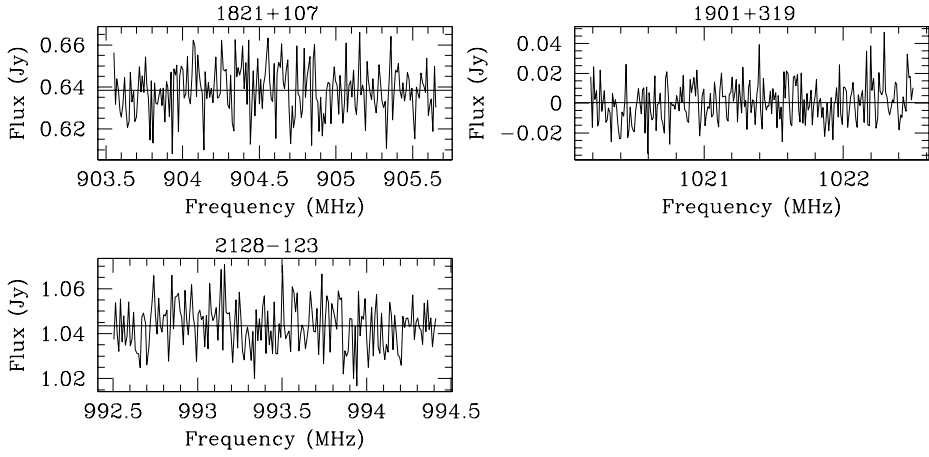
Figure 2.5: (cont'd)

3

Statistics from the 21cm Survey

We combine results from a recent WSRT survey for H I 21cm absorption in Mg II-selected systems with existing literature surveys to create a complete Mg II/21cm sample from which to derive statistical properties of the absorbers. Using known statistical properties of the Mg II systems, we estimate $n_{21cm}(z)$ and $\Omega_{21cm}(z)$ and compare these results to numbers from Damped Lyα surveys.

3.1   Introduction

Just as the identification and study of individual 21cm absorbers at low and intermediate redshifts is important to our understanding of the characteristics of such a system, so is the information to be gained by a systematic and statistical study of the absorbers important to our understanding of their properties as a class of objects, and their evolution over time. Although the numbers are still relatively small, the sample presented here can, with the aid of known properties of the Mg II absorber population from which it is drawn, be used to derive some rough properties of HI-rich absorbers at these intermediate redshifts.

In order to make a complete statistical sample of Mg II-selected systems, we added information from the literature to the WSRT-sample described in Chapter 2. There have been two previous surveys for 21cm absorption in Mg II-selected systems. The first was by Peterson and Foltz (1980), who used the 91m transit telescope in Green Bank, West Virginia, to look for 21cm absorption in 8 Mg II absorbers, all of which lie at redshifts $0.2 < z < 0.9$. They had no detections and their sensitivity limits were generally quite poor. Half of their systems were included in the WSRT-sample, and of the other four, three were observed by Briggs and Wolfe (1983) with greater sensitivity. Hence they contribute only one unique system, 0420-014 at $z = 0.6320$ to our complete sample. This quasar satisfies the other WSRT-sample selection criteria ($S_{1400\,MHz} \geq 0.5$, $\delta \geq -30°$), and would have been observed by the

WSRT except for the presence of rfi at that frequency. In addition to 0420-014, we use their detection limit for the 0952+179 system at $z = 0.239$ because it is more sensitive than the WSRT-survey result.

The Briggs and Wolfe survey (1983), used the Arecibo Telescope to study a sample of 18 Mg II- and Fe II- selected systems, among which they found two 21cm absorbers. In this case the redshifts fell over a wider range, as did the backgrounds source strengths, and it was necessary to refine their sample slightly to match the WSRT sample selection. After excluding Fe II-selected systems, weak radio QSOs, and systems at redshifts outside of $0.2 < z < 1.0$, there are 12 Mg II absorbers left, of which nine are not part of the WSRT-sample (mostly due to rfi). Two of those nine are 21cm detections. Although the actual detections were made separately from the Briggs and Wolfe survey itself, they were studied because of the presence of Mg II absorption and are thus valid members of the survey group.

Combining the 62 systems from the WSRT sample with the 10 taken from the literature, we arrive at a total Mg II/21cm sample of 72 systems. Among these there are five 21cm absorbers. There are two from the Briggs and Wolfe (1983) survey; AO 0235+164 at $z = 0.524$ and PKS 1229-021 $z = 0.395$. The other three come from the WSRT sample; B 0248+430 at $z = 0.394$, OI 363 (B 0738+313) at $z = 0.221$, and B 1127-145 at $z = 0.313$.

There are two systems that are not detected at the sensitivity limits of our spectra in the Mg II/21cm sample which were individually observed due to the known presence of Damped Lyα (DLA) absorption and discovered to be 21cm absorbers as well. The first of these systems is the $z = 0.239$ absorber towards PKS 0952+179. This system was included in the WSRT-sample, but the spectrum suffered from instrumental problems as well as time-dependent rfi, and only reached a 3σ optical depth limit of $\tau_{3\sigma} = 0.062$. Kanekar and Chengalur (2000) obtained a far more sensitive spectrum of this system using the GMRT, in which they detect a 21cm absorption line with a maximum optical depth of approximately $\tau = 1.5\%$. Similarly, they also identify a very weak line with $\tau \approx 0.6\%$, in the spectrum of 0827+243 at $z = 0.5247$. This system was included in the Briggs and Wolfe (1983) survey as well as the WSRT sample, but was not detected due to its very small optical depth. These two systems appear in our Mg II/21cm sample statistics as non-detections. The detection information is included anytime that Mg II-selection is not an issue, in order to better indicate the properties of 21cm absorbers as a group.

These two systems are a very good illustration of the incompleteness which enters our sample due to an imposed sensitivity limit. It is difficult to correct for this bias, because very little information exists on low optical depth 21cm absorption lines. In fact, the two new 21cm lines of Kanekar and Chengalur are among the weakest detected in extra-galactic systems.

3.2   21cm Detection Limits

The detection limit for a line with a width of one channel in a spectrum with a continuum flux density, *S*, and an RMS noise per channel, ΔS, can be written as:

$$\tau_{3\sigma} = -\ln\left(1 - \frac{3\Delta S}{f\,S}\right) \tag{3.1}$$

where $\tau_{3\sigma}$ is the optical depth of a line at a significance of 3σ, and f is the covering factor, or the fraction of the continuum source which is covered by the intervening gas. For the sake of simplicity, and since we know very little about the true distribution of the intervening gas, we assume that $f = 1$ in all non-detection cases. Note that this is likely to be true for compact background QSOs, but not for those radio sources which are very extended.

Using $\tau_{3\sigma}$, we can express the upper limit for the H I column density, N_{HI} on the sight line to the quasar as:

$$N_{\mathrm{HI}} \leq 1.8 \times 10^{18} < T_{\mathrm{s}} > \int \tau_{3\sigma}\,dv \quad \mathrm{cm}^{-2} \tag{3.2}$$

where $< T_{\mathrm{s}} >$ is the harmonic mean spin temperature of all the gas on the sight line in degrees K. The integral represents the area under the absorption curve. If we assume a Gaussian line profile with full width at half maximum Δv and height $\tau_{3\sigma}$ then:

$$\int \tau_{3\sigma}\,dv = 1.06\,\tau_{3\sigma}\,\Delta v \tag{3.3}$$

For non-detections, Δv is the resolution of the spectrum in km s^{-1} and is related to the channel width in frequency space, $\Delta\nu$, of the WSRT spectra by:

$$\Delta v = 3 \times 10^5 \left(\frac{1.2\Delta\nu}{\nu_{abs}}\right) \quad \mathrm{km\ s}^{-1} \tag{3.4}$$

where

$$\nu_{abs} = \frac{1420.4057}{(1 + z_{abs})} \quad \mathrm{MHz} \tag{3.5}$$

is the expected absorption frequency of the 21cm line, and $\Delta\nu$ is in MHz as well. The factor 1.2 comes from the uniform weighting applied to the WSRT spectra, and converts the channel width to a true resolution.

Usually we do not know the $< T_{\mathrm{s}} >$ of the H I on the sight line, so it is more useful to calculate $N_{\mathrm{HI}}/< T_{\mathrm{s}} >$ for each Mg II absorber in our complete sample. The resulting values can be multiplied by a chosen value of $< T_{\mathrm{s}} >$ to estimate N_{HI}.

In Table 3.1 we have listed the individual parameters for all non-detections in our sample. Columns (1), (2), and (3) give the quasar name in B1950 coordinates, the emission redshift of the quasar, and the absorption redshift of the Mg II absorber. Column (4) gives the expected frequency of the associated 21cm absorption feature, while column (5) gives the velocity resolution of the spectrum at that frequency. Column (6) gives the computed value of $\tau_{3\sigma}$, and column (7) lists the values for $N_{\mathrm{HI}}/< T_{\mathrm{s}} >$. For systems that are resolved by the WSRT beam, values against each lobe are listed, separated by commas, for Columns (6) and (7). We have included information at the highest velocity resolution available, rather than smoothing to a common resolution.

Table 3.1: 21cm Absorption Spectra Limits

Object	z_{em}	z_{abs}	Freq. (MHz)	Δv (km s^{-1})	$\tau_{3\sigma}^{a}$	$\frac{N_{\mathrm{HI}}}{<T_s>}^{a} \times 10^{17}$ (cm^{-2} K^{-1})
0051+291	1.828	0.8465	769.242	4.6	0.040	3.5
0109+176	2.155	0.8392	772.295	9.1	0.108	19
0109+200	0.746	0.5346	925.587	7.6	0.029	4.2
0119−046	1.969	0.6577	856.853	8.2	0.011	1.7
		0.7199	825.865	4.3	0.032	2.6
0229+131	2.067	0.4177	1001.908	7.0	0.027	3.6
0229+341	1.240	0.7754	800.048	8.8	0.043	7.2
0235+164[b]	0.940	0.8510	767.372	10	0.006	1.1
0248+430	1.316	0.4515	978.578	3.6	0.039	2.7
0420−014[c]	0.915	0.633	869.814	10.6	0.146	30
0454−234	1.003	0.606	884.437	4.0	0.039	3.0
		0.630	871.415	8.1	0.041	6.3
		0.752	810.734	14.4[d]	0.044	12
0454+039[b]	1.343	0.8597	763.782	10	0.010	1.9
0457+024[b]	2.384	0.4717	965.146	10	0.048	9.2
0710+118	0.768	0.4630	970.886	7.2	0.084,0.051	12,7.0
0735+178		0.4246	997.056	3.5	0.058	3.9
0805+046	2.876	0.7029	834.110	8.4	0.051	8.2
		0.9598	724.771	4.9	0.095	8.9
0827+243	0.939	0.524	932.025	3.8	0.027	2.0
0843+136	1.875	0.6054	884.767	7.9	0.324,0.051	49,7.7
0855−196	0.659	0.6463	862.787	8.1	0.041	6.3
0941+261	2.908	0.7113	830.016	8.5	0.049	7.9
		0.8545	765.924	9.2	0.026	4.6
0952+179[c]	1.472	0.2377	1147.617	8.0	0.032	4.9
0957+003	0.907	0.6720	849.525	8.3	0.105,0.134	17,21
1011+250	1.631	0.2584	1128.739	6.2	0.047	5.6
1011+280[b]	0.899	0.8895	751.736	10	0.010	1.9
1019+309	1.315	0.3461	1055.201	6.7	0.027	3.4
1038+064[b]	1.270	0.4416	985.298	10	0.01	1.9
1040+123	1.029	0.6591	856.130	4.1	0.017	1.3
1049+616	0.422	0.2251	1159.420	6.0	0.027	3.1
		0.3933	1019.454	6.9	0.017	2.23
1137+660	0.652	0.636	868.219	8.1	0.020,0.005	3.1,0.77
1148+387	1.303	0.2130	1170.986	10[d]	0.031	5.9
1206+439	1.396	0.4124	1005.668	7.0	0.027	3.6
1218+339	1.519	0.7423	815.247	8.6	0.020	3.3
1226+105[b]	2.304	0.4308	992.735	10	0.026	5.0
1229−021	1.038	0.7571	808.381	4.3	0.029	2.4
1243−072	1.286	0.436	989.140	3.6	0.067	4.6
1308+326[b]	0.996	0.879	755.937	10	0.007	1.3
1327−206	1.169	0.853	766.544	9.2	0.201	35
1327−214	0.528	0.301	1091.780	6.4	0.115	14
1331+170	2.08	0.7443	814.313	8.6	0.090	15
1354+195	0.719	0.4563	975.352	3.6	0.013	0.89
1354+258	2.004	0.8585	764.275	9.2	0.103	18
		0.8856	753.291	9.3	0.050	8.9
1437+623	1.090	0.8723	758.642	9.2	0.049	8.6
1510−089	0.361	0.351	1051.374	6.7	0.025	3.2
1540+180	1.662	0.7294	821.329	8.5	0.030	4.9
1556−245	2.815	0.7713	801.900	8.8	0.068	11

Table 3.1 – *cont'd*

Object	z_{em}	z_{abs}	Freq. (MHz)	Δv (km s^{-1})	$\tau_{3\sigma}^a$	$\frac{N_{HI}}{<T_s>}\,^a \times 10^{17}$ (cm^{-2} K^{-1})
1622+239	0.927	0.318	1077.698	6.5	0.035	4.3
		0.367	1039.068	6.8	0.027	3.5
		0.6560	857.733	8.2	0.026	4.1
		0.7973	790.300	8.9	0.022	3.7
1629+120	1.795	0.5313	927.582	7.6	0.031	4.5
		0.9004	747.425	9.4	0.080	14
1704+608	0.371	0.2219	1162.457	3.0	0.042	2.4
1756+237	1.726	0.3713	1035.810	6.8	0.060	7.8
1821+107	1.359	0.5702	904.602	7.8	0.048	7.1
1857+566	1.572	0.7151	828.177	8.5	0.031	5.0
1901+319	0.635	0.3901	1021.801	3.4	0.011	0.71
2128−123	0.501	0.4299	993.360	3.5	0.030	2.0
2145+067	0.999	0.7906	793.257	8.8	0.029	4.9
2212−299	2.703	0.6329	869.867	8.1	0.217	34
2249+185	1.758	0.7820	797.085	8.8	0.025	4.2

[a]Assuming a covering factor $f = 1$
[b]Numbers taken from Briggs & Wolfe (1983)
[c]Numbers taken from Peterson & Foltz (1980)
[d]Hanning smoothed. Use a factor of 2 instead of 1.2 in Eq. 3.4

For those systems with detected 21cm line absorption, we measure true values for τ, based on the actual depths of the absorption lines relative to the continuum strength. In Table 3.2 we list the same information as in Table 3.1, with the difference that these are actual values rather than upper limits to τ and $N_{HI}/<T_s>$. The values listed for ΔV are the total velocity spread of all the components for each system, estimated as the separation in centroid velocities plus the FWHM velocity (Δv) of the two most widely separated components. This means that $\Delta V = \Delta v$ at FWHM for single component systems.

While it is still possible to estimate a value for $N_{HI}/<T_s>$, most of these systems have also been observed in the Lyα line which provides an independent measurement of N_{HI}. These values are listed in Column (8) of Table 3.2. By combining the DLA N_{HI} values with the 21cm information, it is possible to derive a value for $<T_s>$.

3.3   Metal-Line Properties of the Sample

3.3.1   Metal-Line Rest Equivalent Widths

All of the systems included in our complete Mg II/21cm sample were initially selected for the presence of a Mg II $\lambda\lambda$ 2796, 2803 Å doublet. Although we did not insist that the strength, as measured by the rest equivalent width of the λ 2796 Å line, be particularly large or even accurately measured, rest equivalent width values for most of our systems exist in the literature. Spectra taken to find the Mg II doublet at a given redshift quite naturally tend to cover the appropriate wavelengths to

Table 3.2: Summary of Absorption Profiles for the 21cm Absorbers

Object	z_{em}	z_{abs}	ΔV^a (km s^{-1})	τ	$\frac{N_{HI}}{<T_s>} \times 10^{18}$ (cm^{-2} K^{-1})	$N_{HI} \times 10^{20}$ (cm^{-2})	Ref.
0235+164	0.940	0.5238	110	0.05-0.6	23.4	50	2,5
0248+430	1.316	0.3939	40	0.07-0.2	5.1		9
0738+313	0.631	0.2213	5.5	0.10	1.1	7.9	9,7
1127−145	1.187	0.3130	60	0.03-0.11	5.3	51	9,7
1229−021	1.038	0.3950	12	0.24	3.0	5.6	8,4
non-Mg II-selected systems							
0809+483	0.871	0.4368	36	0.24	5.6	6.3	3,10,4
0827+243	0.939	0.524	51.5	0.007	0.43	2.0	6,7
0952+179	1.472	0.2377	8	0.013	0.27	21	6,7
1328+307	0.849	0.692	8	0.10	1.7	18	1,4

^{a}Total velocity coverage of absorption components.
References: (1) Davis and May 1978, (2) Wolfe et al. 1978, (3) Brown and Mitchell,
1983, (4) Boisseé et al. 1998, (5) Cohen et al. 1999, (6) Kanekar and Chengalur 2000
(7) Rao and Turnshek 2000, (8) Briggs et al. 2000, (9) This thesis, Chapter 4,
(10) F. Briggs, private communication

observe either the Mg I λ 2852 Å line and/or the Fe II λ 2600 Å line when they are present, and we were often able to find published rest equivalent width values or upper limits for these two lines as well. In cases where the published spectra cover the appropriate wavelength range for these lines but no rest equivalent width values are quoted, we estimated upper limits ourselves.

The information we have compiled on these low ionization metal lines for the 72 systems in our complete Mg II/21cm sample is summarized in Table 3.3. Column (1) gives the QSO's B 1950 coordinate designation, Column (2) gives the emission redshift of the QSO while Column (3) gives the absorption redshift. Columns (4) through (7) list the rest equivalent widths or upper limits for the Mg II λ 2796, Mg II λ 2803, Mg I λ 2852, and Fe II λ 2600 Å absorption lines, and finally Column (8) gives the references for the metal-line data. Blank values in the table indicate systems with no published equivalent width values, for which there are no published spectra suitable for estimating the equivalent widths.

Table 3.3: Metal Line Equivalent Widths

Object	z_{em}	z_{abs}	$W_o^{\lambda 2796}$ Mg II	$W_o^{\lambda 2803}$ Mg II	$W_o^{\lambda 2852}$ Mg I	$W_o^{\lambda 2600}$ Fe II	Ref.
0051+291	1.828	0.8465	...	...	...	...	13,27
0109+176	2.155	0.8392	1.75	1.20	<0.2	1.09	15
0109+200	0.746	0.5346	2.26	1.71	...	...	18
0119−046	1.969	0.6577	0.30	0.22	<0.1	<0.1	4
		0.7199	0.27	0.19	...	...	18
0229+131	2.067	0.4177	0.67	0.75	[<0.35]	...	1
0229+341	1.240	0.7754	1.92	2.02	<1.13	...	8

Metal Line Equivalent Widths *(cont'd)*

Object	z_{em}	z_{abs}	$W_o^{\lambda 2796}$ Mg II	$W_o^{\lambda 2803}$ Mg II	$W_o^{\lambda 2852}$ Mg I	$W_o^{\lambda 2600}$ Fe II	Ref.
0235+164	0.940	0.5238	2.42	2.34	0.91	1.79	29
		0.8510	0.44	0.42	<0.3	0.23	29
0248+430	1.316	0.3939	1.86	1.42	0.70	1.03	2
		0.4515	0.34	0.29	[<0.5]	<0.2	6
0420−014	0.915	0.633	1.02	0.86	<0.36	...	8
0454−234	1.003	0.606	...	...	...	...	19
		0.630	...	...	...	...	19
		0.752	...	...	...	...	19
0454+039	1.343	0.8597	1.53	1.40	0.37	1.11	2,7
0457+024	2.384	0.4717	...	...	...	...	30
0710+118	0.768	0.4630	0.62	0.29	0.24	<0.4	8
0735+178		0.4246	1.33	1.04	0.18	0.87	9,34
0738+313	0.631	0.2213	0.52	0.50	<0.2	<0.6	10
0805+046	2.876	0.7029	0.52	0.39	...	...	15
		0.9598	1.01	0.83	<0.6	0.24	3,20
0827+243	0.939	0.524	2.90	2.20	...	1.90	11,12
0843+136	1.875	0.6054	0.48	0.18[a]	<0.4	<0.7	13
0855−196	0.659	0.6463	...	...	...	...	21
0941+261	2.908	0.7113	0.96	0.83	<0.2	...	15
		0.8545	0.39	0.40	<0.4	...	3
0952+179	1.472	0.2377	0.63	0.79	<0.4	...	2
0957+003	0.907	0.6720	1.77	1.32	...	...	18
1011+250	1.631	0.2584	...	...	...	...	22
1011+280	0.899	0.8895	...	2.01	...	1.46	31
1019+309	1.315	0.3461	0.70	0.68	<0.2	<0.4	2
1038+064	1.270	0.4416	0.66	0.57	<0.15	<0.3	2
1040+123	1.029	0.6591	0.58	0.42	<0.2	<0.4	8
1049+616	0.422	0.2251	0.51	0.56	<0.2	<0.4	10
		0.3933	0.34	0.29	...	<0.2	10
1127−145	1.187	0.3130	2.21	1.90	1.14	1.14	14
1137+660	0.652	0.636	0.15[a]	0.16[a]	...	...	8
1148+387	1.303	0.2130	0.96	0.37	<0.3	...	10
1206+439	1.396	0.4124	>0.6	>0.6	...	...	23,24
1218+339	1.519	0.7423	1.34	1.08	<0.7	<1.0	8
1226+105	2.304	0.4308	...	...	...	...	30
1229−021	1.038	0.3950	2.22	1.93	0.49	1.59	32
		0.7571	0.52	0.48	<0.2	...	8
1243−072	1.286	0.436	...	...	...	...	25
1308+326	0.996	0.879	...	...	...	...	33
1327−206	1.169	0.853	2.11	1.48	<0.4	0.76[a]	16,17
1327−214	0.528	0.301	0.65[a]	0.44	<0.4	<0.6	8
1331+170	2.08	0.7443	0.87	0.76	...	0.27	1
1331+170	2.08	0.7454	0.91	0.66	...	0.34	1
1354+195	0.719	0.4563	0.89	0.82	0.16	0.32	2
1354+258	2.004	0.8585	1.00	0.86	<0.1	...	15
		0.8856	0.81	0.57	<0.2	...	15[b]
1437+623	1.090	0.8723	0.71	0.64	<0.4	<0.5	8
1510−089	0.361	0.351	...	...	...	...	26
1540+180	1.662	0.7294	0.76	0.42	<0.1	<0.2	15
1556−245	2.815	0.7713	2.07	1.91	1.07	<0.2	15
1622+239	0.927	0.318	0.50	0.43	<0.2	<0.4	5
		0.367	[0.54]	0.29	<0.15	<0.3	5
		0.6560	[1.29]	[1.69]	<0.4	1.13	2

Metal Line Equivalent Widths *(cont'd)*

Object	z_{em}	z_{abs}	$W_o^{\lambda 2796}$ Mg II	$W_o^{\lambda 2803}$ Mg II	$W_o^{\lambda 2852}$ Mg I	$W_o^{\lambda 2600}$ Fe II	Ref.
		0.7973	0.42	0.32	<0.2	...	5
1629+120	1.795	0.5313	1.40	1.35	0.31	0.70	8
		0.9004	1.06	0.67	0.44	0.63	15,8
1704+608	0.371	0.2219	0.55	0.33	<0.2	...	10
1756+237	1.726	0.3713	0.14[a]	0.09[a]	...	...	13
1821+107	1.359	0.5702	0.85	0.67	0.32	0.51	2
1857+566	1.572	0.7151	0.65	0.64	<0.3	<0.3	15
1901+319	0.635	0.3901	0.45	0.15	<0.2	...	8
2128−123	0.501	0.4299	0.41	0.37	0.10[a]	0.27	7,28
2145+067	0.999	0.7906	0.52	0.41	<0.2	<0.1	2
2212−299	2.703	0.6329	1.26	1.00	0.36	...	15
2249+185	1.758	0.7820	0.39	0.35	<0.1	...	15

All numbers are rest equivalent widths in Å.

[ ] indicates that the line is part of a blend.

[a]Line has an equivalent width of less than 5σ.

[b]W_{rest} is misquoted in reference 15. Values calculated from W_{obs}.

Upper limits are either given in the reference or estimated from the published spectrum.

References: (1) Sargent et al. 1988, (2) Steidel & Sargent 1992, (3) Sargent et al. 1989, (4) Sargent et al. 1982, (5) Steidel et al. 1997, (6) Womble et al. 1990, (7) Petitjean & Bergeron 1990, (8) Aldcroft, Bechtold, & Elvis 1994, (9) Boksenberg et al. 1979, (10) Boissé et al. 1992, (11) Wills 1978, (12) Ulrich & Owens 1977, (13) Foltz et al. 1986, (14) Bergeron & Boissé 1991, (15) Barthel et al. 1990, (16) Kunth & Bergeron 1984, (17) Bergeron et al. 1987, (18) Bergeron & Boissé 1984, (19) Stickel et al. 1989, (20) Chen et al. 1981, (21) White et al. 1988, (22) Carswell et al. 1976, (23) Aldcroft, Elvis, & Bechtold 1993, (24) Anderson et al. 1987, (25) Wright et al. 1979, (26) Bergeron & Kunth 1984, (27) Burbidge et al. 1977, (28) Bergeron & Kunth 1983, (29) Wolfe & Wills 1977, (30) Roberts et al. 1978, (31) Peterson & Strittmatter 1978, (32) Briggs et al. 1985, (33) Miller, French, & Hawley 1978, (34) Peterson et al. 1977

3.3.2   Mg II $W_o^{\lambda 2796}$ Distribution

Figure 3.1 is a histogram showing the distribution of Mg II $\lambda 2796$ Å rest equivalent widths ($W_o^{\lambda 2796}$) for the Mg II/21cm sample. Only three of our systems have a measured $W_o^{\lambda 2796} < 0.3$ Å, although we made no effort to limit our sample in this way. For reference, the distribution of Mg II widths for the systems which are associated with 21cm absorption is shaded in, as is the distribution of DLA absorbers over the same redshift range. The Mg II absorber distribution peaks near the 0.3 Å detection lower-limit of most Mg II surveys. The 21cm and DLA systems are not yet very numerous but it is clear that most of the large $W_o^{\lambda 2796}$ tail of the Mg II distribution is associated with high column density HI absorption.

3.3.3   Mg I $W_o^{\lambda 2852}$ and the Mg II Doublet Ratio

A plot of Mg II $W_o^{\lambda 2796}$ against Mg I $W_o^{\lambda 2852}$ is shown in Figure 3.2. Mg II $W_o^{\lambda 2796}$ versus the Mg II doublet ratio $W_o^{\lambda 2796}/W_o^{\lambda 2803}$ is shown in Figure 3.3. The 21cm absorbers do not occupy any particular area of these plots, and neither the Mg I strength nor
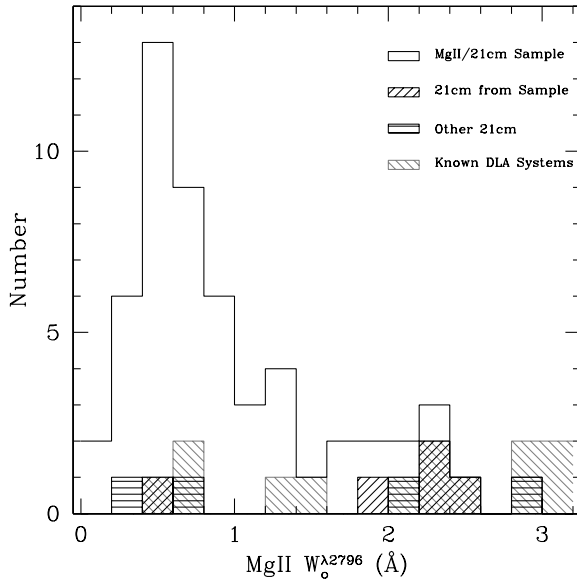
Figure 3.1: A histogram which shows the Mg II $\lambda 2796$ Å rest equivalent width distribution of the Mg II/21cm sample. Systems for which no published values were available are not included. The HI 21cm absorbers identified in the survey are marked by boxes hatched from lower left to upper right, while 21cm absorbers which were not Mg II-selected are indicated with boxes hatched horizontally. For comparison, the distribution of DLA absorbers is indicated with boxes hatched from upper left to lower right.
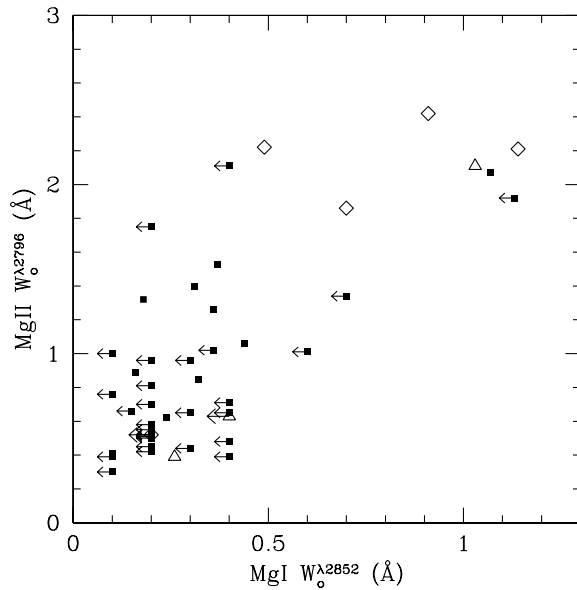
Figure 3.2: A plot of Mg II $W_o^{\lambda 2796}$ vs. Mg I $W_o^{\lambda 2852}$. The Mg II-selected 21cm absorbers are marked with open diamonds and the other known 21cm absorbers are marked by open triangles. Left pointing arrows indicate upper limits to the measured values of $W_o^{\lambda 2852}$, while systems with no spectra at appropriate wavelengths are excluded. There is no correlation between these two quantities, and the 21cm absorbers do not occupy a special portion of the plot.

the Mg II doublet ratio $W_o^{\lambda 2796} / W_o^{\lambda 2803}$ are useful for better selection of systems likely to be 21cm absorbers.
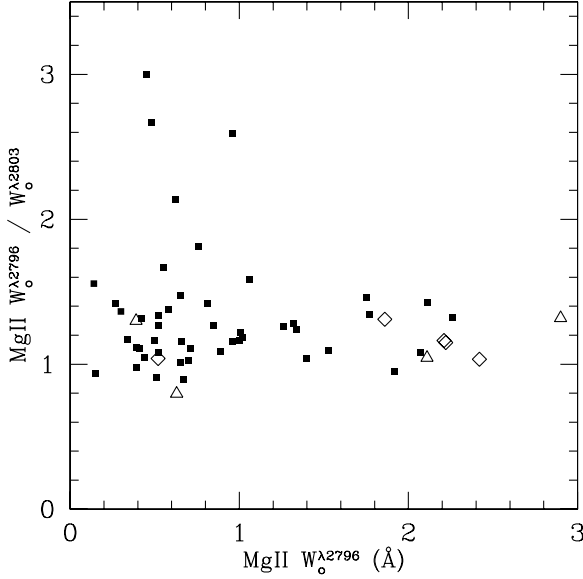
Figure 3.3: A plot showing the distribution of Mg II $W_o^{\lambda2796}$ vs. the doublet ratio of Mg II $W_o^{\lambda2796}$ / Mg II $W_o^{\lambda2803}$. The 21cm absorbers are indicated by open diamonds and 21cm absorbers which are not Mg II-selected are marked by open triangles. No special part of the parameter space is occupied by the 21cm absorbers, although most have doublet ratios ≈ 1.

3.3.4   Fe II $W_o^{\lambda2600}$ Considerations

The rest equivalent width of Fe II $\lambda2600$ Å is plotted against the rest equivalent width of Mg II $\lambda2796$ Å for the systems in the complete Mg II/21cm sample in Figure 3.4. It is immediately obvious that the strength of these two lines is well-correlated. Rao and Turnshek (2000) have identified a selection criteria of $W_o^{\lambda2796} > 0.5$ Å and $W_o^{\lambda2600} > 0.5$ Å above which roughly half of all the systems in their sample exhibit DLA absorption. In the case of 21cm absorption, roughly one-third of the Mg II-selected systems which satsify these criteria are also 21cm absorbers. This fraction increases sharply for systems with both $W_o^{\lambda2796}$ and $W_o^{\lambda2600} > 1.0$ Å. In other words, a 21cm survey of only the broadest equivalent width Mg II and Fe II systems would be considerably more efficient than one which had no equivalent width criteria, such as our WSRT survey.

In Figure 3.5 we plot the Mg II $W_o^{\lambda2796}$ versus the total velocity covered by H I 21cm absorbing components taken from Table 3.2. The Mg II equivalent widths are taken from Table 3.3, with the additions of 3C196: Mg II $W_o^{\lambda2796} = 2.11$ (Aldcroft et al. 1994), and 3C286: Mg II $W_o^{\lambda2796} = 0.39$ (Cohen et al. 1994). Despite the small number (nine) of 21cm absorbers, there is a clear tendency for lower $W_o^{\lambda2796}$ systems to have smaller H I velocity width. If we investigate the H I spectra in more detail, we find that the small $W_o^{\lambda2796}$ systems have one H I absorption component with a FWHM velocity of $\delta v \leq 10$ km s^{-1}. With the exception of 0827+243, for which Kanekar and Chengalur (2000) find one very broad, shallow HI absorption feature, all of the large
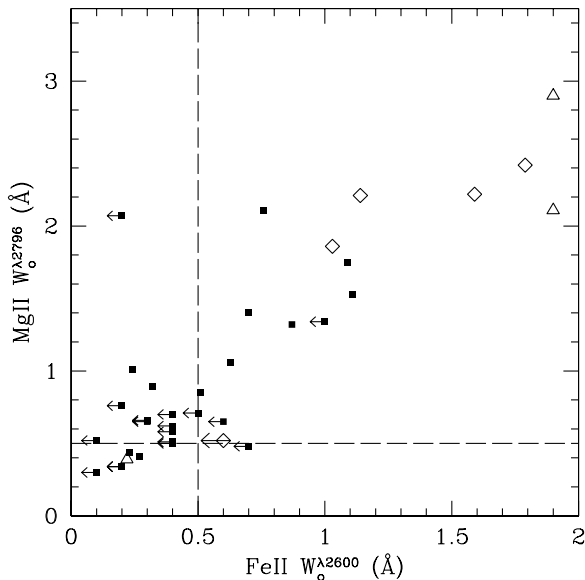
Figure 3.4: This plot shows the correlation between Mg II $W_o^{\lambda2796}$ and Fe II $W_o^{\lambda2600}$ for the Mg II/21cm sample. The 21cm absorbers are marked with open diamonds. Open triangles indicate 21cm absorbers not selected by Mg II absorption. Left pointing arrows indicate upper limits to the measured value of $W_o^{\lambda2600}$. These two ions are well-correlated. Dotted lines mark the 0.5 Å cutoffs above which Rao and Turnshek (2000) find that roughly half of the metal-line systems are also DLA systems. The 21cm absorbers fall into two loose groups; the narrow line systems with $W_o^{\lambda2796} \sim$ 0.5, and the multi-component systems with $W_o^{\lambda2796} \sim 2$.

$W_o^{\lambda2796}$ systems have two or more H I absorption components, spread over a substantial velocity interval.

We conclude that selecting for extremely wide metal-line equivalent widths will most likely select for multi-component absorption systems. This is evident in both high-resolution optical spectra, where broad metal lines are often seen to break up into many components (eg. Lanzetta and Bowen, 1992), and in the HI 21cm absorption spectra. Narrow and single component systems such as the absorber towards B0738+313 or 3C286 would not be discovered using the Mg II $W_o^{\lambda2796} > 0.5$ Å and Fe II $W_o^{\lambda2600} > 0.5$ Å selection criteria, and any derived properties of H I 21cm or DLA absorbers as a class would be necessarily biased against very face-on or single-cloud systems. It is important to continue to search for an effective way to find the narrow-line absorbers as well as the broad-line absorbers.

3.4 Statistics

3.4.1 Detection Probabilities

Following Steidel & Sargent (1992), and in order to make use of their statistics on Mg II absorbers, we divide our sample into several statistical subsamples based on
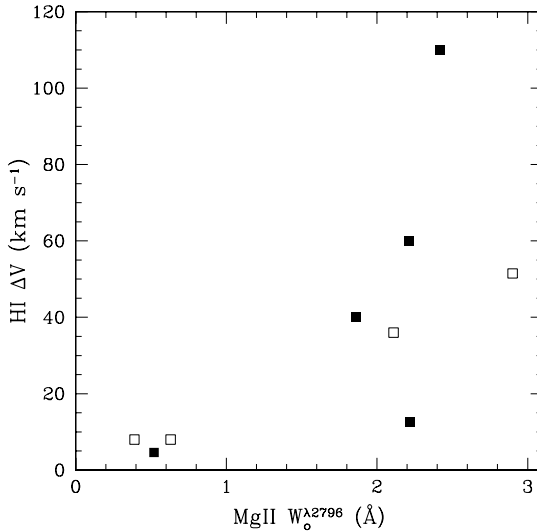
Figure 3.5: Mg II $W_o^{\lambda 2796}$ versus the total velocity spread of the H I 21cm absorption components. Solid squares are the Mg II-selected systems, and open squares are the other absorbers. Single component systems are plotted at their H I FWHM velocities. Multicomponent systems are plotted at the total velocity width spanned by all of the H I components.

Mg II $W_o^{\lambda 2796}$. The first includes the 52^1 absorbers with $W_o^{\lambda 2796} > 0.3$ Å, a second contains the 34 absorbers with $W_o^{\lambda 2796} > 0.6$ Å, and the third sample is composed of the 20 systems for which $W_o^{\lambda 2796} > 1.0$ Å.

The probability of finding a 21cm absorber in any of these samples increases with increasing $W_o^{\lambda 2796}$. The probability of finding a 21cm absorber in the complete Mg II-sample, with no $W_o^{\lambda 2796}$ threshold, is $5/72 = 7\%$. When the threshold requirement $W_o^{\lambda 2796} > 0.3$ Å is introduced this probability increases to $5/52 = 9.6\%$. Similarly, the probability is $4/34 = 11.8\%$ for $W_o^{\lambda 2796} > 0.6$ Å, and $4/20 = 20\%$ if the threshold is increased to $W_o^{\lambda 2796} > 1.0$ Å. Thus a survey which included a selection on $W_o^{\lambda 2796}$ would be more efficient than the WSRT-survey presented in Chapter 2.

Using these same three $W_o^{\lambda 2796}$ thresholds to define statistical samples, Rao and Turnshek (2000) find much higher detection probabilities for DLA absorption in Mg II systems. In their survey they find $11/44 = 25.0\%$ of systems with $W_o^{\lambda 2796} > 0.6$ Å are DLA absorbers. This is slightly more than twice the detection rate which we find for H I 21cm absorbers. There are several factors which contribute to this difference. In the first place, a fraction of our 0.6Å sample includes extended radio quasars, for which the H I absorption sightline differs from the optical Mg II and DLA absorption sight line. However, we are now convinced that a more important effect is the low sensitivity of 21cm spectra to warm H I gas due to the fact that $\tau_{21} \propto T_s^{-1}$. We discuss this topic in more detail in Chapter 5.

The Mg II/21cm survey is not completely insensitive to small column densities of gas. A quick glance through the numbers in the final column of Table 3.1 shows that *cold* gas with $T_s \approx 100$ K, which was unbroadened by bulk kinematical motions and fell into only one 19.5 kHz wide spectral channel, could be detected by most of the

---

[1]The 1331+170 sight-line has been excluded from the statistical samples because its two Mg II-systems are separated by < 350 km s^{-1} in redshift.

spectra in our survey down to column densities of a few $\times 10^{19}$ cm^{-2}. This is well below the canonical column density threshold for DLA systems which is $N_{HI} = 2 \times 10^{20}$ cm^{-2}. However, it is rare that gas clouds are not kinematically broadened beyond a few km s^{-1} in width, and even rarer for such a cloud to be perfectly centered in one channel of the spectrum. It is also uncommon to encounter cold gas without surrounding warm gas, while the reverse - a lot of warm gas with only a little cold gas - is more probable (Kulkarni and Heiles 1988). Therefore, in practice, the 21cm absorbers are found to be a high column density subset of the DLA absorbers.

3.4.2 $\quad$ $\mathbf{n}_{21cm}(z)$

The redshift evolution of the number density of Mg II systems, $n(z, W_o^{\lambda2796})$, can be parameterized as:

$$n(z, W_o^{\lambda2796}) = n_o(W_o^{\lambda2796})(1 + z)^{\gamma(W_o^{\lambda2796})} \tag{3.6}$$

Steidel and Sargent (1992) used their Mg II samples to find values for $n(z, W_o^{\lambda2796})$ and $\gamma(W_o^{\lambda2796})$ which they report in Table 4 of their paper. From these it is possible to estimate values for $n_o(W_o^{\lambda2796})$, which allow the equation to be generalized to other values of z.

Starting from the numbers for Mg II, $n_{21cm}(z)$ can then be determined from the fraction of Mg II systems which are H I 21cm absorbers:

$$n_{21cm}(z) = \left(\frac{\#\ of\ \text{H\,I}\ 21cm\ absorbers\ found}{\#\ of\ \text{Mg\,II}\ absorbers\ searched} \right) \times n_{\text{Mg\,II}}(z, W_o^{\lambda2796})$$

where the error in the $\#\ of$ H I $absorbers\ found$ can be estimated from small-number Poisson statistics (Gehrels 1986).

For our $W_o^{\lambda2796} > 0.3$ Å statistical subsample, $< z >= 0.589$, and:

$$n_{21cm}(z = 0.589) = \left(\frac{5^{+3.38}_{-2.16}}{52} \right) (0.54 \pm 0.18)(1 + 0.589)^{0.78 \pm 0.42},$$

$$n_{21cm}(z = 0.589) = 0.075^{+0.058}_{-0.043}$$

while for $W_o^{\lambda2796} > 0.6$ Å, $< z >= 0.603$ and:

$$n_{21cm}(z = 0.603) = \left(\frac{4^{+3.16}_{-1.91}}{34} \right) (0.24 \pm 0.10)(1 + 0.603)^{1.02 \pm 0.53},$$

$$n_{21cm}(z = 0.603) = 0.046^{+0.043}_{-0.031}$$

and finally for $W_o^{\lambda2796} > 1.0$ Å, $< z >= 0.657$ and:

$$n_{21cm}(z = 0.657) = \left(\frac{4^{+3.16}_{-1.91}}{20} \right) (0.041 \pm 0.027)(1 + 0.657)^{2.24 \pm 0.76}$$

$$n_{21cm}(z = 0.0657) = 0.026^{+0.029}_{-0.024}$$

Due to the large errors on these numbers that they should be considered, at best, rough estimates. Most of the 21cm absorbers are part of the $W_o^{\lambda 2796} > 1.0$ Å sample, and so the final estimate is perhaps the most valid. Unfortunately, this sample has the largest errors both on our measurement of the fraction of HI absorbers and on the parameters taken from the Mg II survey (Steidel and Sargent 1992), leading to greater than 100% errors on the value for $n_{21cm}(z)$.

3.4.3 $\Omega_{21cm}(z)$

The cosmological mass density of neutral gas in 21cm systems, $\Omega_{21cm}(z)$, can be derived using $n_{21cm}(z)$. In addition we will need to know the mean column density of the 21cm systems, $< N_{\mathrm{HI}}(z) >$. Because determinations of N_{HI} from H I 21cm absorption profiles depends upon the spin temperature of the gas, which we generally do not know, we will use instead the N_{HI} measured from fits to the DLA line in each system, as listed in Table 3.2. This applies to all of our systems except B 0248+430, for which we have estimated N_{HI} using a mean spin temperature of $< T_s > = 700$ K and the 21cm absorption parameters. Only the Mg II-selected 21cm absorbers are included in calculating $< N_{\mathrm{HI}}(z) >$. With values for $n_{21cm}(z)$ and $< N_{\mathrm{HI}}(z) >$ in hand, we can calculate:

$$\Omega_{21cm}(z) = \frac{\mu 8\pi G m_H}{3cH_o} \frac{n_{21cm}(z) < N_{\mathrm{HI}}(z) >}{(1+z)} \tag{3.7}$$

for $q_o = 0$, and

$$\Omega_{21cm}(z) = \frac{\mu 8\pi G m_H}{3cH_o} \frac{n_{21cm}(z) < N_{\mathrm{HI}}(z) >}{(1+z)^{1/2}} \tag{3.8}$$

for $q_o = 0.5$. The constant $\mu = 1.3$ corrects for a neutral gas composition which is 25% He and 75% H by mass. G is the gravitational constant and m_H is the mass of the hydrogen atom. We use a Hubble constant, $H_o = 75$ km s^{-1} Mpc^{-1}. Because the majority of the 21cm absorbers fall into the $W_o^{\lambda 2796} > 1.0$ Å category, we would ideally like to use these numbers in our calculations. However this introduces extremely large ($> 100\%$) errors into the result, so we also calculate the $W_o^{\lambda 2796} > 0.6$ Å value for comparison. Both the 1.0Å and the 0.6Å subsamples include the same set of four H I 21cm absorbers, and have $< N_{\mathrm{HI}}(z) > = 3.1 \pm 0.4 \times 10^{21}$ cm^{-2}.

For $W_o^{\lambda 2796} > 0.6$ Å,

$$\Omega_{21cm}(z = 0.603) = \left(0.0015^{+0.0014}_{-0.0010}\right), \quad q_o = 0$$

$$\Omega_{21cm}(z = 0.603) = \left(0.0019^{+0.0018}_{-0.0013}\right), \quad q_o = 0.5.$$

Similarly

$$\Omega_{21cm}(z = 0.657) = \left(0.00080^{+0.00090}_{-0.00075}\right), \quad q_o = 0$$

$$\Omega_{21cm}(z=0.657) = \left(0.0010^{+0.0011}_{-0.0009}\right), \quad q_o = 0.5.$$

for the $W_o^{\lambda 2796} > 1.0$ Å sample.

The only other values for $\Omega_{21cm}(z)$ have been measured at $z = 0$ (eg. Rao and Briggs, 1993, Zwaan et al. 1997). There are, however, values for $\Omega_{DLA}(z)$ in the literature, at redshifts roughly $0.1 < z < 4.7$. We use the $z = 0$ value and the DLA values to study the redshift evolution of $\Omega_{HI}(z)$. In Figure 3.6, we plot $\log \Omega_{HI}(z)$ against redshift. The open diamonds, triangles, and dotted circles show DLA results taken from the literature (Storrie-Lombardi and Wolfe 2000, Wolfe et al. 1995, Rao and Turnshek 2000), while the asterisk and circle at $z = 0$ represent values for Ω_{stars} and Ω_{21cm} respectively (Zwaan et al. 1997, Fukugita et al. 1998). The 21cm results from this survey are marked with a solid square ($W_o^{\lambda 2796} > 0.6$ Å) and a solid triangle ($W_o^{\lambda 2796} > 1.0$ Å) respectively. In the top panel we have used $q_o = 0$ and in the bottom panel $q_o = 0.5$. We have scaled all the numbers to $H_o = 75$ km s^{-1} Mpc^{-1}.

The 21cm result is in close agreement with the other low redshift points, both taken from the Rao and Turnshek (2000) DLA survey. The agreement is particularly strong for the $W_o^{\lambda 2796} > 0.6$ Å result. This is not entirely surprising given that the DLA value was derived from an Mg II-selected sample with $W_o^{\lambda 2796} > 0.6$ Å, using the same steps that we have used to go from Mg II statistics to H I statistics. However, our $W_o^{\lambda 2796} > 1.0$ Å result is also consistent with the DLA values, despite the huge error bars.

Previous values for $\Omega_{HI}(z)$ at redshifts $z < 1.5$ were much smaller, (eg. Wolfe et al. 1995), and it was thought that $\Omega_{gas}(z)$ peaked around a redshift $z \approx 3$ and then decreased smoothly to the $z = 0$ value as gas was converted into stars. This worked particularly nicely because the peak $\Omega_{gas}(z)$ was roughly equal to $\Omega_{stars}(z = 0)$. The Rao and Turnshek (2000) result first suggested that $\Omega_{gas}(z)$ is roughly flat until much smaller redshifts before decreasing to its present value. The new 21cm result supports this view.

3.5   Conclusions

Combining the WSRT-sample described in Chapter 1 with existing data from the literature (Peterson and Foltz 1980, Briggs and Wolfe 1983) we have created a complete Mg II/21cm sample of 72 absorbers. Of these, 5 are seen to be H I 21cm absorbers. We find that Mg I $\lambda 2852$ and the doublet ratio of Mg II $\lambda 2796, 2803$ do not seem to be related to the presence of H I 21cm absorption. However, a high percentage of systems with both large Fe II $W_o^{\lambda 2600}$ and large Mg II $W_o^{\lambda 2796}$ values are H I 21cm absorbers, and the combination of these criteria make a better selector than Mg II alone.

We also find a rough correlation between Mg II $W_o^{\lambda 2796}$ and the type of 21cm absorption seen. Small $W_o^{\lambda 2796}$ systems tend to be narrow single component H I 21cm absorbers, while large $W_o^{\lambda 2796}$ systems have many H I components spread over a wide velocity range. This suggests that selecting for large Mg II $W_o^{\lambda 2796}$ and Fe II $W_o^{\lambda 2600}$

may bias resulting surveys against face-on or non-rotating absorbers. It is important to continue searching for a better selector to find the narrow-line absorbers.

Finally we use Mg II statistics from Steidel and Sargent (1992) to estimate $n_{21cm}(z)$ and $\Omega_{21cm}(z)$. Comparing these numbers to existing $n(z)$ and $\Omega(z)$ values for DLA systems, we find that our results are in good agreement with those of Rao and Turnshek (2000).

References

Aldcroft, T. L., Bechtold, J., and Elvis, M. 1994, ApJS, 93, 1

Aldcroft, T. L., Elvis, M., and Bechtold, J. 1993, AJ, 105, 2054

Anderson, S. F., Weymann, R. J., Foltz, C. B., and Chaffee, F. H., J. 1987, AJ, 94, 278

Barthel, P. D., Tytler, D. R., and Thomson, B. 1990, A&AS, 82, 339

Bergeron, J. and Boissé, P. 1984, A&A, 133, 374

Bergeron, J. and Boissé, P. 1991, A&A, 243, 344

Bergeron, J. and Kunth, D. 1983, MNRAS, 205, 1053

Bergeron, J. and Kunth, D. 1984, MNRAS, 207, 263

Bergeron, J., Kunth, D., and D'Odorico, S. 1987, A&A, 180, 1

Boissé, P., Boulade, O., Kunth, D., Tytler, D., and Vigroux, L. 1992, A&A, 262, 401

Boissé, P., Le Brun, V., Bergeron, J., and Deharveng, J. M. 1998, A&A, 333, 841

Boksenberg, A., Carswell, R. F., and Sargent, W. L. W. 1979, ApJ, 227, 370

Briggs, F. H., Lane, W. M., and de Bruyn, A. G. 2000, in prep.

Briggs, F. H. and Wolfe, A. M. 1983, ApJ, 268, 76

Briggs, F. H., Wolfe, A. M., Turnshek, D. A., and Schaeffer, J. 1985, ApJ, 293, 387

Brown, R. L. and Mitchell, K. J. 1983, ApJ, 264, 87

Burbidge, E. M., Smith, H. E., Weymann, R. J., and Williams, R. E. 1977, ApJ, 218, 1

Carswell, R. F., Coleman, G., Williams, R. E., and Strittmatter, P. A. 1976, A&A, 53, 275

Chen, J. S., Morton, D. C., Peterson, B. A., Wright, A. E., and Jauncey, D. L. 1981, MNRAS, 196, 715

Cohen, R. D., Barlow, T. A., Beaver, E. A., Junkkarinen, V. T., Lyons, R. W., and Smith, H. E. 1994, ApJ, 421, 453

Cohen, R. D., Burbidge, E. M., Junkkarinen, V. T., Lyons, R. W., and Madejski, G. 1999, BAAS, 194, 7101

Davis, M. M. and May, L. S. 1978, ApJ, 219, 1

Foltz, C. B., Weymann, R. J., Peterson, B. M., Sun, L., Malkan, M. A., and Chaffee, F. H., J. 1986, ApJ, 307, 504

Fukugita, M., Hogan, C. J., and Peebles, P. J. E. 1998, ApJ, 503, 518

Gehrels, N. 1986, ApJ, 303, 336

Kanekar, N. and Chengalur, J. 2000, in prep.

Kulkarni, S. R. and Heiles, C. 1988, in *Galactic and Extragalactic Radio Astronomy*, ed. G. Verschuur and K. Kellerman, (New York: Springer-Verlag), 95

Kunth, D. and Bergeron, J. 1984, MNRAS, 210, 873

Lanzetta, K. M. and Bowen, D. V. 1992, ApJ, 391, 48

Miller, J. S., French, H. B., and Hawley, S. A. 1978, in *Pittsburgh Conference on BL Lac Objects, Pittsburgh, Pa., April 24-26, 1978, Proceedings. (A79-30026 11-90)*, ed. A. Wolfe, (Pittsburgh, PA: Univ. of Pittsburgh), 176

Peterson, B. M. and Foltz, C. B. 1980, ApJ, 242, 879

Peterson, B. M. and Strittmatter, P. A. 1978, ApJ, 226, 21

Peterson, B. M., Strittmatter, P. A., Williams, R. E., and Coleman, G. D. 1977, ApJ, 218, 605

Petitjean, P. and Bergeron, J. 1990, A&A, 231, 309

Rao, S. and Briggs, F. 1993, ApJ, 419, 515

Rao, S. and Turnshek, D. 2000, astro-ph/9909164

Roberts, D. H., Burbidge, G. R., Crowne, A. H., Junkkarinen, V. T., Burbidge, E. M., and Smith, H. E. 1978, ApJ, 224, 344

Sargent, W. L. W., Boksenberg, A., and Young, P. 1982, ApJ, 252, 54

Sargent, W. L. W., Steidel, C. C., and Boksenberg, A. 1988, ApJS, 68, 539

Sargent, W. L. W., Steidel, C. C., and Boksenberg, A. 1989, ApJS, 69, 703

Steidel, C. C., Dickinson, M., Meyer, D. M., Adelberger, K. L., and Sembach, K. R. 1997, ApJ, 480, 568

Steidel, C. C. and Sargent, W. L. W. 1992, ApJS, 80, 1

Stickel, M., Fried, J. W., and Kuehr, H. 1989, A&AS, 80, 103

Storrie-Lombardi, L. and Wolfe, A. 2000, astro-ph/00060444

Ulrich, M. H. and Owen, F. N. 1977, Nature, 269, 673

White, G. L., Jauncey, D. L., Wright, A. E., Batty, M. J., Savage, A., Peterson, B. A., and Gulkis, S. 1988, ApJ, 327, 561

Wills, B. J. 1978, in *Pittsburgh Conference on BL Lac Objects, Pittsburgh, Pa., April 24-26, 1978, Proceedings. (A79-30026 11-90)*, ed. A. Wolfe, (Pittsburgh, PA: Univ. of Pittsburgh), 235

Wolfe, A. M., Broderick, J. J., Johnston, K. J., and Condon, J. J. 1978, ApJ, 222, 752

Wolfe, A. M., Lanzetta, K. M., Foltz, C. B., and Chaffee, F. H. 1995, ApJ, 454, 698

Wolfe, A. M. and Wills, B. J. 1977, ApJ, 218, 39

Womble, D. S., Junkkarinen, V. T., Cohen, R. D., and Burbidge, E. M. 1990, AJ, 100, 1785

Wright, A. E., Peterson, B. A., Jauncey, D. L., and Condon, J. J. 1979, ApJ, 229, 73

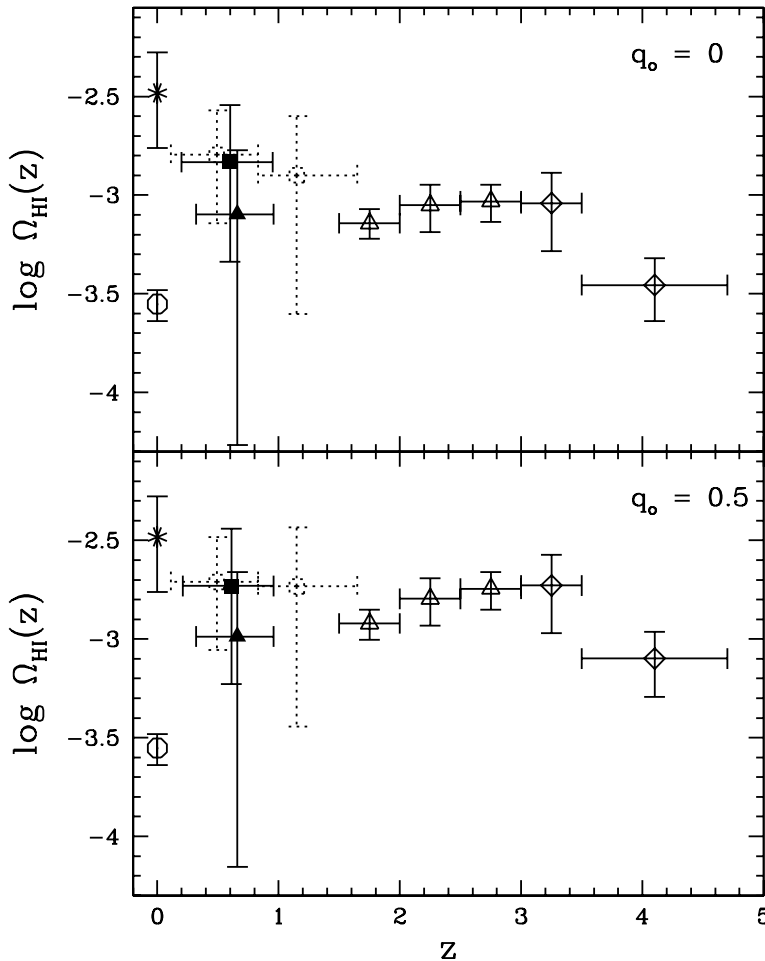Zwaan, M. A., Briggs, F. H., Sprayberry, D., and Sorar, E. 1997, ApJ, 490, 173

Figure 3.6: $\log \Omega_{\mathrm{H\,I}}(z)$ versus redshift. Vertical bars show 1σ errors, while the horizontal bars indicate bin size. The open diamonds are points from the DLA results of Storrie-Lombardi, et al. (2000), while the open triangles show DLA results from Wolfe et al. (1995). The dotted line open circles are taken from the Rao & Turnshek (2000) low redshift DLA survey, based on Mg II-selected systems with $W_o^{\lambda 2796} > 0.6$ Å. At $z = 0$ the open circle marks Ω_{21cm} measured by Zwaan et al. (1997), and the asterisk is Ω_{stars} as measured by Fukugita, Hogan, & Peebles (1998). The filled square is our 21cm result from the $W_o^{\lambda 2796} > 0.6$ Å sample, while the filled triangle marks the $W_o^{\lambda 2796} > 1.0$ Å result.

4

The new H I 21cm Absorbers

We present new H I 21cm spectra and summarize existing information for the three new absorbers found in our recent WSRT survey. The three systems are $z = 0.2212$ toward B 0738+313, $z = 0.313$ toward B 1127-145, and $z = 0.3941$ toward B 0248+430. We discuss the velocity and temperature information which can be derived from their 21cm absorption profiles. We conclude with a general discussion of temperature in redshifted DLA/21cm absorbers.

4.1   Introduction

Among the rarest of the QSO absorption lines, H I 21cm absorption features provide unique information about physical conditions in the systems in which they arise. The non-point-source nature of most radio QSOs on terrestrial baselines allows the spatial distribution of the various absorbing components to be mapped giving a direct look at the geometry of the gas in the host system. The opacity of the 21cm line is sensitive to the excitation or spin temperature, T_s, of the gas. This temperature is coupled to the kinetic temperature, T_k, of the gas under usual conditions in the interstellar medium (ISM) of the Milky Way (Dickey and Lockman 1990), so an H I 21cm absorption feature can be used to estimate the temperature of the absorbing gas. Finally the 21cm absorption features, because they are resolved in velocity space, provide kinematical information on the H I in the intervening absorber. In the optical, the Lyα lines for 21cm absorbers are heavily saturated and provide no details on the gas kinematics. Optical and UV observations of metal lines do provide kinematical information on the low ionization gas that is associated with the H I.

A harmonic mean spin temperature, $< T_s >$, of all of the H I clouds on a given sight line can be determined by a comparison of H I 21cm absorption and an inferred 21cm emission profile for the same sight line (eg. Dickey and Lockman, 1990), or by comparison of the 21cm absorption line parameters to a column density from the damped Lyα (DLA) absorption feature on the same sight line. However the values

of $< T_s >$ derived in the second manner for sight lines through redshifted DLA/H I 21cm absorbers are consistently higher than those found in clouds of similar optical depth in the Galaxy using the first method (eg. Carilli et al. 1996).

An upper limit to the thermal kinetic temperature, T_k in the 21cm absorbing gas can be estimated directly from the line-widths of the absorption profiles. However, only the most narrow velocity lines provide interesting constraints on the gas temperature.

In this chapter we present high velocity resolution radio spectra for three new low-redshift H I 21cm absorbers identified in the WSRT-survey described in Chapter 2. Two of these, B 0738+313 at $z_{abs} = 0.2212$ and B 1127-145 at $z_{abs} = 0.3127$ have been identified as DLA absorbers as well (Rao and Turnshek 2000), allowing us to derive $< T_s >$ values in addition to kinematical information from the data. The third object B 0248+430 at $z_{abs} = 0.394$ does not have a measured DLA absorption line, but we are able to put upper limits on T_k for the 21cm absorption components based on their velocity widths, and thus estimate a total N_{HI}.

4.2   Deriving the Temperature

The equation relating neutral hydrogen column density, N_{HI}, to the observed H I 21cm absorption profile is:

$$N_{HI} = 1.8 \times 10^{18} T_s \int \tau(v) \, dv \ \text{cm}^{-2} \tag{4.1}$$

where T_s is the spin temperature of the absorbing gas. $\tau(v)$ is the optical depth of the line at velocity v, calculated as:

$$\tau(v) = -\ln \left(1 - \frac{\Delta S(v)}{f \, S} \right) \tag{4.2}$$

where f is the fraction of the continuum source covered by the absorber, S is the continuum flux density, and $\Delta S(v)$ is the line depth at velocity v. For a single line with a Gaussian profile, the integral of the optical depth over velocity is

$$\int \tau(v) \, dv = 1.06 \, \tau_{21cm} \, \Delta v \tag{4.3}$$

where τ_{21cm} is the peak optical depth of the line at the line center and Δv is the full width at half maximum velocity in km s^{-1}. This quantity, which is proportional to the column density divided by the spin temperature, is usually labeled EW_{21} although it is only equal to a true equivalent width as measured for optical absorption features in the limit $\tau(v) << 1$ over the entire absorption profile.

If we assume that the same gas is responsible for the 21cm absorption and the DLA absorption, the value for N_{HI} measured from the DLA absorption combined with the EW_{21} can be used in Equation 4.1 to derive the spin temperature of the gas. When calculated in this way, individual cloud information is lost and the derived
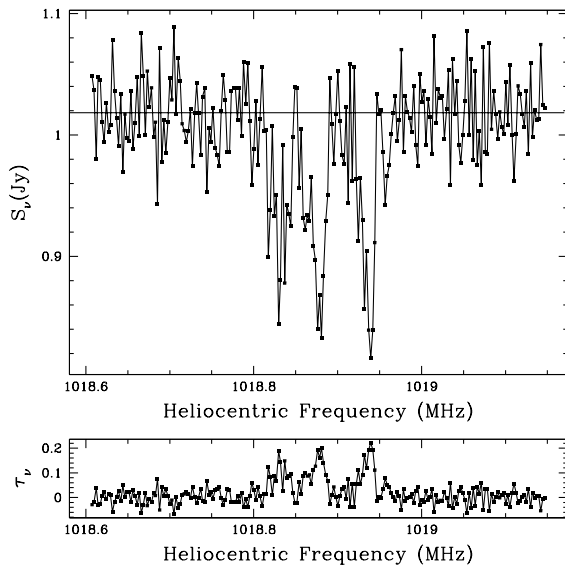
Figure 4.1: A WSRT/DZB high resolution spectrum of the $z = 0.3941$ H I 21cm absorber toward B 0248+430 at a channel spacing of 2.44 kHz, or a velocity resolution of 0.81 km s^{-1}. The lower panel shows the optical depth of the lines, which are all roughly 15 to 18%.

temperature, denoted $< T_s >$, is a column density weighted harmonic mean spin temperature of all the gas along the line of sight.

In some circumstances, thermal broadening of an absorption feature provides an independent constraint on the thermal kinetic temperature, T_k, of the gas:

$$T_k \leq \frac{1.2119 \times 10^2 \Delta v^2}{8 \ln 2} \text{ K} \tag{4.4}$$

where Δv is the FWHM velocity measured in km s^{-1}. Because bulk kinematical motions and turbulence in the absorbing H I gas will also broaden the absorption line, this is a less stringent constraint than the derived value of $< T_s >$ for many H I absorbers.

4.3   B 0248+430, $z_{abs} = 0.3941$

B 0248+430 is a core dominated quasar at an emission redshift $z_{em} = 1.31$. The metal line system at $z_{abs} = 0.394$ was originally identified in a spectrum taken to study absorption associated with a pair of merging galaxies at $z = 0.05$ (Womble et al. 1990). This initial detection of Mg II and Mg I was confirmed, and a detection of Fe II and Ca II absorption was reported by Sargent and Steidel (1990), who also suggested that a concentration of faint galaxies around the QSO could be a cluster at the absorption redshift. There is no detection of the damped Lyα line for this system. Although it was included in the survey of Rao and Turnshek (2000), the UV spectrum of B 0248+430 had an extremely low S/N ratio at the expected wavelength of the DLA absorption line due to the sharp FOS-G160L filter cutoff, and it was not possi-

ble to detect the line. For this reason, there is no reliable measure of the total neutral column density in this system.

Table 4.1: The Four Component Fit to the B 0248+430 21cm line Profile

Component	ΔV_{offset} (km s^{-1})	τ_{21}	FWHM Δv (km s^{-1})	EW_{21} (km s^{-1})	T_k (K)
4	-6.2 ± 0.6	0.07 ± 0.03	1.9 ± 0.4	0.14 ± 0.07	79
1	0	0.20 ± 0.03	4.3 ± 0.4	0.92 ± 0.16	405
2	17.8 ± 0.6	0.16 ± 0.03	6.2 ± 0.4	1.05 ± 0.21	840
3	31.0 ± 0.6	0.12 ± 0.03	6.9 ± 0.4	0.88 ± 0.23	1040

A 21cm spectrum was obtained on 19 September 1999 using the WSRT and the DZB correlator. The total integration time was just under 4 hours. A bandwidth of 0.625 MHz centered at 1018.94 MHz is divided into 256 channels to provide a channel width of 2.44 kHz. No on-line smoothing was applied giving a velocity resolution of 0.86 km s^{-1}. After editing to remove the shortest baselines, the twelve antennas provided 48 baselines in each of two linear (XX and YY) polarizations. Observations of 3C48 were used to calibrate the flux density scale and the passband using standard routines in AIPS. The data were self-calibrated to continuum maps. After removing the continuum emission with UVSUB and UVLIN, a map cube was made and the spectrum was extracted at the position of the QSO using ISPEC. We have offset the y-axis to the measured continuum flux density of the QSO in the spectrum presented in Figure 4.1.

The H I 21cm absorption feature is composed of a complex of lines, roughly clustered in three groups, which combined cover ~ 40 km s^{-1}. The 3σ RMS noise in the spectrum is quite high, equivalent to an optical depth of $\tau_{3\sigma} = 0.09$. The best simultaneous 4-Gaussian fit to the data is shown in Figure 4.2. The fitted line parameters are listed in Table 4.1. We have placed the system velocity, $\Delta V = 0$, at a frequency of 1018.94 MHz, corresponding to both the center of the deepest absorption component and the metal-line redshift of $z_{abs} = 0.394$. Conservative errors for τ are estimated from the RMS of the residuals. The errors on Δv are assumed to be one-half of a resolution element.

The 21cm line integral, $EW_{21} = 2.99 \pm 0.36$ km s^{-1}, leads to an estimated column density of $N_{HI} = 5.4 \pm 0.6 \times 10^{18} \times T_s$ atoms cm^{-2} K^{-1}. Even if the spin temperature of each component is as low as $T_s \sim 100$ K, this system would have a combined $N_{HI} \approx 5 \times 10^{20}$ cm^{-2}, well above the canonical lower limit in DLA systems. Using Eq. 4.4, we calculate upper limits to T_k for each component. These are listed in column 6 of Table 4.1. Setting $T_s \approx T_k$, we find a column density $N_{HI} \leq 3.9 \times 10^{21}$ cm^{-2} is contained in the detected profile. This estimate could be missing a significant column density of warm-phase H I which would create a broad shallow absorption component not detected at the sensitivity levels of this spectrum (Lane et al. 2000).
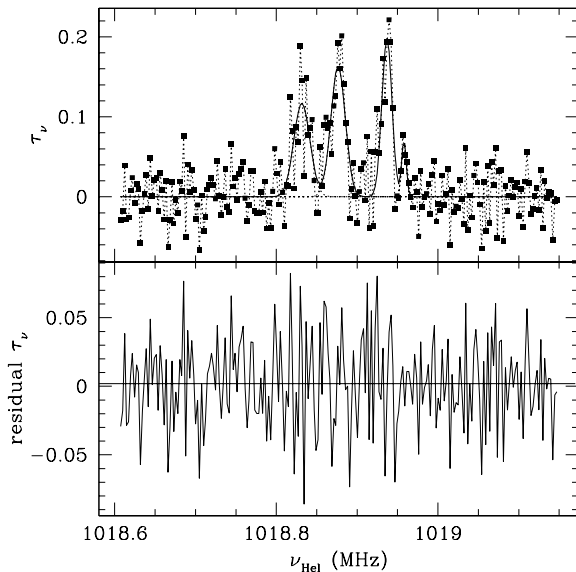
Figure 4.2: The 4 component fit to the WSRT/DZB spectrum of B 0248+430 is shown. In the upper panel, the points are the data connected by the dotted line, and the heavy solid line is the combined fit. In the bottom panel, the residuals are shown.

4.4   B 0738+313, $z_{abs} = 0.2212$

OI 363 (0738+313) is a core dominated quasar at $z_{em} = 0.630$. Observations at 1640 MHz (Murphy et al. 1993) show that the faint lobes extending $\approx 30''$ from the core emit only 3% of the total L-Band flux of the quasar, and deep observations with the WSRT confirm this at 1300 MHz (Lane et al. 2000). At 408 MHz, monitoring the quasar over a 9 year period reveals a 7% variability, corresponding to ~ 110 mJy about an average continuum strength of 1.59 Jy (Bondi et al. 1996a).

The $z_{abs} = 0.22$ metal line absorption system was originally reported by Boulade, et al. (1987) at a redshift of $z = 0.2213$, and subsequently by Boissé, et al. (1992) at a redshift of $z = 0.2216 \pm 0.0003$. The only identified lines in the spectrum are the Mg II $\lambda\lambda 2796, 2803$ doublet and a possible Mg I line. There is an additional DLA/21cm absorber on this sight line at $z = 0.0912$ which we will discuss in Chapter 5. There is no evidence for gravitational lensing on this sight line (Rao and Turnshek 1998). Gas from the $z = 0.22$ system is thought to lie in the outskirts of an elliptically shaped galaxy at a separation of about 20 h_{65}^{-1} kpc from the QSO sight line (Chapter 6, this thesis).

We used the WSRT to make a 12-hour integration for this source on 27 December 1997. A 1.25 MHz bandwidth centered at a Heliocentric frequency of 1163.15 MHz and divided into 256 channels gave a channel width of 4.88 kHz, corresponding to an unsmoothed resolution of 1.51 km s^{-1}. Thirteen antennae and the DXB correlator provided 36 baselines in each of two polarizations (XX and YY). Observations of the calibrator source 3C147 were used for flux and passband calibration. The data were reduced using standard routines in the NEWSTAR data reduction package developed for use with WSRT data. The final spectrum is shown in Figure 4.3. The
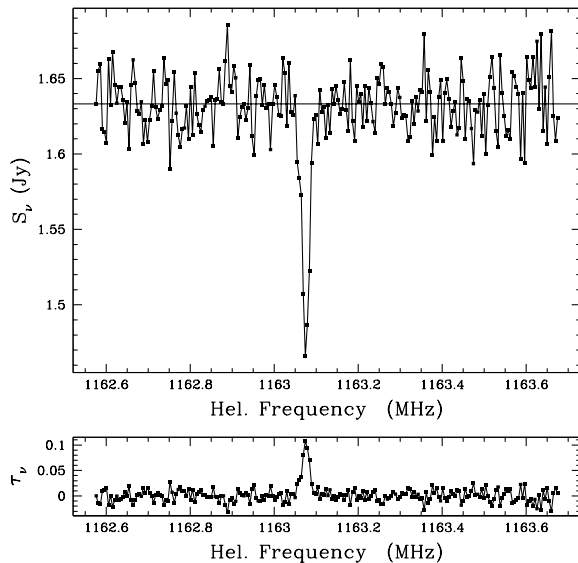
Figure 4.3: A WSRT/DXB spectrum of the $z = 0.2212$ 21cm absorber toward B 0738+313. The channel spacing is 4.9 kHz, corresponding to a velocity resolution of 1.52 km s^{-1}. The lower panel shows the optical depth of the line, which is $\tau \approx 0.10$.

small spikes near 1162.9 MHz and 1163.35 MHz are both caused by radio frequency interference (rfi) which appears in both the calibrator and the object datasets. The 3σ noise in the spectrum corresponds to an optical depth of $\tau_{3\sigma} = 0.034$.

The single H I 21cm absorption line can be well-fit by a Gaussian with an optical depth of $\tau_c = .104 \pm 0.008$, and a full width at half maximum (FWHM) velocity of $\Delta v = 5.4 \pm 0.5$ km s^{-1}. It has a slight asymmetry on the low frequency side. This may be due to a blend with a second weak line, but it is also consistent with random noise in the spectrum. Using the line width and depth, and assuming that the gas only covers the quasar core, and not the weak extended lobes (i.e. the covering factor $f \leq 0.98$), we can derive a $< T_{\rm s} >$ value by comparison with the value for neutral column density, $N_{\rm HI} = 7.9 \pm 1.4 \times 10^{20}$ cm^{-2}, from the DLA line. The resulting value, $< T_{\rm s} > = 735 \pm 155$ K, is typical of $z > 0$ systems. If we convert the 21cm line width directly into a thermal kinetic temperature using Eq. 4.4, we find $T_{\rm k} = 635 \pm 120$ K. Because the profile may also be broadened by bulk motions, the line width indicates an upper limit to the spin temperature, $T_{\rm s} < T_{\rm k}$, for the gas detected in the 21cm absorption feature.

4.5   B 1127$-$145, $z_{abs} = 0.3127$

PKS B 1127-145 is a compact, gigahertz peaked radio source at $z_{em} = 1.187$. VLBI observations at 1670 MHz show a slightly elongated core-jet structure with an extent of approximately 20 mas, which exhibits structural variations between observations taken 7 years apart (Bondi et al. 1996b). A 15 year monitoring program at 408 MHz finds a flux variability of 30% or roughly 1.7 Jy around an average continuum strength of 5.5 Jy (Bondi et al. 1996a). Observations at 1080 MHz (the frequency of
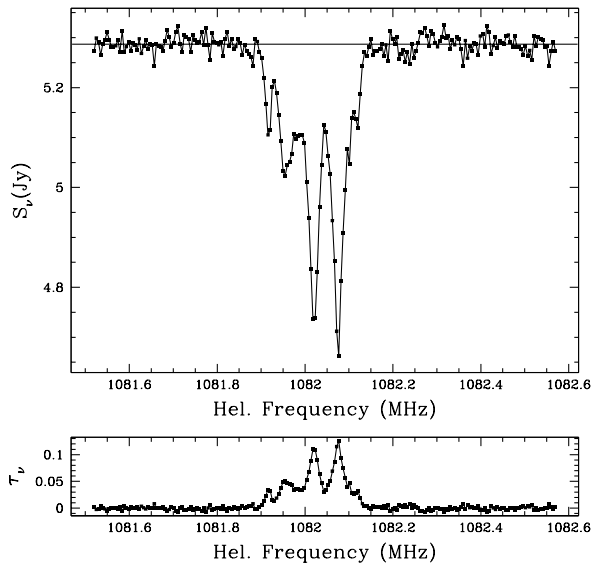
Figure 4.4: A WSRT/DZB spectrum showing the complex 21cm absorption at $z = 0.3127$ toward the quasar B 1127−145. The channel spacing is 4.9 kHz, giving a velocity resolution of 1.6 km s^{-1}. The absorption complex covers roughly 60 km s^{-1} in total. The lower panel shows the optical depth across the profile.

the 21cm absorption) have found a continuum strength which varies between 5 and 6 Jy, but can reach extremes of 4 to 8 Jy (Kanekar and Chengalur 2000a). Bergeron and Boissé (1991) originally identified the metal-line system based on Mg II, Fe II and Mg I absorption in the QSO spectrum. The average redshift of the metal lines is $z = 0.3127 \pm 0.0002$.

A 6 hour observation of the 21cm line in this system was obtained on 25 October 1998 with the WSRT and the new DZB correlator, which was in its commissioning phase. The 1.25 MHz bandwidth was centered at 1082.11 MHz and divided into 256 channels to provide channel widths of 4.88 kHz. No on-line smoothing was applied. The final spectral resolution is 1.6 km s^{-1}. Because the DZB correlator was not fully implemented, we were unable to observe the complete set of 91 baselines + 14 autocorrelations in two polarizations that this system can provide. A subset of 64 baselines in each of the two linear polarizations (XX,YY) were recorded. Data calibration and reduction was performed in AIPS. The calibrator sources 3C147 and 3C286 were used to calibrate the flux density and passband. The data were self-calibrated to a continuum image of the field. The continuum emission was then subtracted using UVSUB and UVLIN, and ISPEC was used to extract the spectrum from a map cube.

The spectrum is displayed in Figure 4.4, and we have scaled the y-axis to show the measured continuum of the unresolved QSO. The 3σ RMS noise in the spectrum corresponds to an optical depth of $\tau_{3\sigma} = 0.0096$. The H I 21cm absorption profile is very complex and extends over about 60 km s^{-1}, reaching optical depths of up to $\tau \approx 0.11$. Unusually for a 21cm absorption feature, the deepest component is on the low velocity (high frequency) edge of the profile. this 'edge-leading' shape is more typically found in metal-lines, and can be explained if the line of sight passes through
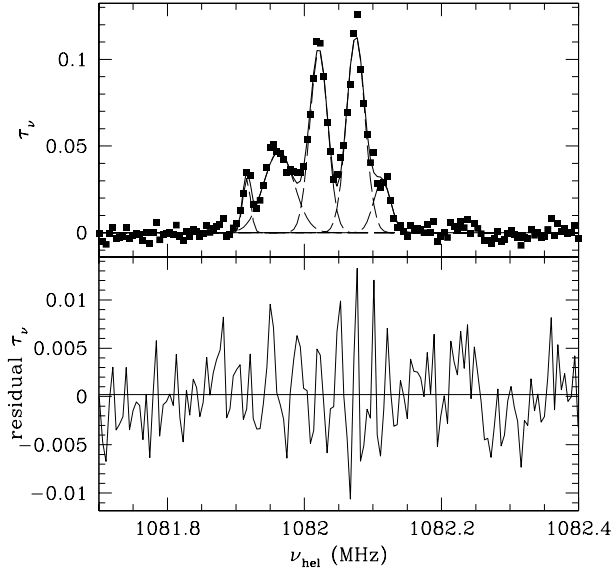
Figure 4.5: The 5 component fit to the WSRT/DZB spectrum for 1127-145. In the upper panel, the points are the data, the dashed lines are individual components and the heavy solid line is the combined fit. In the bottom panel, the residuals are shown.

a thick rotating gas disk (Prochaska and Wolfe 1998). Using the Giant Meterwave Radio Telescope (GMRT), Kanekar and Chengalur (2000a) have observed the 21cm line depths to vary in this source, in a manner that is uncorrelated with the quasar flux variability. However, they find no evidence for change in the velocity centroids and widths of the lines.

Table 4.2: Five Component Fit to the 1127-145 21cm line Profile

Component	ΔV_{offset} (km s^{-1})	τ_{21}	FWHM Δv (km s^{-1})	EW_{21} (km s^{-1})
1	-25.6 ± 0.6	0.030 ± 0.004	8.1 ± 0.4	0.26 ± 0.05
2	-15.0 ± 0.6	0.113 ± 0.005	8.7 ± 0.4	1.04 ± 0.06
3	0	0.105 ± 0.004	8.5 ± 0.4	0.95 ± 0.06
4	16.1 ± 1.7	0.048 ± 0.004	14.6 ± 1.6	0.74 ± 0.19
5	29.2 ± 0.6	0.031 ± 0.004	3.7 ± 0.4	0.12 ± 0.02

An iterative fitting routine was used to decompose the observed H I 21cm absorption profile into individual components. The best fit was obtained using 5 Gaussian components which are summarized in Table 4.2 and shown in Figure 4.5.

We have placed the velocity center ($\Delta V = 0$) at 1082.02 MHz, which is the center of Component 2 as well as the z_{abs} of the metal-lines. Conservative errors in τ_{21} are taken from the RMS noise in the residual to the fit, while errors in Δv are estimated to be one-half of a resolution element, with the exception of Component 4 for which

we quote larger errors because the uncertainty in the velocity offset of the profile center was quite high. The integrated line depth $EW_{21} = 3.11 \pm 0.21$ km s^{-1}. The H I column density from the DLA profile is $N_{HI} = 5.1 \pm 0.9 \times 10^{21}$ cm^{-2}, and we calculate that $< T_s > = 910 \pm 170$ K. A velocity width of $\Delta v = 8$ km s^{-1} corresponds to a $T_k = 1400$ K. Four of the five fitted components have $\Delta v \geq 8$ km s^{-1}, and thus we cannot use the velocity widths of the individual components to provide better temperature constraints for this system.

4.6   Spin Temperature in Redshifted Systems

Table 4.3: Summary of DLA/21cm Absorbers

Object	z_{em}	z_{abs}	$N_{HI\,DLA}$ 10^{20} cm^{-2}	EW_{21} km s^{-1}	$< T_s >$ K	ref
0201+113	3.61	3.388	25 ± 12 [a]	0.90 ± 0.27	1530 ± 865	8,9
0235+164	0.940	0.5238	50 ± 25 [a]	13 ± 0.6	215 ± 110	2,11
0458-020	2.286	2.038	50 ± 25 [a]	7.29 ± 0.17	380 ± 190	7,6
0738+313	0.631	0.0912	15 ± 2	1.12 ± 0.02	725 ± 100	14,13
		0.2213	7.9 ± 1.4	0.58 ± 0.07	735 ± 155	14,16
0827+243	0.939	0.5248	2 ± 0.2	0.34 ± 0.08	330 ± 70	14,12
0952+179	1.472	0.2377	21 ± 2.5	0.57 ± 0.07	2050 ± 345	14,12
1127$-$145	1.187	0.3127	51 ± 9	3.11 ± 0.05	910 ± 170	14,16
1157+014	1.986	1.944	63 ± 10	2.19 ± 0.21	1595 ± 400	4
1229$-$021	1.038	0.3950	5.6 ± 0.9	3.0 ± 0.8	105 ± 30	10,15
1328+307	0.849	0.692	18 ± 1	0.91 ± 0.09	1100 ± 125	1,10
1331+170	2.081	1.776	15 ± 7 [a]	0.43 ± 0.11	1925 ± 1025	3,5

[a]Numbers with no published uncertainties were arbitrarily assigned 50% errors.
References: (1) Davis and May 1978, (2) Wolfe et al. 1978, (3) Wolfe and Davis 1979
(4) Wolfe et al. 1981, (5) Chaffee et al. 1988, (6) Briggs et al. 1989
(7) Wolfe et al. 1993, (8) White et al. 1993, (9) Briggs et al. 1997
(10) Boisseé et al. 1998, (11) Cohen et al. 1999, (12) Kanekar and Chengalur 2000
(13) Lane et al. 2000, (14) Rao and Turnshek 2000, (15) Briggs et al. 2000,
(16) This Chapter.

Figure 4.6 shows $< T_s >$ vs. redshift and N_{HI}, and log(EW_{21}) vs. redshift and N_{HI} for known DLA/H I 21cm absorber systems, calculated from the literature and tabulated in Table 4.3. It is clear that these quantities are uncorrelated. We have deliberately excluded the absorber at $z_{abs} = 0.437$ toward 3C196, because it is known that the radio and optical sight lines in this system are not coincident (Brown and Mitchell 1983, Cohen et al. 1996), and any value for $< T_s >$ derived by comparing

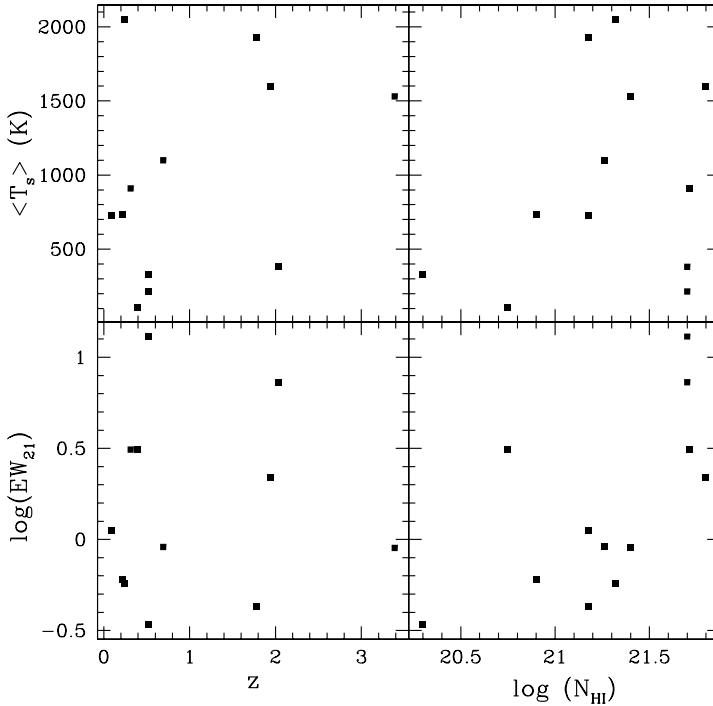Figure 4.6: A plot showing $< T_s >$ vs. redshift and column density in the upper two panels, and $\log(EW_{21})$ vs. redshift and column density in the bottom two panels. There is no significant correlation between any of these quantities.

them is thus meaningless.

Estimates of T_s for the present epoch are based on studies of the Milky Way and/or Andromeda galaxies (Dickey and Brinks 1988, Braun and Walterbos 1992), and find values in the range $70 < T_s < 600$, with a strong inverse correlation between optical depth and T_s. It was originally considered possible that the high $< T_s >$ values derived for redshifted DLA/21cm absorbers could be a result of redshift evolution in either the temperature of H I gas or the relative amounts of warm and cold-phase H I gas in gas-rich galaxies (Carilli et al. 1996). We now have $< T_s >$ values for absorbers spanning the redshift range $0.1 < z < 3.5$ and there is no discernible trend of this quantity with redshift. We consider redshift evolution an unlikely explanation for the high $< T_s >$ values.

In Figure 4.7 we show the dependence of N_{HI} and $< T_s >$ on the maximum optical depth τ of the 21cm absorption feature. τ and N_{HI} are uncorrelated, but τ and $< T_s >$ show a strong inverse-correlation despite the wide range of redshifts covered by the absorption systems. The solid and dotted lines in the bottom panel indicate
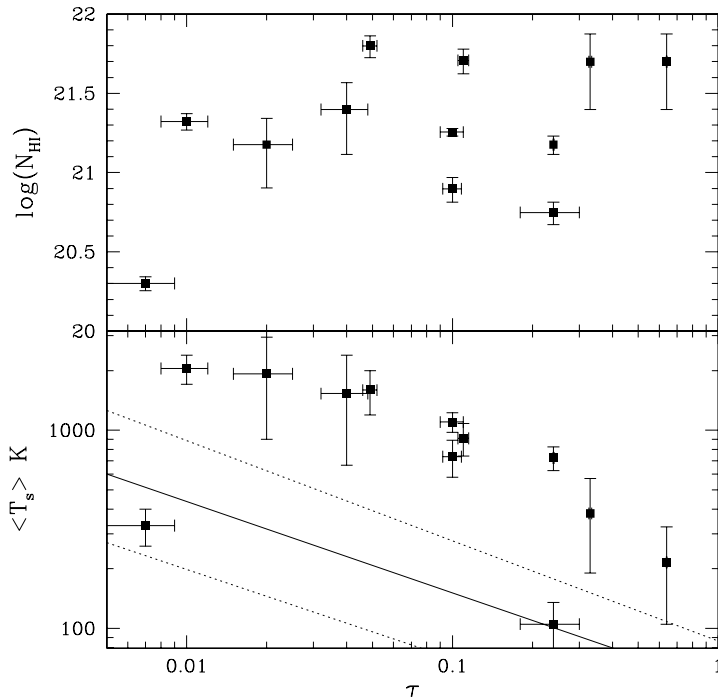
Figure 4.7: The upper panel shows $\log(N_{HI})$ vs. τ for the entire sample of DLA/21cm absorbers from Table 4.3. For multi-component systems, τ is measured at the deepest point in the profile. The lower panel shows $< T_s >$ vs. τ, where τ is defined in the same way. The solid line marks median values for the Galaxy and the dotted lines indicate scatter in the Galactic relation (Braun and Walterbos 1992). With the exception of 0827+243 and 1229-021, all of the redshifted absorbers fall above the Galactic values at a given τ.

the Galactic $\tau - < T_s >$ relationship and its scatter (Braun and Walterbos 1992). The two redshifted systems which fall among the Galactic values are 1229-021, which is not inconsistent with the other high-redshift systems, and 0827+243 which has an unusually low $< T_s >$ for the measured τ. The slope of the $\tau - < T_s >$ relationship appears to be somewhat steeper for the redshifted systems than for the Galactic data, but the uncertainties in the redshifted numbers are quite large.

DLA absorption lines are sensitive to both warm- and cold- phase gas, while H I 21cm absorption is most sensitive to cold gas. A comparison between the two lines would produce a high $< T_s >$ estimate if there is a substantial component of warm-phase gas on the sight line. In our own galaxy, warm-phase gas (WNM) has a much higher filling factor than the cold-phase gas (CNM), and also extends to larger vertical scale heights (Kulkarni and Heiles 1988). Observations of local dwarf galaxies (Young 1999, Young 2000) find a similar distribution of WNM and CNM H I gas. We

would expect, then, that it is uncommon to find cold-phase H I without warm-phase H I on any sight line through an absorber. Lane et al. (2000; also Chapter 5 of this thesis) identified a warm-phase gas absorption component in the 21cm spectrum of the $z = 0.0912$ absorber toward B 0738+313. This broad, low optical depth component represents gas with a column density of $N_{HI} \sim 1 \times 10^{21}$ cm^{-2} and observationally confirms the two-phase nature of H I gas in redshifted gas-rich systems.

The implication is that a substantial fraction of the total column density of H I gas sensed by the DLA absorption line can be easily missed in 21cm absorption spectra due to its low optical depth. Large amounts of warm-phase gas can explain two puzzling features of the high redshift absorbers. The DLA absorbers which are found to contain no 21cm absorption at a sensitive detection limit are likely sight lines which pass through warm-phase H I and no or very little cold-phase H I. Because $< T_s >$ is a *column density weighted* harmonic mean spin temperature, large column densities of warm-phase H I would lead to large derived $< T_s >$ values compared to Galactic T_s measurements.

The 21cm spectrum of B 0738+313 at $z_{abs} = 0.0912$ also contains two narrow velocity absorption features, one of which has a velocity dispersion of less than 1 km s^{-1} and an optical depth of only a few percent. Using the upper limit to T_k from the line width and setting $T_k = T_s$, the total column density in this feature is $N_{HI} \approx 1 \times 10^{19}$ cm^{-2}. This nicely illustrates the fact that an individual cloud does not require a large column density to be detected in H I 21cm absorption. However, the probability of a sight line intercepting an isolated, cold H I cloud at redshifts $z > 0$ is low, so in practice H I absorption is rarely detected in any but the highest neutral column density systems.

High $< T_s >$ values can also result from differences in the radio and optical sight lines. The sizes of the radio emission regions of quasars are much larger than the optical regions, and usually larger than an average cloud as well. It is therefore likely that the optical and radio lines of sight actually sense different clouds in a redshifted galaxy, and hence have different column densities of neutral gas. This implies that the spin temperatures derived by assuming DLA and 21cm column densities are equal may be meaningless. The absorber at $z = 0.437$ on the 3C196 sight line provides an extreme example of this problem; the QSO is lobe dominated at radio frequencies, and there is little radio continuum at the position of the optical sight line (Brown and Mitchell 1983, Cohen et al. 1996). Unfortunately, the resolution obtained in most radio survey observations (with single dishes or synthesized beams from arrays like the WSRT) is at least as large on the sky as compact background radio sources, and gives no spatial information about the clouds in front of the quasar. VLBI techniques are necessary to precisely pinpoint the radio continuum which corresponds to the optical sight line, as we will demonstrate in a study of the $z_{abs} = 0.0912$ H I 21cm absorber in Chapter 5.

References

Bergeron, J. and Boissé, P. 1991, A&A, 243, 344

Boissé, P., Boulade, O., Kunth, D., Tytler, D., and Vigroux, L. 1992, A&A, 262, 401

Boissé, P., Le Brun, V., Bergeron, J., and Deharveng, J. M. 1998, A&A, 333, 841

Bondi, M., Padrielli, L., Fanti, R., Ficarra, A., Gregorini, L., and Mantovani, F. 1996a, A&AS, 120, 89

Bondi, M., Padrielli, L., Fanti, R., Ficarra, A., Gregorini, L., Mantovani, F., Bartel, N., Romney, J. D., Nicolson, G. D., and Weiler, K. W. 1996b, A&A, 308, 415

Boulade, O., Kunth, D., Tytler, D., and Vigroux, L. 1987, in *High Redshift and Primeval Galaxies*, ed. J. Bergeron et al., (Paris: Edit. Frontieres), 349

Braun, R. and Walterbos, R. A. M. 1992, ApJ, 386, 120

Briggs, F. H., Brinks, E., and Wolfe, A. M. 1997, AJ, 113, 467

Briggs, F. H., Lane, W. M., and de Bruyn, A. G. 2000, in prep.

Briggs, F. H., Wolfe, A. M., Liszt, H. S., Davis, M. M., and Turner, K. L. 1989, ApJ, 341, 650

Brown, R. L. and Mitchell, K. J. 1983, ApJ, 264, 87

Carilli, C. L., Lane, W., de Bruyn, A. G., Braun, R., and Miley, G. K. 1996, AJ, 111, 1830

Chaffee, F. H., Black, J. H., and Foltz, C. B. 1988, ApJ, 335, 584

Cohen, R. D., Beaver, E. A., Diplas, A., Junkkarinen, V. T., Barlow, T. A., and Lyons, R. W. 1996, ApJ, 456, 132

Cohen, R. D., Burbidge, E. M., Junkkarinen, V. T., Lyons, R. W., and Madejski, G. 1999, BAAS, 194, 7101

Davis, M. M. and May, L. S. 1978, ApJ, 219, 1

Dickey, J. M. and Brinks, E. 1988, MNRAS, 233, 781

Dickey, J. M. and Lockman, F. J. 1990, ARA&A, 28, 215

Kanekar, N. and Chengalur, J. 2000a, in prep.

Kanekar, N. and Chengalur, J. 2000b, in prep.

Kulkarni, S. R. and Heiles, C. 1988, in *Galactic and Extragalactic Radio Astronomy*, ed. G. Verschuur and K. Kellerman, (New York: Springer-Verlag), 95

Lane, W., Briggs, F., and Smette, A. 2000, ApJ, 532, 146

Murphy, D. W., Browne, I. W. A., and Perley, R. A. 1993, MNRAS, 264, 298

Prochaska, J. X. and Wolfe, A. M. 1998, ApJ, 507, 113

Rao, S. and Turnshek, D. 2000, astro-ph/9909164

Rao, S. M. and Turnshek, D. A. 1998, ApJ, 500, L115

Sargent, W. L. W. and Steidel, C. C. 1990, ApJ, 359, L37

White, R. L., Kinney, A. L., and Becker, R. H. 1993, ApJ, 407, 456

Wolfe, A. M., Briggs, F. H., and Jauncey, D. 1981, ApJ, 248, 460

Wolfe, A. M., Broderick, J. J., Johnston, K. J., and Condon, J. J. 1978, ApJ, 222, 752

Wolfe, A. M. and Davis, M. M. 1979, AJ, 84, 699

Wolfe, A. M., Turnshek, D. A., Lanzetta, K. M., and Lu, L. 1993, ApJ, 404, 480

Womble, D. S., Junkkarinen, V. T., Cohen, R. D., and Burbidge, E. M. 1990, AJ, 100, 1785

Young, L. M. 1999, AJ, 117, 1758

Young, L. M. 2000, AJ, 119, 188

5

The $z = 0.0912$ H I 21cm Absorber toward B 0738+313[1]

We present a detailed study of the H I 21cm absorption system at $z = 0.0912$ toward the radio quasar B0738+313. Although the harmonic mean spin temperature calculated by comparison of the 21cm absorption profile to the damped Lyα line is $< T_s > = 725 \pm 100$ K, the thermal kinetic temperatures of the two narrow absorption components, calculated from their widths, are much lower: $T_k \leq 297 \pm 3$ and $\leq 103 \pm 10$ K respectively. This is the first case of a redshifted absorption system for which T_k is measured to be *less* than $< T_s >$. We discuss this result in the context of a two-phase gas model, in which the damped Lyα gas is sensitive to a significant neutral column density of warm-phase gas as well as the cold-phase gas of the narrow 21cm lines. The third absorption component is interpreted as representing the warm-phase gas with with T_k $\leq 5050 \pm 950$ K. The combined column density of the three 21cm components is approximately equal to that derived from fits to the damped Lyα line.

We also search for an H I emission signal from this system over a velocity range of ± 500 km s^{-1} around the narrow 21cm absorption features. Although a spectral dynamic range of 5500 to 1 is achieved at full resolution, no H I emission is detected. The RMS noise in the final spectra is sufficiently low to place a 3σ upper limit on the H I mass of the absorber which rules out the presence of a normal L=L* spiral galaxy at arbitrary inclination, unless the velocity range of the emission overlaps that of the strong 21cm absorption.

---

[1]Based in part on a paper by W.M. Lane, F.H. Briggs, and A. Smette, 2000, ApJ, 532, 146.

5.1 Introduction

Damped Lyα (DLA) and H I 21cm absorption lines are the spectral signatures of systems with high neutral hydrogen column densities. Such systems are the major contributors to the mass density of neutral gas at high redshifts ($z \approx 3$). Despite the success of several surveys in identifying DLA absorption lines in both the optical (Wolfe et al. 1986, Lanzetta et al. 1991, Wolfe et al. 1995, Storrie-Lombardi et al. 1996) and the UV regimes (Lanzetta et al. 1995, Rao and Turnshek 2000), our understanding of the morphology and evolution of the host galaxies in which they arise remains poor. Until recently, most of the known DLA systems were at high redshift, making identification and study of the host galaxies difficult.

The profiles of associated metal lines in these systems are consistent with the hypothesis that DLAs arise in rapidly rotating large disks with substantial vertical scale heights (Prochaska and Wolfe 1997, Prochaska and Wolfe 1998), which fits well with the standard paradigm that DLAs arise in luminous disk galaxies or their progenitors (Wolfe et al. 1995). However, there is a growing body of evidence in both theory and observations that this model might not be applicable to all DLA absorbers. Models based on DLA simulations suggest that the interactions of relatively small systems or even protogalactic clumps might account for the line profiles and neutral column densities of these absorbers (Rauch et al. 1997, Haehnelt et al. 1998). A number of spectral and imaging studies of low- and moderate-redshift DLAs have identified a variety of host galaxies with moderate to high luminosities, including compact objects and amorphous low surface brightness (LSB) galaxies as well as spiral disks (Steidel et al. 1997, Le Brun et al. 1997, Rao and Turnshek 1998).

Just as the morphology of DLA systems is poorly understood, so are their physical conditions, and in particular the temperature of the gas in which the absorption arises. Under usual conditions in the interstellar medium (ISM), the excitation, or spin temperature, T_s, describing the hyperfine level populations in the ground state of neutral hydrogen is coupled to its thermal kinetic temperature, T_k. A harmonic mean spin temperature, $< T_s >$, of all of the neutral clouds on a given sight line can be determined by a comparison of H I 21cm absorption and an inferred 21cm emission profile for the same sight line, or by comparison of the 21cm absorption line parameters to a column density from the DLA absorption feature on the same sight line. However the values of $< T_s >$ derived in this manner for redshifted DLA/H I 21cm absorbers are consistently higher than those found in clouds of similar optical depth in the Galaxy(Lane et al. 1998, Carilli et al. 1996).

The two DLA absorption systems identified in the UV spectrum of the $z_{em} = 0.630$ QSO B0738+313 (OI 363), are both examples of low-redshift absorbers associated with no identifiable luminous disk galaxy (Rao and Turnshek 1998). They are both H I 21cm absorbers, and both have very narrow 21cm lines (Lane et al. 1998, Chengalur and Kanekar 1999). The first absorber is the lowest redshift system for which the DLA line has been observed (the "DLA System" at $v \approx 1170$ km s^{-1} reported by Miller, Knezek, & Bregman (1999) was not observed in the Lyman lines, and a measurement of x-ray absorption was used to infer the neutral H I column density). It has a redshift $z_l = 0.0912$ and a neutral hydrogen column density of

$N_{HI} = 1.5 \pm 0.2 \times 10^{21}$ cm^{-2}. It was discovered serendipitously in a *Hubble Space Telescope* Faint Object Spectrograph (*HST*-FOS) spectrum taken to observe the Ly-α line associated with the previously known metal-line absorption system at $z_2 = 0.2212$ on the same sight line. This second system is also damped, with a slightly lower column density of $N_{HI} = 7.9 \pm 1.4 \times 10^{20}$ cm^{-2}. In ground-based optical images only one candidate host galaxy is visible near the QSO sight line. Based on its optical brightness and the assumption that it is a moderately luminous galaxy, this candidate absorber has been associated with the higher redshift system, although it has no confirming spectroscopic redshift(Le Brun et al. 1993). The other absorption system must arise in either a low surface brightness (LSB) galaxy or a small galaxy which falls under the image of the QSO(Rao and Turnshek 1998).

Here we present new information on the lower redshift ($z_1 = 0.0912$) system on the B0738+313 sight line. Very little is known about the associated metal lines, because the wavelength coverage of the only published optical spectrum (Boissé et al. 1992) does not include the expected wavelengths of any strong lines belonging to this system, while the *HST*-FOS spectrum (Rao and Turnshek 1998) has insufficient signal to noise ratio (S/N) and resolution to allow the detection of small equivalent width lines. We present WHT/ISIS[2] observations of Ca II H and K, the only metal lines observed so far in this system. We discuss observations of the H I 21cm absorption made with the VLA (Very Large Array)[3], and the Arecibo Radio Telescope[4], and the estimates of temperature which we derive from them. We also present Very Long Baseline Array (VLBA)[3] data that was used to investigate the line characteristics and gas covering factor on parsec, or typical ISM cloud scales. The VLBA achieves subarcsecond resolution which provides a fair comparison to the UV and optical absorption lines, because the optically emitting region of a QSO is subparsec in size. Finally we present the results of a very sensitive Westerbork Synthesis Radio Telescope (WSRT)[5] search for emission associated with this H I absorber.

5.2 Observations

5.2.1 WHT/ISIS

The initial redshift determination from the DLA discovery spectrum of the $z = 0.09$ absorber on the B0738+313 sight line had an unreasonably large uncertainty due largely to the difficulties in fitting damped absorption profiles, and the low signal to noise of the *HST* detection spectrum. Because an accurate redshift facilitates the

---

[2]The William Herschel Telescope (WHT) is operated on the island of La Palma by the Isaac Newton Group in the Spanish Observatorio del Roque de los Muchachos of the Instituto de Astrofísica de Canarias

[3]operated by The National Radio Astronomy Observatory, a facility of the National Science Foundation operated under cooperative agreement by Associated Universities, Inc.

[4]The Arecibo Observatory is part of the National Astronomy and Ionosphere Center, which is operated by Cornell University under a cooperative agreement with the National Science Foundation

[5]The Westerbork Synthesis Radio Telescope is operated by the Netherlands Foundation for Research in Astronomy (NFRA/ASTRON) with support from the Netherlands Foundation for Scientific Research(NWO).
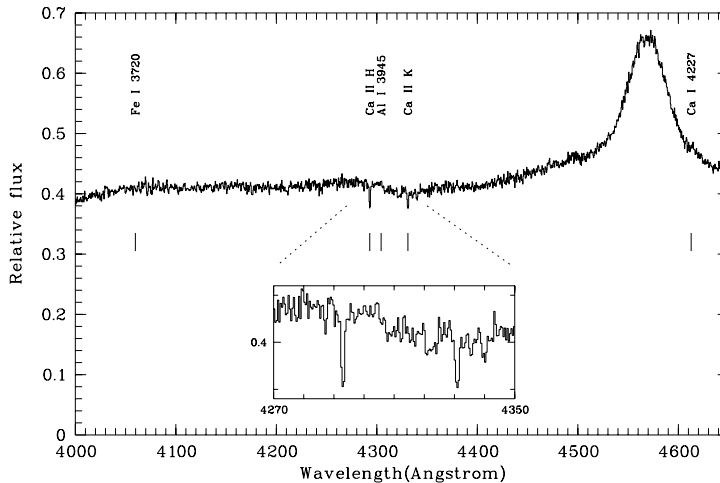
Figure 5.1: Ca II H and K absorption features at a redshift of $z = 0.0910$ are marked. No significant absorption is seen at the expected positions for Fe I $\lambda 3270$, Al I $\lambda 3945$, or Ca I $\lambda 4227$.

search for associated 21cm absorption, observations were made of strong metal lines which fall in the optical window at this redshift. Spectra were obtained using the WHT+ISIS in service mode on the night of 1997 November 9-10, by R. Rutten. The detector was the 2148x4200 EEV10 CCD. We used the R600B grating with a central wavelength of 4300 Å, so that the spectrum covers the range $\lambda\lambda$ 3420Å– 5200Å. The slit was oriented along the parallactic angle, and its width was $1''.00$ providing a spectral resolution of ~ 1Å. Two exposures of 900s and one exposure of 1800s were obtained, for a total integration time of 1 hour. The data were reduced with standard MIDAS routines.

An excerpt of the resulting spectrum is presented in Fig. 5.1. It shows the Ca II H and K absorption lines with rest frame equivalent widths of 0.11 ± 0.02 Å and 0.15 ± 0.02 Å, respectively, at a mean redshift $z = 0.09103 \pm 0.00007$, where the uncertainty represents mainly the RMS of the wavelength calibration. No significant absorption is seen at the expected positions for Fe I $\lambda 3720$, Al I $\lambda 3945$, or Ca I $\lambda 4227$. This spectrum also covers emission line features from the QSO at $z = 0.63$. The large peak near 4570 Å is Mg II emission, and the region between 4050 and 4320 Å contains a complex of emission lines attributed to Fe II $\lambda 2500$.

5.2.2   VLA

The VLA was used in D-array configuration for 4 hours on 1998 January 3 to look for associated H I 21cm absorption at the redshift of the Ca II lines. The sources 3C147

and B0735+331 were used to calibrate the amplitude and passband. The observations were made in 2 polarizations, with a bandwidth of 3.125 MHz centered at a helio-centric frequency of 1301.81 MHz. The band was divided into 128 spectral channels which gave a channel separation of 5.6 km/s. The data were reduced using standard routines in AIPS. An unresolved 21cm absorption line was observed at a redshift of $z = 0.09118$, with an optical depth $\tau = 0.08$ and a FWHM velocity $\Delta v = 13.4$ km s^{-1}. By comparing the 21cm line characteristics with the column density from the DLA measurement, a harmonic mean spin temperature of $< T_s > = 775 \pm 100$ K was derived. This temperature represents a column density weighted harmonic mean of the spin temperatures of all of the neutral gas clouds along the sight line. The derived harmonic mean spin temperature is typical of values found in most other redshifted 21cm/DLA absorbers, and is considerably higher than typical values at similar optical depths in the Milky Way (Lane et al. 1998 and references therein).

5.2.3   VLBA

The $z = 0.0912$ line was observed on 1998 October 8 for just under 6 hours, using the VLBA, as part of a project that observed both 21cm lines on this QSO sight line simultaneously. All 10 VLBA stations participated in the experiment, but due to technical problems, data from Kitt Peak and Los Alamos were not useful. Pie Town had a fatal clock error which was corrected halfway through the experiment. The compact source B0742+103 was observed for calibration purposes. The data were reduced using standard routines in the AIPS data reduction package. The VLBA telescopes have a poor sensitivity at 1163 MHz because it lies at the lower edge of the L-band. As a result the observations of the $z = 0.2212$ system provided little useful information, and were only able to confirm the line detection.

The observations of the $z = 0.0912$ absorber were more successful. At 1302 MHz the QSO center is lightly resolved into a core and an extended component, as shown in Figure 5.2, and all of the "core" flux from unresolved observations is recovered. The symmetric, weak, extended lobes, which lie at roughly $30''$ to the north and south of the quasar (Murphy et al. 1993), have been resolved away. Spectra from three locations across the QSO have been extracted. The upper spectrum is offset by one synthesized beam-width (full width at half power) to the north; the lower offset is one beam-width to the south, and two beam-widths to the east, corresponding to a position along the extension of the QSO. Although nearly 65% of the continuum level in the upper spectrum is due to contaminating signal from the center sight line, the lower position is nearly completely independent and is unlikely to be contaminated at a detectable level. The total shift in position on the sky between the center and lower-most sight line is 13.2 mas, which corresponds to 20 h_{75}^{-1} pc at the redshift of the absorber.

5.2.4   Arecibo

The Arecibo Radio Telescope was used to make three one-hour on source integrations of the 1665 and 1667 MHz OH lines in the two absorption systems on the
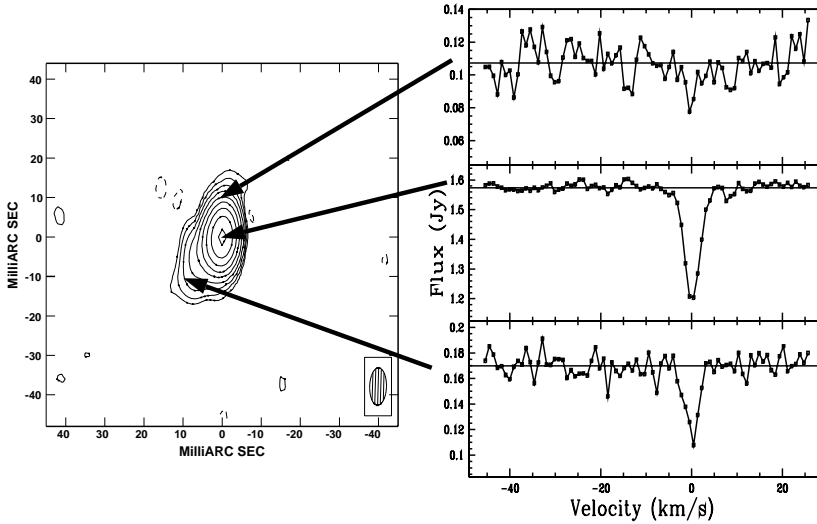
Figure 5.2: Contour plot of the core of B0738+313 observed with the VLBA at 1302 MHz. The quasar is lightly resolved showing a slight extension to the southeast. Spectra have been extracted at the three positions indicated by the arrows. The top spectrum is at $\delta x = 0, \delta y = 10$ mas, the center is at $\delta x = 0, \delta y = 0$, and the bottom at $\delta x = -10$ mas, $\delta y = -10$ mas. At a redshift of $z = 0.0912$, 10 mas corresponds to 15 h_{75}^{-1} pc. The synthesized beam (FWHP) is roughly 5 mas by 10 mas. The velocity scale is centered with $v = 0$ at a heliocentric frequency of 1301.65 MHz.

B0738+313 sight line. Given the narrowness of the 21cm absorption features at both redshifts (Lane et al. 1998, Chengalur and Kanekar 1999), we knew that the absorbing clouds must be very cold and therefore might contain detectable molecular gas. The observations were carried out by K. O'Neill on 1998 November 30 and 1998 December 1&3. Using the post-upgrade system, the L-Band wide receiver, and the new autocorrelation spectrometer, it was possible to observe both OH lines at the redshifts of both DLA systems simultaneously by placing 4 bandpass subcorrelators at appropriate frequencies. A bandwidth of 3.125 MHz and 1024 channels gave a velocity resolution of 0.7 km s^{-1} in two polarizations. The observations were made in an on/off "total power" mode. Total power spectra for the calibration source 3C236 were processed to form gain templates for the spectral passbands, and these templates were applied to the B0738+313 difference spectra using Analyz software. The band centered on the OH 1665 MHz line at $z_1 = 0.0912$ was badly corrupted by interference, and could not be used. No OH was detected in the other three bands (OH 1667 MHz at $z_1 = 0.0912$ and both OH 1667 and 1665 MHz at $z_2 = 0.2212$), which were Hanning smoothed to a velocity resolution of $\delta v = 1.4$ km s^{-1} and had a 3σ detection limit of $\tau = 0.0012$.
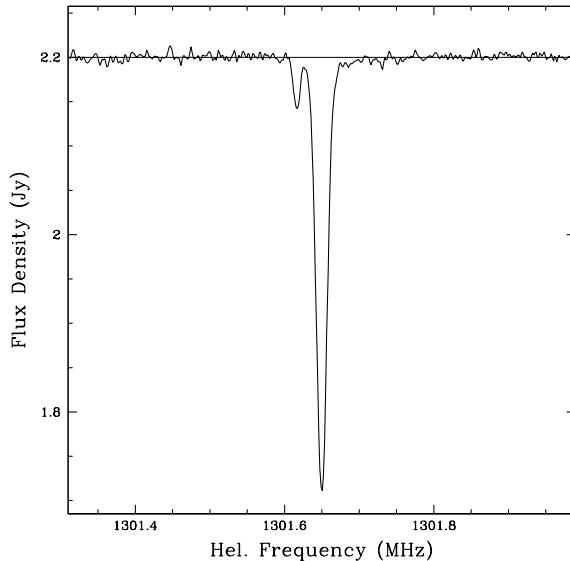
Figure 5.3: An Arecibo spectrum showing the H I 21cm line at $z = 0.0912$ towards the QSO B0738+313. Channel spacing is 0.35 km s^{-1}, allowing this extremely narrow line system to be resolved for the first time. The thin horizontal line marks the continuum level. A second absorption feature is clearly separated from the main line. The shallow feature on the high frequency side of the main absorption is real.

On 1999 April 24-25, we observed the 21cm line in the $z_1 = 0.0912$ system for 45 minutes on source using the on/off observation technique, in two polarizations. Placing 2048 channels across the 3.125 MHz bandwidth gave a velocity resolution of 0.35 km s^{-1}. The nearby source J0745+317 was observed as a calibrator. After gain calibration and averaging, a linear baseline was removed from the data using Analyz to produce the spectrum shown in Figure 5.3. Two narrow absorption lines, the principal component observed in the VLA data and the weak secondary component first seen in the GMRT spectrum of Chengular & Kanekar (1999), are clearly resolved and separated from each other in the Arecibo spectrum. In fitting the absorption features we assume that the signal from any 21cm emission in this system is negligible at this velocity resolution.

5.2.5 WSRT

Using the WSRT, we attempted a sensitive search for HI emission associated with the $z = 0.0912$ absorber. The observations were made on five separate days with the WSRT (6 November 1998, 16 November 1998, 2 December 1998, 18 December 1998, and 14 January 1999), for a standard 12 hours each, or as close to that as scheduling of the instrument allowed. The standard sources 3C48 and 3C147 were observed for primary flux and passband calibration. A bandwidth of 5 MHz, divided into 256 channels, provided roughly 5.4 km s^{-1} resolution. The new DZB correlator as well as the new cooled 21cm MFFE receivers were used to provide the greatest sensitivity possible. Due to the ongoing upgrade, all 14 telescopes were never available, and most of the data used either 10 or 11 telescopes only.

Several of the data sets had their U and V values switched. This was visible in the
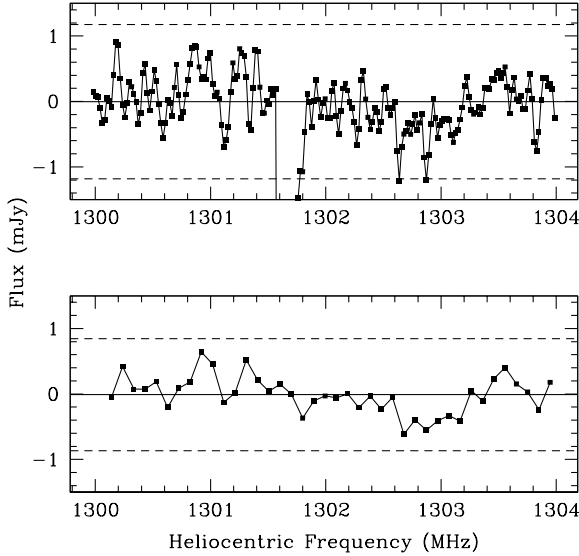
Figure 5.4: Continuum subtracted WSRT spectra extracted from the QSO core position. The top panel shows the full resolution spectrum, with channel spacings $\Delta v = 5.4$ km s^{-1}. The bottom panel shows the same spectrum after it has been Hanning smoothed and resampled at a velocity spacing of $\Delta v = 22.5$ km s^{-1}. The 3σ RMS noise levels are marked in both panels by dashed lines.

map plane as a 90 degree rotation and a distortion of the sources, due to incorrect application of the cos(dec) factor. All of the datasets are affected by a clock error, which led to errors in the delay corrections applied by the on-line system. The roughly 10 second error was constant over a given observation, changing value only between sources, which allowed each dataset to be fixed before calibration by applying an appropriate phase correction to the raw visibilities. We modified the NEWTASK routine in AIPS to fix both the delay and U/V switching errors, as described in Appendices A,B, and C.

After these corrections, the five datasets were calibrated individually using standard AIPS tasks. They were combined using the task DBCON, which applies scaling to account for the slight change in frequency on the different observing dates. Map image cubes at full spatial resolution (FWHP = 15.8" x 28.7" at PA 1.3) and tapered to lower spatial resolution (FWHP = 49.5" x 53.5" at PA 8.0) were synthesized and spectra were extracted at the position of the QSO. The spectra were then Hanning smoothed and resampled at a resolution of 22.5 km s^{-1}. Channels affected by the absorption lines were given a zero weight in the smoothing and averaging. The full resolution spectra and the smoothed version, both at full spatial resolution, are shown in Figure 5.4. In order to search for extended emission around the QSO position, the continuum subtracted data in the central 25 channels were made into a small cube at full velocity and spatial resolution, in which each plane had been individually cleaned to remove side-lobes from the strong absorption.

No convincing H I emission signal was detected. Section 5.4 presents a discussion of the limits this places on the H I mass of the intervening system.

5.3 H I Absorption

5.3.1 The Covering Factor of the Gas

The equation relating neutral hydrogen column density, N_{HI}, to the observed H I 21cm absorption profile is:

$$N_{HI} = 1.8 \times 10^{18} T_s \int \tau(v) \, dv \ \text{cm}^{-2} \tag{5.1}$$

where T_s is the spin temperature of the absorbing gas. $\tau(v)$ is the optical depth of the line at velocity v, calculated as:

$$\tau(v) = -\ln\left(1 - \frac{\Delta S(v)}{f\, S}\right) \tag{5.2}$$

where f is the fraction of the continuum source covered by the absorber, S is the continuum flux density, and $\Delta S(v)$ is the line depth at velocity v. For a single line with a Gaussian profile, the integral of the optical depth over velocity is

$$\int \tau(v) \, dv = 1.06 \ \tau_{21cm} \, \Delta v \tag{5.3}$$

where τ_{21cm} is the peak optical depth of the line at the line center and Δv is the full width at half maximum velocity in km s^{-1}. We call this quantity, which is proportional to the column density divided by the spin temperature, EW_{21} although it is only equal to a true equivalent width as measured for optical absorption features in the limit $\tau(v) << 1$ over the entire absorption profile.

The covering factor f of the gas in 21cm absorbers is usually assumed to be $f \equiv 1$ for compact QSOs, based on a variety of arguments (for a summary, see Carilli et al. 1996). VLBI measurements can be used to refine estimates for f for more complex sources (Briggs and Wolfe 1983). Adoption of a value for f allows a calculation of either the column density, if the temperature is known, or of the temperature if the neutral column density is known from a DLA measurement.

The quasar B0738+313 is core dominated, but has two very weak and diffuse lobes at roughly $\pm 30''$ separation from the core along a nearly north-south line (Murphy et al. 1993). This extended structure is lightly resolved by the synthesized beam in the WSRT data. We extract spectra at the position of the peak in each lobe as identified by the clean components. The northern lobe peaks at an offset of $\delta x = -10'', \delta y = 30''$ from the QSO center, while the southern is at $\delta x = 10'', \delta y = -35''$. These positions are in very good agreement the 18cm maps of Murphy et al. (1993). A contour map of the QSO and the off-center spectra are shown in Figure 5.5.

The southern spectrum shows no sign of absorption. In the northern spectrum, the small absorption feature is caused by contamination from the strong absorption against the core. Neither spectrum shows any significant evidence for emission. The RMS noise gives optical depth limits of $\tau_{north} = 0.03$ and $\tau_{south} = 0.08$ for velocity resolution $\delta v = 5.4$ km s^{-1}) over velocities in a range of several hundred km s^{-1} to either side of the main component redshift. These limits can be compared to the
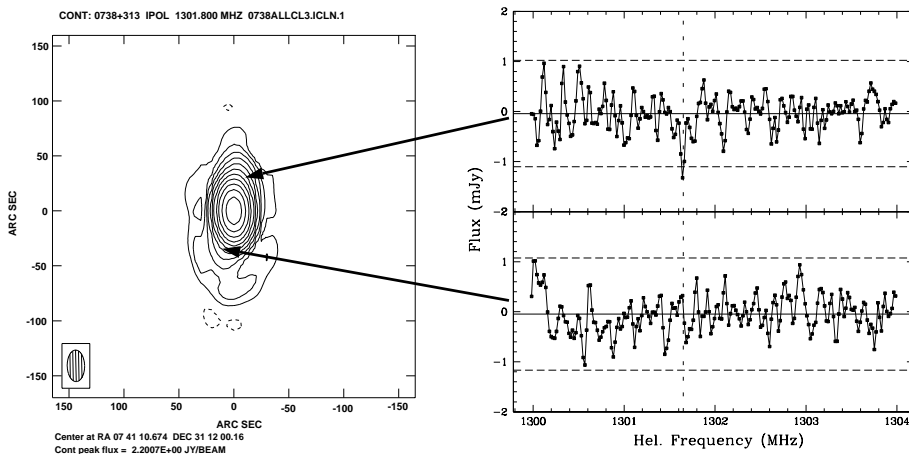
Figure 5.5: Spectra extracted at the position of the weak north and south lobes. The three σ noise levels are shown by horizontal lines, and the dotted vertical line marks the frequency of the main absorption line against the core of the QSO.

absorption line optical depth of $\tau_{21} = 0.11$ measured against the QSO core. These spectra allow us to directly estimate the covering factor of the absorbing gas against the QSO. Since we see no absorption against the lobes, which comprise roughly 2% of the total QSO flux, the absorbing gas must have a covering factor $f \leq 98\%$.

Within the errors, the width, depth and redshift of the main absorption line do not change across the core of the quasar in the VLBA data, as seen in Figure 5.2. The size scale and low velocity dispersion of the gas causing the main absorption feature suggest that it belongs to a single cold cloud or cloud complex. More sensitive VLBA measurements would be necessary to determine if the weak secondary absorption is also present over this size scale, or is part of a smaller scale feature. The constancy of the primary line characteristics over the slightly resolved core in the VLBA data suggests that it is completely covered ($f_{\rm core} = 1$) by the absorbing gas in that component, and we assume this is true for the weaker component as well. We therefore adopt the view that the absorbing gas entirely covers the core but not the extended weak lobes, and that the covering factor of the gas is $f \approx 0.98$.

5.3.2 Kinetic Temperature

The extreme narrowness of the absorption features (as measured in the Arecibo data) places a firm upper limit on the amount of thermal broadening in the lines, and consequently on any turbulence or bulk motions of the absorbing gas. As a result, an upper limit to the kinetic temperature for each cloud can be found directly from the widths of the lines, without having to rely on a comparison between the DLA

and 21cm line characteristics to calculate a harmonic mean spin temperature for the entire ensemble of clouds which lie on the sight line. The kinetic temperature of the gas is related to the width of the absorption line by:

$$T_k \leq \frac{1.2119 \times 10^2 \Delta v^2}{8 \ln 2} \ \text{K} \tag{5.4}$$

where Δv is the FWHM velocity measured in km s^{-1}.

5.3.3   H I Gas in Two Temperature Phases

In order to further analyze the kinematics of the absorbing H I gas, we fit the 21cm profile with overlapping Gaussian components. A simultaneous two component fit to the Arecibo spectrum left large residuals and had a reduced $\chi^2 = 2.34$. By adding a third component to the fit, the reduced $\chi^2 = 1.02$, and the residuals were all within the noise. The first or main component has a velocity width at half maximum (FWHM) of $\Delta v = 3.687 \pm 0.019$ km s^{-1}, and an optical depth of $\tau = 0.2462 \pm 0.0010$. It lies at a heliocentric frequency of 1301.6496 MHz, corresponding to $z = 0.09123$. The second, weaker line is separated from the first by $\Delta V_{\text{offset}} = 7.69 \pm 0.04$ km s^{-1}. It has a FWHM velocity of $\Delta v = 2.18 \pm 0.11$ km s^{-1} and an optical depth $\tau = 0.0253 \pm 0.0010$. The third component has an optical depth $\tau = 0.0063 \pm 0.0008$ and FWHM velocity $\Delta v = 15.2 \pm 1.4$ km s^{-1}. The absorption is shifted by $\Delta V_{\text{offset}} = -1.59 \pm 0.66$ km s^{-1} with respect to the main narrow absorption feature. Attempts to force the third component to lie at the position of either of the other two components resulted in much poorer fits. Figure 5.6 shows the Arecibo spectrum after the fits to the first two components have been removed. The fit to the third component has been marked, and the residuals after removing all three Gaussian fits are shown. Parameters for each of the absorption components are summarized in Table 5.1.

Table 5.1: Three Component Fit to the 21cm Absorption

Component:	1	2	3
Optical depth:	0.2462±0.0010	0.02527±0.0010	0.0063±0.0008
ΔV_{offset} (km s^{-1})		7.69±0.04	-1.59±0.66
FWHM(km s^{-1})	3.687±0.019	2.18±0.11	15.2±1.4
T_k (K)	297±3	103±10	5046±953
N_{HI} (10^{20} cm^{-2})	5.27 ± 0.02	0.11 ± 0.01	9.4 ± 2.3

Using equation 5.4, the kinetic temperature is $T_k \leq 297 \pm 3$ K for the main component and $T_k \leq 103 \pm 10$ K for the secondary line. Both of these temperatures would fall within the scatter in the Galactic relation for $< T_s > $-$\tau$ (Braun and Walterbos 1992), unlike the considerably higher temperature $< T_s > = 725 \pm 100$ K. This is the first redshifted system for which it can be shown that T_k is less than $< T_s >$, ie. that
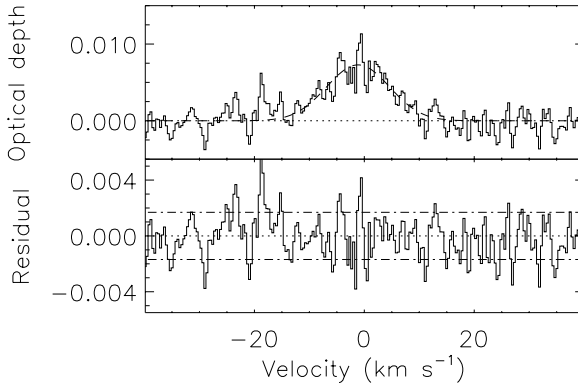
Figure 5.6: Arecibo spectrum showing the warm component and its fit. The velocity scale is set so that $v = 0$ corresponds to a redshift of $z_1 = 0.09123$. The upper panel shows the spectrum after the Gaussian fits to the two cold component absorption lines have been subtracted. The third warm component is clearly visible, and a dashed line shows the Gaussian fit to it simultaneously with the two cold components. The lower panel shows the residuals after subtracting all 3 components, with 1σ error levels marked by the dash-dot lines.

the kinetic temperature in the individual cold phase gas clouds is less than the derived harmonic mean spin temperature for all of the neutral gas on the sight line. The kinetic temperature of the third line, derived from the velocity width of the line, is $T_k \leq 5046 \pm 953$ K, in reasonable agreement with measurements of temperature in the WNM of our own Galaxy (Kulkarni and Heiles 1988, Carilli et al. 1998), where typical temperatures fall in the range 5000-8000 K.

For a given cloud, $T_s \approx T_k$ under usual conditions found in the ISM (Kulkarni and Heiles, 1988). For the two cold absorption components, we set $T_s = T_k$ and $f = 0.98$ (because the Arecibo beam covers both the core and the extended lobes of the quasar), and calculate the column density for each 21cm line component from equations 5.1 and 5.3. Adding the two together, and bearing in mind that our values for T_k are upper limits, we find a total column of $N_{\text{HI 21cm}} \leq 5.4 \pm 0.1 \times 10^{20}$ cm^{-2} in the narrow absorption features. This is approximately one third of the measured H I column density in the DLA line: $N_{\text{HI DLA}} = 1.5 \pm 0.2 \times 10^{21}$ cm^{-2} (Rao and Turnshek 1998).

The calculated column density in the warm component is $N_{\text{HI}} \leq 9.4 \pm 2.3 \times 10^{20}$ cm^{-2} for a covering factor of $f = 0.98$. Although we do not have the needed sensitivity to determine the core covering factor for this component in the VLBA data, warm gas in our Galaxy is distributed more widely and more uniformly than the cold gas (Dickey and Lockman 1990), so it seems unlikely that the gas would have a lower core covering factor than the cold gas. There is the possibility that the warm gas covers one or both of the weak extended radio lobes as well as the core (ie. that $f > 0.98$), but given that $30'' \approx 45 \ h_{75}^{-1}$ kpc at $z_1 = 0.0912$, it seems unlikely. The absorption limits against the extended lobes measured using the WSRT data and the

EW_{21} of the warm absorption in the Arecibo spectrum rule out the possibility that the absorption covers one of the lobes but not the core as well.

When the warm and cold component column densities are added together, the total column density in 21cm absorption on this sight line is $N_{HI21cm} \leq 1.48 \pm 0.24 \times 10^{21}$ cm^{-2}. This is in remarkable agreement with the column density from the fit to the DLA line.

5.3.4 Discussion of Warm Phase H I Gas

The existence of a second gas phase has often been suggested to explain the large harmonic mean spin temperature values, typically $< T_s > \approx 1000$ K (Carilli et al. 1996) found in redshifted DLA/21cm absorbers. If the gas on the sight line has two (or more) temperature phases, then the T_s calculated by comparing the 21cm and DLA absorption profiles will not be equal to the kinetic temperature in either phase, but rather to a column-density weighted harmonic mean of the temperature of each phase. Thus a sight line with mostly warm phase gas will have a higher calculated $< T_s >$ than one with mostly or only cold phase gas. The values found for $< T_s >$ can then best be interpreted as an upper limit to the temperature of the cold phase gas. When this quantity is derived for redshifted systems, it is usually a value somewhere between the measured temperatures of stable cold and stable warm neutral gas in our own Galaxy. In most redshifted 21 cm absorbers, the absorption lines are broadened by bulk kinematic motions of the gas, and the limit on the kinetic temperature is higher than that of the $< T_s >$.

This is the first redshifted 21cm absorber measured for which the calculated thermal T_k which constrains the cold gas temperature more tightly than the derived $< T_s >$, and shows directly that not all of the gas column density seen in the DLA line appears in the cold components of the 21cm lines. It suggests that some two-thirds of the column density on this sight line, if not more, is contained in warm phase gas. If the broad shallow component we have detected in our Arecibo data were to be resolved by more sensitive observations into a collection of shallow narrow absorptions lines, then the conclusion that warm phase gas is necessary to explain all of the DLA fitted neutral column density in this system would still remain. The integrated N_{HI} in such an ensemble of little narrow cold components would be very small, and we would still need to find the rest of the gas sensed by the DLA observation. The logical place for it to be "hiding" from the 21cm absorption measurement would still be in a warm neutral component, appearing as an even broader and shallower absorption feature.

This system offers an explanation for why some DLA absorbers which fall in front of radio-bright QSOs do not show 21cm absorption. There is $N_{HI} \approx 10^{21}$ cm^{-2} column of gas which was "unseen" in the 21cm spectrum until extremely sensitive observations were made. This amount is well over the canonical lower limit for DLA systems, and its existence here suggests that some fraction of the DLA systems may arise in entirely warm phase gas. This idea is strengthened by the lower limits found on $< T_s >$ for 21cm non-detections, which are typically several times 10^3 K, suggestive of either unstable or warm phase gas (WNM) (Carilli et al. 1996).

Given that the WNM is more widely and uniformly distributed than the CNM in our own Galaxy (Dickey and Lockman 1990) and in observations of local Dwarfs (Young and Lo 1996, Young and Lo 1997a, Young and Lo 1997b), it seems likely that the gas responsible for any detection of DLA absorption would include a large fraction of warm phase neutral gas.

5.4   H I Emission

No significant emission was seen in any of the WSRT spectra (Figure 5.4, nor at any off-center location in the map cubes. The original data were taken with a channel spacing of 4.5 km s^{-1} in order to more carefully separate the narrow absorption features from any possible emission. The absorption affected a total of 12 channels (roughly 55 km s^{-1}) which were given a zero weight before the data were smoothed to 22.5 km s^{-1} in order to search for weak emission. At the smoothed resolution, the absorption completely fills the central channel, and affects one channel to each side as well.

The full resolution spectrum has an RMS noise per 4.5 km s^{-1} channel of $\sigma = 0.393$ mJy. This is equal to the WSRT expected theoretical noise for a 60 hour integration at this frequency, and implies a spectral dynamic range of $\approx$ 5500:1 for this 2.2 Jy continuum source. However the spectrum suffers from the presence of a broad sinusoidal feature which has an amplitude of $\sim 5\sigma$ peak to peak, and appears in the individual as well as the combined data sets at roughly the same level of significance. As a result, the RMS noise in the smoothed spectrum does not decrease as much as expected. The RMS noise in the 22.5 km s^{-1} resolution spectrum is $\sigma = 0.285$ mJy, as opposed to the theoretical value of $\sigma_{theor} = 0.175$ mJy. While we are uncertain as to the cause of this sinusoid, it is possible that more frequent passband calibrations (van Gorkom et al. 1993) could be used to minimize or remove it in future observations.

5.4.1   Limits on $M_{\text{H I}}$

In order to convert the measured spectral noise into an upper limit on the H I mass of the 21cm absorber, we need to assume a shape and a velocity width for the emission profile. For simplicity, we choose a rectangular emission profile with width ΔV in km s^{-1} and height S measured in mJy. The H I mass is then given by:

$$M_{\text{H I}} \leq 235 \times S \times \Delta V \times D_L^2 \ M_\odot \tag{5.5}$$

where D_L is the luminosity distance to the system in Mpc, and $D_L = 372.8$ Mpc for $z = 0.0912$ (H$_o = 75$ km s^{-1} Mpc^{-1}). Using the smoothed, 22.5 km s^{-1} resolution spectrum, the 3σ limit to the line flux is $S = 0.855$ mJy, and the 3σ upper limit to the H I mass is

$$M_{\text{H I}} \leq 2.8 \times 10^7 \Delta V \ M_\odot$$

The H I mass of a typical (L~L*) spiral galaxy is $M^\star_{\rm H\,I} \sim 5 \times 10^9\ M_\odot$.

The velocity width, ΔV, of the 21cm emission profile varies with the inclination of a galaxy's disk to the line of sight. In face on spirals, ΔV can be as little as 20-30 km s^{-1}, which is comparable to the resolution of our smoothed spectrum. Using $\Delta V = 22.5$ km s^{-1}, the upper limit of the mass in this system is $M_{\rm H\,I} \leq 6.3 \times 10^8\ M_\odot$. This is only valid if the bulk of the emitting H I is separated in velocity from the H I absorbing gas. However, it seems likely that the emission would in fact overlap the strong absorption features at least in part, making the mass limit in the face-on case very tentative.

More stringent constraints apply to a galaxy viewed at a greater inclination, for which the H I emission profile is likely to be much broader, thus extending beyond the absorption in velocity, even should an overlap occur. For a moderately inclined galaxy, velocity widths of $70 - 100$ km s^{-1} are typical. If we set $\Delta V = 100$km s^{-1}, we obtain a mass limit $M_{\rm H\,I} \leq 2.8 \times 10^9\ M_\odot$, which is still slightly less than the expected mass of an L* galaxy.

However, a common emission profile for inclined, and particularly for highly inclined spirals is not rectangular but rather "double-horned", and shows two narrow peaks of emission, each a few tens of km s^{-1} in width, separated by a wide plateau. In this case, we would expect to see at least one of the two horns in our spectrum. The upper limit for the mass in one such undetected horn is the same as that derived for a face-on galaxy.

The limits placed on the mass and inclination of the H I for this system agree with optical images of the QSO and surrounding field, in which there is no obvious luminous spiral galaxy which could be responsible for the absorption (Rao and Turnshek 1998), and add strength to the argument for either a dwarf or low surface brightness host-galaxy.

5.5   Conclusions

In conclusion, we are able to derive not only a harmonic mean spin temperature for the $z = 0.09$ H I absorption system, but also a thermal kinetic temperature for the gas in the narrow-line absorbing clouds. For the first time in a redshifted H I 21cm absorber, the kinetic temperature derived from the velocity width of the absorption is observed to be smaller than the derived spin temperature. The neutral gas must be split into warm and cold phases in order to account for this discrepancy. We find that the 21cm absorption spectrum is best fit by three components; two narrow deep lines, assumed to arise in cold gas with $T_{\rm k} \leq 300$ & 105 K, and a broad shallow absorption feature which we identify with the warm phase gas at $T_{\rm k} \leq 5050$ K. Within the errors, all of the neutral hydrogen column density seen in the DLA measurement is recovered by these three 21cm absorption components. This is the first detection of warm phase gas in absorption in an extragalactic system, and the highest redshift detection of warm neutral phase gas known. It is also the first time limits on temperature have been made in a redshifted DLA system which show a two temperature distribution of the neutral gas, comparable to that found in our own Galaxy.

We are unable to place stringent limits on the H I emission from this absorber. If the galaxy is an inclined rotating disk system, then we find a limiting mass of $M_{\mathrm{H\,I}} \leq 2.8 \times 10^9\ M_\odot$, which is slightly less than the mass of a typical L* galaxy. This combined with the lack of an obvious luminous spiral in optical images of the QSO field suggests that the absorption arises in some sort of dwarf or LSB-type galaxy, which may in fact lie under the PSF of the ground-based images.

Acknowledgements

References

Boissé, P., Boulade, O., Kunth, D., Tytler, D., and Vigroux, L. 1992, A&A, 262, 401

Braun, R. and Walterbos, R. A. M. 1992, ApJ, 386, 120

Briggs, F. H. and Wolfe, A. M. 1983, ApJ, 268, 76

Carilli, C. L., Dwarakanath, K. S., and Goss, W. M. 1998, ApJ, 502, L79

Carilli, C. L., Lane, W., de Bruyn, A. G., Braun, R., and Miley, G. K. 1996, AJ, 111, 1830

Chengalur, J. N., de Bruyn, A. G., and Narasimha, D. 1999, A&A, 343, L79

Chengalur, J. N. and Kanekar, N. 1999, MNRAS, 302, L29

Dickey, J. M. and Lockman, F. J. 1990, ARA&A, 28, 215

Haehnelt, M. G., Steinmetz, M., and Rauch, M. 1998, ApJ, 495, 647

Kulkarni, S. R. and Heiles, C. 1988, in *Galactic and Extragalactic Radio Astronomy*, ed. G. Verschuur and K. Kellerman, (New York: Springer-Verlag), 95

Lane, W., Smette, A., Briggs, F., Rao, S., Turnshek, D., and Meylan, G. 1998, AJ, 116, 26

Lanzetta, K. M., McMahon, R. G., Wolfe, A. M., Turnshek, D. A., Hazard, C., and Lu, L. 1991, ApJS, 77, 1

Lanzetta, K. M., Wolfe, A. M., and Turnshek, D. A. 1995, ApJ, 440, 435

Le Brun, V., Bergeron, J., Boissé, P., and Christian, C. 1993, A&A, 279, 33

Le Brun, V., Bergeron, J., Boisse, P., and Deharveng, J. M. 1997, A&A, 321, 733

Miller, E. D., Knezek, P. M., and Bregman, J. N. 1999, ApJ, 510, L95

Murphy, D. W., Browne, I. W. A., and Perley, R. A. 1993, MNRAS, 264, 298

Prochaska, J. X. and Wolfe, A. M. 1997, ApJ, 487, 73

Prochaska, J. X. and Wolfe, A. M. 1998, ApJ, 507, 113

Rao, S. and Turnshek, D. 2000, astro-ph/9909164

Rao, S. M. and Turnshek, D. A. 1998, ApJ, 500, L115

Rauch, M., Haehnelt, M. G., and Steinmetz, M. 1997, ApJ, 481, 601

Steidel, C. C., Dickinson, M., Meyer, D. M., Adelberger, K. L., and Sembach, K. R. 1997, ApJ, 480, 568

Storrie-Lombardi, L. J., McMahon, R. G., Irwin, M. J., and Hazard, C. 1996, ApJ, 468, 121

van Gorkom, J. H., Bahcall, J. N., Jannuzi, B. T., and Schneider, D. P. 1993, AJ, 106, 2213

Wolfe, A. M., Lanzetta, K. M., Foltz, C. B., and Chaffee, F. H. 1995, ApJ, 454, 698

Wolfe, A. M., Turnshek, D. A., Smith, H. E., and Cohen, R. D. 1986, ApJS, 61, 249

Young, L. M. and Lo, K. Y. 1996, ApJ, 462, 203

Young, L. M. and Lo, K. Y. 1997a, ApJ, 476, 127

Young, L. M. and Lo, K. Y. 1997b, ApJ, 490, 710

A   The U/V Error

Consider a matrix for the U,V, and W values expressed in units of wavelength, λ:

$$\begin{pmatrix} U \\ V \\ W \end{pmatrix} = \frac{1}{\lambda} \begin{pmatrix} \sin H_o & \cos H_o & 0 \\ -\sin\delta\cos H_o & \sin\delta\sin H_o & \cos\delta \\ \cos\delta\cos H_o & -\cos\delta\sin H_o & \sin\delta \end{pmatrix} \begin{pmatrix} B_x \\ B_y \\ B_z \end{pmatrix} \tag{5.6}$$

where H_o, δ are the Hour Angle and Declination of a reference position, and B_x, B_y, and B_z are the coordinates for the difference in position between two antennae. For an East-West array, $B_x, B_z = 0$ and $B_y = B$, which leaves the (much simpler) set of equations:

$$U_\lambda = \frac{1}{\lambda} B \cos H_o \tag{5.7}$$

$$V_\lambda = \frac{1}{\lambda} B \sin H_o \sin\delta \tag{5.8}$$

$$W_\lambda = -\frac{1}{\lambda} B \sin H_o \cos\delta \tag{5.9}$$

where U_λ, V_λ, $and W_\lambda$ are are expressed in wavelengths.

During part of the WSRT/DZB commissioning phase, there was an error which resulted in the U,V, and W values of the data being miscalculated. In fact, they were calculated as if $B_y, B_z = 0$ and $B_x = B$. The effect in the data was to make it appear that the U and V values had been "switched". In terms of our formulae, this resulted in the following erroneous values:

$$U_{\lambda err} = \frac{1}{\lambda} B \sin H_o \tag{5.10}$$

$$V_{\lambda err} = -\frac{1}{\lambda} B \cos H_o \sin\delta \tag{5.11}$$

$$W_{\lambda err} = \frac{1}{\lambda} B \cos H_o \cos\delta \tag{5.12}$$

This error can be easily corrected by combining the two sets of equations to find that:

$$U_\lambda = \frac{-V_{\lambda err}}{\sin \delta} \tag{5.13}$$

$$V_\lambda = U_{\lambda err} \sin \delta \tag{5.14}$$

$$W_\lambda = -U_{\lambda err} \cos \delta \tag{5.15}$$

We chose to correct only the errors in U and V by modifying the NEWTASK routine in AIPS to apply the corrections from Equations 5.13 and 5.14.

B The Delay Error

There was a period of time during the commissioning phase of the WSRT/DZB there was a clock problem which caused an error in the online delay correction applied in the correlator, as well as small errors in the U,V, and W values. In effect, everything was calculated for an array geometry at a time $t + \Delta t$. In general, $\Delta t \sim 10$ seconds. According to the "shift theorem" of Fourier transforms, the error in delay, τ_{err}, leads to a small phase offset in the cross-correlated spectrum which varies linearly with frequency, ν. In fact, affected data showed a slope in phase across the band which varied with Hour Angle and baseline length (it was steeper for HA~ 0 and the longest baselines).

Because Δt is found to be constant over a given observation, it is possible to apply a correction for this error directly to the visibilities. Consider the real and imaginary part of each complex visibility, $Ve^{i\Phi_V}$, which can be written as:

$$Real = |V| \cos \Phi_V \tag{5.16}$$

$$Im = |V| \sin \Phi_V \tag{5.17}$$

We need to add a phase correction $\Delta \Phi_e(\nu)$ to each measured phase Φ_V. Expanding according to cos and sin angle addition rules, we find:

$$Real_{corr} = |V| (\cos \Phi_V \cos \Delta \Phi_e(\nu) - \sin \Phi_V \sin \Delta \Phi_e(\nu))$$

$$Im_{corr} = |V| (\sin \Phi_V \cos \Delta \Phi_e(\nu) + \cos \Phi_V \sin \Delta \Phi_e(\nu))$$

However this can be more easily expressed as:

$$Real_{corr} = Real \cos \Delta \Phi_e(\nu) - Im \sin \Delta \Phi_e(\nu) \tag{5.18}$$

$$Im_{corr} = Im \cos \Delta \Phi_e(\nu) + Real \sin \Delta \Phi_e(\nu) \tag{5.19}$$

Thus, once we now what $\Delta \Phi_e(\nu)$ is, we can easily modify the existing visibilities to correct for the delay error.

We begin by writing:

$$\Delta\Phi_e(\nu) = 2\pi\tau_{err}\Delta\nu \tag{5.20}$$

where the $\Delta\nu = \nu - \nu_o$ accounts for the frequency dependence across the band and is taken relative to the fringe stopping frequency, which is positioned at the center of the band, ν_o. τ_{err} is the delay error and depends on the error made in the computed W. We compute this error from the equation:

$$\tau_{err} = \frac{1}{c}\frac{dW}{dt}\Delta t \tag{5.21}$$

Differentiating Equation 5.9, we find that

$$\tau_{err} = -\frac{B}{c}\cos H_o \cos\delta\frac{dH_o}{dt}\Delta t \tag{5.22}$$

or

$$\tau_{err} = -\frac{U_\lambda}{\nu_o}\cos\delta\frac{dH_o}{dt}\Delta t \tag{5.23}$$

Substituting Equation 5.23 into Equation 5.20 and re-arranging, we find:

$$\Delta\Phi_e(\nu) = -2\pi\frac{dH_o}{dt}\Delta t\frac{(\nu - \nu_o)}{\nu_o}U_\lambda\cos\delta \tag{5.24}$$

The change in hour angle over time, is always 1 turn every 24 hours. Adjusting this to radians and accounting for the slight difference between 1 second of UT time and 1 second of LST, we find an expression in seconds:

$$\frac{dH_o}{dt} = \frac{2\pi \times 1.0027}{86400} \tag{5.25}$$

which in its turn can be substituted into Equation 5.24, to get:

$$\Delta\Phi_e(\nu) = \frac{-4\pi^2(1.0027)}{86400}\Delta t\frac{(\nu - \nu_o)}{\nu_o}U_\lambda\cos\delta \tag{5.26}$$

Using this expression for $\Delta\Phi_e(\nu)$, our modified visibility equations 5.18 and 5.19, and knowledge about the size of the timing error Δt, we can now correct for the delay error.

We modified the AIPS routine NEWTASK to apply the visibility modifications. Each dataset taken during the period when the timing offsets were an issue was examined separately for time errors over the range $-10sec < \Delta t < 20sec$ at 5 second intervals. Typically the timing errors found were either 5 or 10 seconds.

C   Positional Errors

The timing error also causes small errors in U and V, which translate into small positional errors in the map, especially for sources far from the phase center. Rough calculations suggest that even far away from the phase center the effect should be only a fraction of the synthesized beam-size, and we have considered them to be negligible. This is particularly true for fields which were self-calibrated.

6

The Host Galaxies of H I 21cm Absorbers

We present near infrared images of the fields around QSOs B 0738+313 and B 1127-145. There are three low-redshift Damped Lyα/H I 21cm absorption line systems present on the sight lines toward these two QSOs. We argue that the absorbing gas at $z = 0.2212$ toward B0738+313 arises in the outskirts of a small elliptically shaped galaxy with L≈ 0.1L* in the K-Band. The $z = 0.0912$ absorber on the same sight line is apparently part of a galaxy which falls under the point-spread-function (PSF) of the bright QSO, although there is a faint spiral arm-like structure at a projected separation of 10 kpc from the QSO sight line if it has a redshift $z = 0.0912$. The multi-component H I 21 cm absorber at $z = 0.313$ toward B1127-145 most likely arises in interaction gas among a small group of galaxies near the QSO sight line.

6.1 Introduction

The spectroscopic identification and study of damped Lyα/H I 21cm absorbers and their associated metal-line absorption provides a range of information about the characteristics of the neutral absorbing gas, including estimates of metallicity, dust content, temperature, and velocity distribution. At high- and moderate- redshifts, DLA absorbers have low-metallicities (Pettini et al. 1999), a low dust-to-gas ratio (Pei et al. 1991), and little molecular gas (Levshakov et al. 1992). The mean spin temperature of the neutral Hydrogen is of the order $< T_s > \sim 1000$ K, much higher than that seen in our own Galaxy (Carilli et al. 1996). Theoretical models can explain the observed metal-line absorption profiles at high-redshift by either thick rotating neutral gas disks (Prochaska and Wolfe 1997, Prochaska and Wolfe 1998) or by the mergers of proto-galactic clumps (Rauch et al. 1997, Haehnelt et al. 1998). At high redshift DLA systems dominate the cosmic mass density, $\Omega_{H I}(z)$, of neutral Hydrogen

gas, and are the likely progenitors of the gas-rich galaxies which dominate $\Omega_{H\,I}(z)$ at $z \approx 0$ (Wolfe et al. 1995).

Despite the theoretical models, we know very little about the true morphology of these neutral-gas rich absorbers. The apparent surface brightness of any redshifted object is dimmed by a cosmological factor of $(1 + z)^{-4}$, and at high redshift it is simply very difficult to image and obtain spectra for candidate DLA-host galaxies. This problem is made worse by the necessary presence of a bright QSO on a sight line passing through some part of the absorbing galaxy. In order to relate the observed absorption lines to physical systems which can be compared to gas rich galaxies at $z \approx 0$, it is crucial to identify the host-galaxy. The recently expanded sample of known low-redshift DLA (Rao and Turnshek 2000) and H I 21cm absorbers (Chapter 4, this thesis) provides an ideal set of sources for study to address this identification problem.

A variety of imaging and spectroscopic studies over the past few years have indicated that the DLA/21cm absorption systems actually select galaxies with a range of morphologies rather than one characteristic type of system. The likely host galaxy for the H I 21cm absorber at $z = 0.437$ on the 3C196 sight line has been identified as a luminous barred spiral (type SBc) with extended arms covering the radio-lobes of the QSO (Cohen et al. 1996, Le Brun et al. 1997). There are two known DLA systems associated with compact objects at small angular separations from QSO sight lines: the $z = 1.01$ absorber towards 0302-223 (Le Brun et al. 1997), and the $z = 0.8596$ absorber on the sight line to 0454+039 (Steidel et al. 1995, Le Brun et al. 1997). There are a couple of absorbers associated with amorphous low surface brightness objects. These include the $z = 0.395$ H I 21cm absorber on the 1229-021 sight line and the $z = 0.692$ H I 21cm absorber toward 3c286 (Steidel et al. 1994, Le Brun et al. 1997). The host-galaxy of the DLA absorber at $z = 0.656$ toward 3c336 has yet to be identified despite an extensive imaging and spectroscopic study of this field (Steidel et al. 1997), and it is thought to arise in a low surface brightness galaxy which has not yet been identified. The $z = 0.2212$ DLA/21cm absorber toward 0738+313 is associated with a slightly under-luminous elliptical, while the $z = 0.0912$ DLA/21cm absorber on the same sight line has no identified host galaxy (Rao and Turnshek 1998, Turnshek et al. 2000). In the case of AO 0235+164 it is entirely unclear what type of object is responsible for the $z = 0.524$ H I 21cm absorption, despite observations made with the *HST* (Burbidge et al. 1996). There is a spiral galaxy with unknown redshift at an angular separation of $1.3''$ to the East of the QSO, while $2''$ to the south there is an AGN at $z_{em} = 0.524$, surrounded by a nebulosity which covers the QSO position.

It is clear that the low redshifts of these systems do not necessarily make it easier to identify the host galaxy. In most cases the best candidates are at such small impact parameters that they fall at least partially under the QSO PSF in ground-based images. In order to confirm the reality of such detections it is necessary to obtain more than one observation, and preferably to use telescopes with adaptive optics or the *HST* to improve the angular resolution of the image. Unfortunately telescope time on such instruments is difficult to obtain.

Imaging at a variety of wavelengths allows the derivation of colors and photometric redshifts for the host-galaxy candidates. Near-infrared colors are particu-

larly useful in this respect, because we expect the absorbing galaxies to be quite red in color, and because they better constrain the photometric models of low-redshift objects. Here we present near-infrared images for the fields of three low-redshift DLA/21cm absorbers for two of which a firm identification of the host galaxy has not yet been made. These include the $z = 0.0912$ and $z = 0.2212$ absorbers on the B 0738+313 sight line, and the $z = 0.313$ absorber toward B 1127-145. The infrared images reveal low surface brightness and sub-$L^\star$ objects in both fields which we identify as the likely host systems for the absorption.

6.2 B 0738+313

6.2.1 The Observations

A K-Band image of the B 0738+313 field was obtained on 12 December 1998 at the 3.0m NASA Infrared Telescope Facility (IRTF) using the NSFCAM instrument and a 256×256 InSb detector array. The image scale is $0.30''$ per pixel, and the seeing is $\approx 0.55''$. In order to properly remove the bright K-band sky the telescope was offset by small amounts between each frame, a procedure called dithering. This changes the position of the bright field objects sufficiently to allow the construction of an object-free sky frame. We chose a 5-point dither pattern with a 2-minute integration at each pointing. This was repeated 6 times for a combined integration time of 60 minutes. The 60 individual images were flatfielded using domeflats. The median of the 5 frames in each dither pattern was used to subtract the sky background. Each image was shifted to remove the dither pattern offset, and the shifted images were combined to create the final image. The final K-band image is presented in Figure 6.1. In order to better see the faint structure near the QSO, the image has been smoothed and the QSO PSF has been subtracted in Figure 6.2, as have the PSFs of stars in the field.

6.2.2 Discussion

The galaxy, G1, that lies to the southeast of the QSO is the only galaxy that is clearly visible near the QSO sight line in optical R-band images, although both Rao and Turnshek (1998) and Le Brun et al.(1993) were also able to identify a fuzzy feature that lies a few arcseconds to the west-southwest of the QSO. There are two DLA absorbers on this sight line – one at $z_1 = 0.0912$ and one at $z_2 = 0.2212$. Both of these have substantial column densities ($N_{HI} = 1.5 \times 10^{21}$ cm^{-2} and $N_{HI} = 7.9 \times 10^{20}$ cm^{-2} respectively) and both have associated H I 21cm absorption lines.

The lower redshift system, as described in Chapter 5, has two very narrow H I 21cm absorption components with velocity widths of only a few km s^{-1}, and a third shallow component with a velocity width of 15 km s^{-1}. The three components are spread over less than 10 km s^{-1} in total. The very narrow, unsaturated Ca II H and K lines are the only identified metal-lines associated with this system (Lane et al. 2000), and while they are consistent with the velocity spread of the 21cm gas, they do not
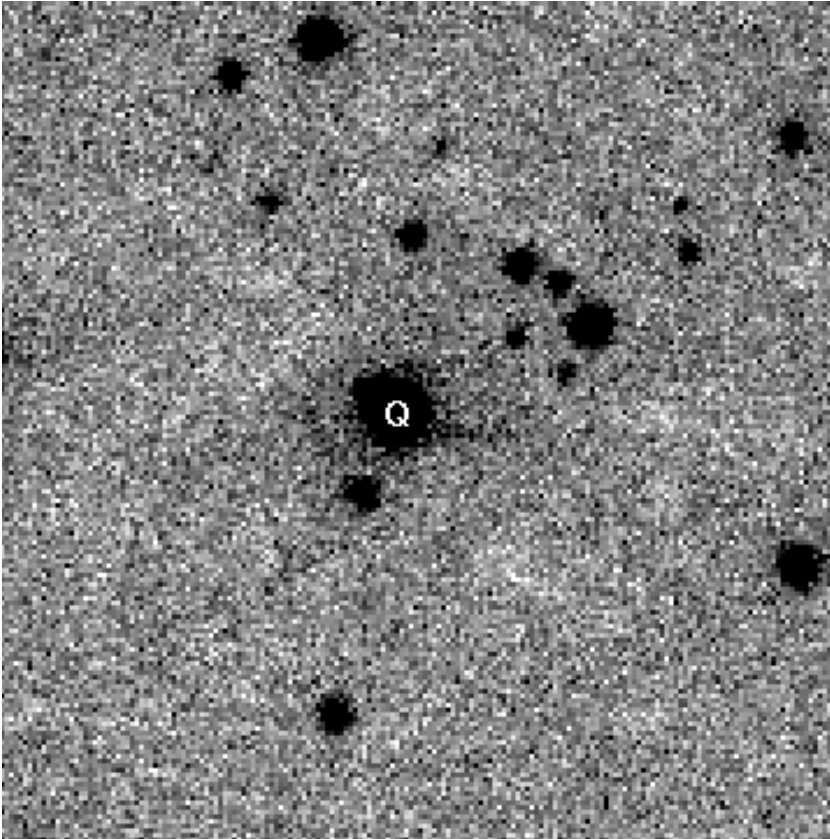
Figure 6.1: K-Band image of the B 0738+313 field. North is up and East is left. The QSO (labeled Q) presents a slightly asymmetric shape because of a close star on the northeast side. The pixel scale is $0.30''$, and the seeing is $\approx 0.55''$. The entire image covers roughly $1'$ by $1'$. The 3σ limiting surface brightness is 22.0 mag/arcsec^2.

further constrain the gas kinematics. The $z = 0.2212$ system has narrow Mg II and Fe II absorption lines, with Mg II $W_o^{\lambda 2796} = 0.52$ Å corresponding to a velocity spread of ≥ 55 km s^{-1}. Its H I 21cm absorption profile contains a single component with a velocity width of ~ 5.5 km s^{-1} (Chapter 4). The information on velocity structure indicates that if either of these absorbers is a large rotating disk it must be viewed nearly face-on.
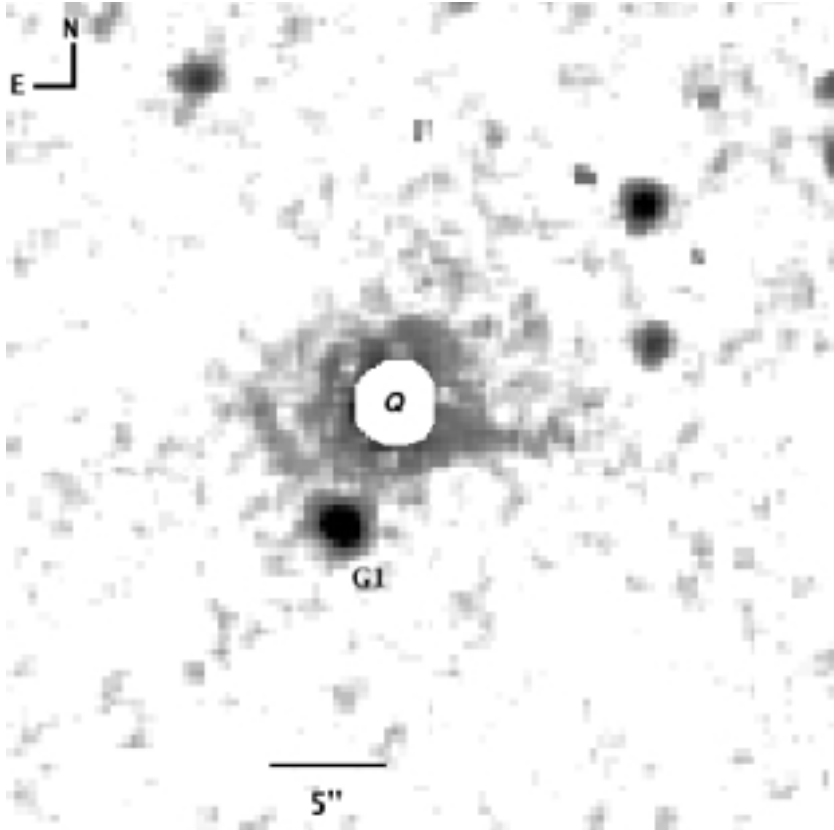
Figure 6.2: Extract from the K-Band image of the B 0738+313 field. The PSF of the QSO has been subtracted to bring out the structure near it and it is labeled Q. The image covers roughly $35''$ by $35''$, and has a 3σ limiting surface brightness of 23.3 mag/arcsec^2. At a redshift $z = 0.0912$, $5''$ is about 9 h_{65}^{-1} kpc, and at $z = 0.2212$ it is 17.5 h_{65}^{-1} kpc. Galaxy G1 is separated from the QSO by $5.7''$.

6.2.3   The $z_{abs} = 0.2212$ Host Galaxy

Turnshek et al. (2000) associate G1 with the $z = 0.2212$ absorber, based on its photometric colors (UBRIJHK) and optical spectrum. This identification does not, however, come from direct measurements of emission lines, as none have been detected. The optical spectrum is typical of an early type galaxy or a bulge. They fit elliptical isophots to an R-Band image of this galaxy, and find that the brightness profile

is well described by an $r^{1/4}$ law in the center, while the outer isophots are better fit by an exponential. Typically dwarf elliptical galaxies have exponential brightness profiles; central surface brightness excesses are seen in bright dwarf ellipticals and spheroidals (eg. Jerjen et al. 2000).

In the K-Band image, G1 is a compact object with little extended low-surface brightness light. It does not appear to overlap the QSO or the low surface brightness structure around the QSO at the sensitivity levels of this image. Measured over a $1.4''$ aperture, G1 has an apparent luminosity, of $m_K = 17.7 \pm 0.1$. The unusually small aperture was chosen to include most of the galactic light detectable above the sky background while minimizing the error. The derived absolute magnitude of G1 is $M_K = -22.3$ for $z = 0.2212$. Loveday (2000) measures the luminosity function of local field galaxies, and finds $M_K^\star = -24.5$ for $H_o = 65$ km s^{-1} Mpc^{-1}. G1 is 2.2 magnitudes fainter than this, so L≈ 0.1L*. The apparent R-band magnitude for G1 is $m_R = 20.8$ mag (Rao and Turnshek 1998), and the derived R - K≈ 3 is slightly redder than typical colors (R-K~ 2.5) of spiral galaxies (de Jong 1996b).

At an impact parameter of $5.7''$, or roughly 20 h_{65}^{-1} kpc at the absorption redshift, the neutral gas in G1 obviously extends to greater radii than the stars visible in either the optical or infrared images. It is possible that G1 is actually the bulge of a low surface brightness disk which we do not detect in our present images. However, it seems more likely in view of the optical and spectroscopic evidence as well as the K-band magnitude and R-K color that it is a regular, slightly under-luminous galaxy with an extended HI disk.

6.2.4 The $z_{abs} = 0.0912$ Candidate Host Galaxy

The QSO is surrounded by a roughly circular region of emission that has a surface brightness that ranges from 22.8 to 23.2 mag arcsec^{-2} in the smoothed image (Figure 6.2. The faint object seen near the QSO in the R-Band images of Rao and Turnshek (1998) and Le Brun et al. (1993) corresponds to the elongated linear feature running nearly directly west from the southwest part of the QSO in Figure 6.2. It has an average surface brightness of 23.0 mag/arcsec^2 and a total apparent magnitude of $m_K = 20.1$ mag, measured in the smoothed and PSF subtracted image. On the other side of the QSO, there is a distinct arc feature to the southeast. This is separate from, but concentric with the bulk of the light around the QSO, and looks like the arm of a spiral galaxy seen face-on. It has an average surface brightness of 23.0 mag/arcsec^2 and a total apparent magnitude $m_K = 20.4$ mag.

The magnitudes of both the arm and the linear feature correspond to ~ 0.002L* at a redshift of $z = 0.09$, but this is not unexpected since it is unlikely that either feature is an entire system at that redshift. If the linear feature is an edge-on galaxy at the QSO emission redshift of $z_{em} = 0.635$, it would have an absolute magnitude which is L~ 0.1L*. The measured surface brightness of the linear feature in the R-band is $\mu_R = 25.3$ mag arcsec^{-2}, barely larger than the 25.4 mag arcsec^{-2} 1σ limiting surface brightness in the image (Rao and Turnshek 1998). Using this information we derive a color R-K≈ 2.5 for the linear feature and a lower limit to the color of the

spiral arm of R-K$>$ 2.5. This is consistent with the colors of typical spiral galaxies (de Jong 1996b).

Excluding the linear feature, the angular diameter of the nearly concentric structure around the QSO is about $10''$, although there is a hint of even lower surface brightness emission further to the northwest which, if real, would increase the angular diameter to $\sim 13''$. At a redshift of $z = 0.0912$ this corresponds to 17.5 h_{65}^{-1} kpc. Galaxies are usually smaller in the infrared than in the optical; Jarret (2000) finds that the K-Band isophotal diameter of 2MASS galaxies measured at 20 mag arcsec^{-1} is typically 60-75 % of the B-Band optical radius measured at 25 mag arcsec^{-1}. The K-Band to B-Band diameter ratio is smaller for late-type spirals and larger for early-types and ellipticals. The concentric structure in our field has a surface brightness of 23.0 mag arcsec^{-2} measured at a radius of 10 h_{65}^{-1} kpc. If we assume a scale length of 2.3 h_{65}^{-1} kpc, a common value among spirals in the K-Band (de Jong 1996a), we find that the surface brightness would be 20 mag arcsec^{-2} at a diameter of $d_{20} \sim 7.5\ h_{65}^{-1}$ kpc. This corresponds to a diameter $10 < d_{25} < 12.5$ kpc in the B-Band. Although isophotal diameters are not the best way to compare the sizes of galaxies and our numbers are crudely estimated, the concentric fuzz is a reasonable size for a spiral galaxy at $z = 0.09$.

McLure et al. (1999) have studied the host galaxies of low redshift luminous quasars. They find that all radio loud quasars and most radio quiet quasars with $M_R \leq -24.0$ mag have luminous (L$\sim$ 2L*), large (average scale length $\sim 8\ h_{65}^{-1}$ kpc), elliptical host galaxies. The R-band image of the 0738+313 QSO is saturated (Rao and Turnshek 1998), but the QSO has an apparent B-band magnitude of 16.1 mag, and assuming B-R$\sim$ 1, $M_R \sim -27$, and is certainly brighter than the McLure et al. cutoff magnitude. An L$\sim$ 2L* galaxy would have a K-band magnitude of $M_K \approx -25.3$ mag, or an apparent magnitude of $m_K \approx 16.8$ mag. The typical scale length of 8 kpc corresponds to $1.3''$ at the QSO redshift of $z_{em} = 0.635$, while the blanked-out QSO in Figure 6.2 has a radius of just over $2''$. Based on this information, a portion of the fuzz surrounding the QSO could well be the QSO host galaxy.

The probable contribution of a QSO-host galaxy at a redshift $z = 0.653$ and the faint nature of the emission in the K-band image, make it difficult to draw firm conclusions about the nature of the $z = 0.0912$ absorber. The interpretation that it is a spiral galaxy viewed face-on is consistent with both the narrow velocity 21cm absorption features and the suggestion of spiral arm structure in the K-band image. The galaxy must lie at a very small impact parameter, centered nearly on the QSO sight line, and is very red in color. It most likely accounts for some or all of the structure seen around the QSO in Figure 6.2. Deeper optical images to obtain better color information and/or images at smaller angular resolution would both help to distinguish the QSO, its host-galaxy, and the foreground absorbing galaxy at $z = 0.0912$.

6.3 B 1127−145

6.3.1 The Observations

A J-Band image for B 1127-145 was obtained with the ESO 3.5m New Technology Telescope (NTT) and the SofI (Son of Isaac) instrument on 10 February 1999. The pixel scale is $0.292''$ per pixel over the $4.9'$ field of view, and the seeing was $0.8''$. Instead of observing in a repeating dither pattern, the telescope was "jittered" in a series of random offsets that optimize sky background filtering (Devillard 1999). Each frame had a 2-minute integration, and the total integration time was 80 minutes. The data were reduced with the pipeline data reduction package ECLIPSE developed specifically for use with SOFI and ISAAC data. Data were dark subtracted, flat fielded with dome flats, sky subtracted, shifted and added together to form one image using the JITTER routine. The resulting J-band image is presented in Figure 6.3. Figure 6.4 shows the region closest to the QSO after PSF subtraction and smoothing to bring out the extended low-surface brightness structures. The PSF of nearby stars has also been subtracted in this image.

6.3.2 Objects in the Field

The galaxy-rich field around B 1127-145 makes a sharp contrast to the relatively empty field around B 0738+313, and includes two large luminous disk galaxies, G1 to the east and G2 to the northeast of the QSO. Bergeron and Boissé (1991) obtained emission spectra for these two galaxies which have emission lines at average redshifts of $z_1 = 0.3130 \pm 0.0007$ and $z_2 = 0.3119 \pm 0.0002$ respectively. They chose the disturbed edge-on disk galaxy G1 as the likely host galaxy for the $z = 0.3129$ Mg II absorption, despite its large impact parameter of $b \geq 42\ h_{65}^{-1}$ kpc. Both G1 and G2 present obviously disturbed profiles in the J-band image and appear to be interacting, implying that tidally generated arms or debris may extend to the QSO sight line.

On the west side of the QSO and separated from it by $3.7''$, is a faintly visible knot labeled G3. In optical images the fuzz around G3 is not visible, and the knot has a spectroscopic redshift of $z_3 = 0.3121 \pm 0.0002$ (Lane et al. 1998). G4, the bright, compact object nearly $6''$ to the east-southeast of the quasar is visible in optical images as well, and does not have a known spectroscopic redshift.

There are two faint patches of fuzz, one to the northwest and one to the southwest of the QSO. These are clearly separate from the QSO image. It is unclear if these patches and G4 are three separate objects, or whether they are connected by even lower surface brightness material not detected here. The small condensation just below G1 does not appear in optical images of the field. We call this G5, as it may be a high redshift dropout galaxy. The QSO B 1127-145 has an emission redshift of $z = 1.187$, at which redshift its host galaxy should fall completely under the QSO PSF.

In Table 6.1 we present a summary of the objects near the B 1127-145 sight line. In columns 2-4 we list the angular separation between the quasar center and the
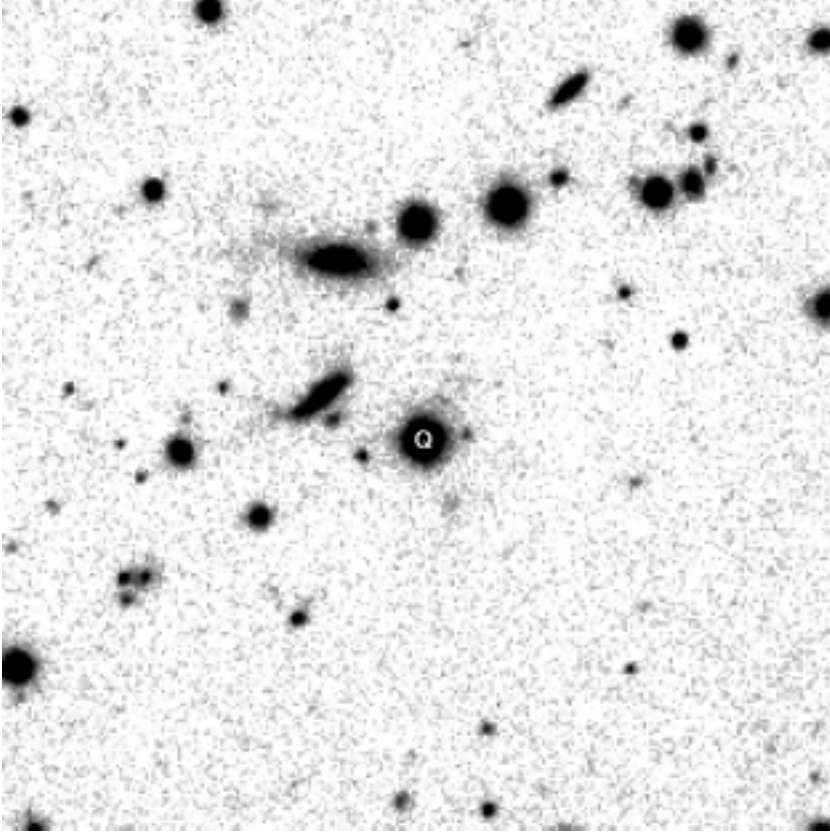
Figure 6.3: J-Band image of the B 1127-145 field. The QSO is labeled Q. The pixel scale is 0.292″, and the seeing is $\approx 0.8″$. The entire image extends 1′15″ by 1′15″. The 3σ limiting surface brightness is 22.9 mag/arcsec².

objects in terms of $\Delta\alpha$, $\Delta\delta$, and the true separation $\Delta\theta$. In column 5 we convert $\Delta\theta$ to a projected physical distance, or impact parameter, b. In column 6 we list the peak surface brightness, and in column 7 we give the total magnitude of each object, measured from the unsmoothed image. Column 8 lists the spectroscopic redshift if known. The k-corrected M_J of each object listed in column 9 is calculated at a redshift of $z = 0.313$.

No J-Band luminosity function of galaxies is currently available in the literature. To place the absolute magnitudes for this field into some context, we convert them
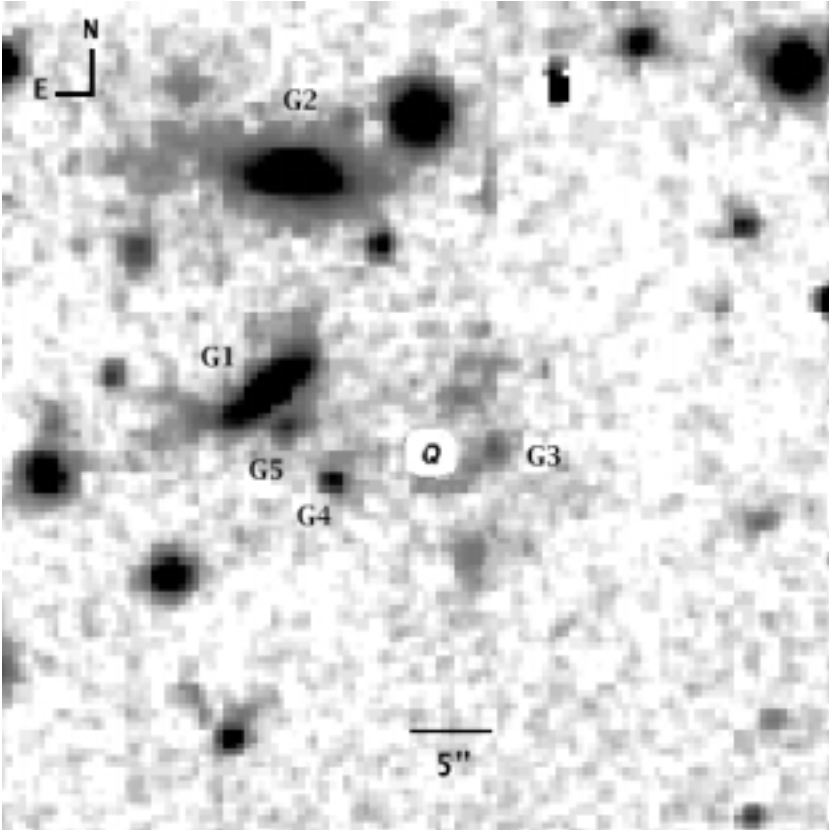
Figure 6.4: Extract from the J-Band image of the B 1127-145 field. The PSF of the QSO has been subtracted and the image has been smoothed to bring out the faint structure. The entire image extends 1′ by 1′. At a redshift $z = 0.313$, 5″ is about 22 h_{65}^{-1} kpc.

to K-band values using the color relationship J-K$\approx$ 1 which applies to all galaxy types (Jarrett 2000). For field galaxies, $M_K^\star = -24.5$ (Loveday 2000) when $H_o = 65$ km s^{-1} Mpc^{-1}. The estimated K-band luminosities for G1 and G2 are L$\sim$ 0.25L* and L$\sim$ 0.6L* respectively, while G3 has L$\sim$ 0.01L*. If we assume that the NW and SW fuzz are part of a single LSB galaxy with G3 at the center, then the total magnitude is $M_J = 20.3$ mag, or L$\sim$ 0.04L*. The three components span about 50 - 60 h_{65}^{-1} kpc at the redshift of G3, which would be a large diameter for a galaxy this faint.

The complex H I 21 cm absorption profile for this system contains at least 5 com-

Table 6.1: Objects in the B 1127-145 Field

Object	$\Delta\alpha$ (arcsec)	$\Delta\delta$ (arcsec)	$\Delta\theta$ (arcsec)	b^a (kpc)	Peak μ_J mag arcsec^{-2}	m_J mag	redshift	M_J mag
G1	9.0	4.0	9.8	42.5	18.8	17.9 ± 0.1	0.3132	-22.5
G2	7.7	16.1	17.9	77.7	18.7	17.4 ± 0.1	0.3125	-23.0
G3	-3.7	0.4	3.7	16.1	21.5	21.9 ± 0.3	0.3121	-18.5
G4	5.4	-1.5	5.6	24.3	20.9	20.9 ± 0.2		-19.5
G5	8.1	1.8	8.3	36.0	21.3	21.0 ± 0.2		-19.4
NW fuzz	-1.9	3.3	3.8	16.5	22.5	21.2 ± 0.3		-19.3
SW fuzz	-2.6	-5.7	6.2	26.9	22.7	21.6 ± 0.3		-20.1

$^a H_o = 65$ km s^{-1} Mpc^{-1}

ponents spanning a velocity of about 85 km s^{-1} (Chapter 4). Similarly, the Mg II, Fe II, and Mg I metal-lines are all very strong. The Mg II $W_o^{\lambda 2796} = 2.21$ Å corresponds to a velocity width of 240 km s^{-1}. The H I column density $N_{HI} = 5.1 \pm 0.9 \times 10^{21}$ cm^{-2} is also very large. The absorption lines indicate a large amount of neutral and low ionization gas spread over a wide velocity range, such as might be found in a large spiral galaxy viewed at high inclination.

Of the large bright spirals in the field, it seems unlikely that G1, at a projected separation from the QSO of 43 kpc, could be responsible for the multi-component velocity structure and total column density of H I gas observed, and G2 is even more distant. If the NW fuzz, SW fuzz, and G3 are all part of one LSB galaxy, the projected separation of 16 kpc is much more reasonable, but the redshift of G3, $z = 0.3121 \pm 0.0003$ is slightly lower than the observed absorption redshift of $z = 0.3129 \pm 0.0003$. The difference in redshift corresponds to $\Delta V \approx 240 \pm 125$ km s^{-1}, which is larger than the velocity spanned by the H I 21cm absorption, but not inconsistent with the spread of the Mg II absorption.

Observations of nearby tidally interacting galaxies show that gas with a broad velocity dispersion and high H I column density can be found well-outside the optical emission regions of the galaxies in compact groups (eg. Williams et al. 1991). In CDM-based theoretical models, Haehnelt, Steinmetz, and Rauch (1998, also Rauch et al. 1997) show that the observed velocity profiles of metal lines in DLA systems can be explained by the interactions of small (proto)galaxies. Taking into account the three galaxies for which the spectroscopic redshifts are known, the disturbed appearances of the two spirals, the broad velocity spread of the absorption lines and the presence of a number of other small galaxies and low surface brightness objects near the QSO, we propose an alternate source for the observed absorption: *interaction gas in a small group of galaxies*. Future observations such as spectroscopy of the other galaxies in the field and narrow-band imaging will be necessary to prove or disprove this theory.

6.4   Summary

We have presented near infrared images for three low redshift DLA/21cm absorbers in two fields. We argue that the $z = 0.2212$ absorber toward B0738+313 arises in the outskirts of an elliptically shaped galaxy which lies at a separation of 20 h_{65}^{-1} kpc from the QSO sight line, and has L= 0.1L* in the K-Band. The $z = 0.0912$ absorber appears to fall under the image of the QSO and its host galaxy. We deduce its face-on nature from the H I 21cm absorption profile, and suggest that an LSB feature shaped like a spiral arm may in fact be part of the host-galaxy. The absorber at $z = 0.313$ toward B1127-145 most likely arises in interaction gas among a small group of galaxies near the QSO sight line.

The images presented in this chapter are part of a larger program to image the fields of low- and moderate- redshift DLA/21cm absorbers in an effort to better characterize their host galaxies. They add to the growing body of evidence which suggests that there is no "typical" host galaxy for DLA/21cm absorbers at these redshifts.

References

Bergeron, J. and Boissé, P. 1991, A&A, 243, 344

Burbidge, E. M., Beaver, E. A., Cohen, R. D., Junkkarinen, V. T., and Lyons, R. W. 1996, AJ, 112, 2533

Carilli, C. L., Lane, W., de Bruyn, A. G., Braun, R., and Miley, G. K. 1996, AJ, 111, 1830

Cohen, R. D., Beaver, E. A., Diplas, A., Junkkarinen, V. T., Barlow, T. A., and Lyons, R. W. 1996, ApJ, 456, 132

de Jong, R. S. 1996a, A&A, 313, 45

de Jong, R. S. 1996b, A&A, 313, 377

Devillard, N. 1999, in *ASP Conf. Ser. 172: Astronomical Data Analysis Software and Systems VIII*, Vol. 8, (San Francisco: Astronomical Society of the Pacific), 333

Haehnelt, M. G., Steinmetz, M., and Rauch, M. 1998, ApJ, 495, 647

Jarrett, T. H. 2000, PASP, 112, 1008

Jerjen, H., Binggeli, B., and Freeman, K. C. 2000, AJ, 119, 593

Lane, W., Briggs, F., and Smette, A. 2000, ApJ, 532, 146

Lane, W., Smette, A., Briggs, F., Rao, S., Turnshek, D., and Meylan, G. 1998, AJ, 116, 26

Le Brun, V., Bergeron, J., Boissé, P., and Christian, C. 1993, A&A, 279, 33

Le Brun, V., Bergeron, J., Boisse, P., and Deharveng, J. M. 1997, A&A, 321, 733

Levshakov, S. A., Chaffee, F. H., Foltz, C. B., and Black, J. H. 1992, A&A, 262, 385

Loveday, J. 2000, MNRAS, 312, 557

McLure, R. J., Kukula, M. J., Dunlop, J. S., Baum, S. A., O'Dea, C. P., and Hughes, D. H. 1999, MNRAS, 308, 377

Pei, Y. C., Fall, S. M., and Bechtold, J. 1991, ApJ, 378, 6

Pettini, M., Ellison, S. L., Steidel, C. C., and Bowen, D. V. 1999, ApJ, 510, 576

Prochaska, J. X. and Wolfe, A. M. 1997, ApJ, 487, 73

Prochaska, J. X. and Wolfe, A. M. 1998, ApJ, 507, 113

Rao, S. and Turnshek, D. 2000, astro-ph/9909164

Rao, S. M. and Turnshek, D. A. 1998, ApJ, 500, L115

Rauch, M., Haehnelt, M. G., and Steinmetz, M. 1997, ApJ, 481, 601

Steidel, C. C., Bowen, D. V., Blades, J. C., and Dickenson, M. 1995, ApJ, 440, L45

Steidel, C. C., Dickinson, M., Meyer, D. M., Adelberger, K. L., and Sembach, K. R. 1997, ApJ, 480, 568

Steidel, C. C., Dickinson, M., and Persson, S. E. 1994, ApJ, 437, L75

Turnshek, D., Rao, S., Nestor, D., Lane, W., Monier, E., Bergeron, J., Briggs, F., and Smette, A. 2000, in prep.

Williams, B. A., McMahon, P. M., and van Gorkom, J. H. 1991, AJ, 101, 1957

Wolfe, A. M., Lanzetta, K. M., Foltz, C. B., and Chaffee, F. H. 1995, ApJ, 454, 698

7

Summary and Future Work

In this thesis we have sought to provide insight into how high column density neutral atomic hydrogen gas evolves from the high redshift damped Lyα absorber population to the $z \approx 0$ gas-rich galaxies. Our approach was two-pronged: in the first half of the thesis we present a large survey designed to identify new high column density systems through the H I 21cm absorption line and to study their statistical properties, while in the latter half we attempt to identify and characterize the individual galaxies or systems in which absorbing gas is found. Here we give a brief summary of the main results from this work, before discussing on-going and future projects.

7.1   Survey and Statistics

Chapter 2

The purpose of this research is to bridge the gap between the extensive H I emission studies of high column density H I gas at low redshift and the high redshift, $z > 1.65$, high column density absorbers identified through large surveys for damped Lyα (DLA) absorption. In Chapter 2 we present the data from a WSRT survey for H I 21cm absorption in 62 Mg II-selected absorption systems. Taking advantage of the new UHF-High receivers at the WSRT, our survey included systems at redshifts $0.2 < z < 1.0$. We identify 3 new H I 21cm absorbers: $z_{abs} = 0.2212$ toward the QSO B 0738+313, $z_{abs} = 0.3127$ toward B 1127-145, and $z_{abs} = 0.3941$ toward B 0248+430. In addition we identify a strong candidate absorber at $z_{abs} = 0.432$ toward B 1243-072.

Chapter3

In Chapter 3 we combine our WSRT-survey with 10 Mg II-selected systems from previous H I 21cm surveys (Peterson and Foltz 1980, Briggs and Wolfe 1983). There

are 5 confirmed 21cm absorbers in this combined sample. For the non-detected systems, the data places upper limits on on the quantity $N_{\text{HI}}/< T_{\text{s}} >$, (the column density over the harmonic mean spin temperature). For $< T_{\text{s}} > = 100$ K and velocity widths in the range 5 - 10 km s^{-1}, we are sensitive to H I gas at column densities of $N_{\text{HI}} \geq 1 \times 10^{20}$ atoms cm^{-2} in the majority of our systems, while in some cases this limit is as low as $N_{\text{HI}} \geq 1 \times 10^{19}$ cm^{-2}.

We compare the metal-line properties for the non-detected systems with those of the H I 21cm absorbers. The presence of 21cm absorption does not depend sensitively on the rest equivalent widths Mg II $W_o^{\lambda 2796}$, Fe II $W_o^{\lambda 2600}$, or Mg I $W_o^{\lambda 2852}$. We do find that the detection probability is increased by requiring that both Mg II $W_o^{\lambda 2796}$ and Fe II $W_o^{\lambda 2600}$ be greater than 0.5 Å, however we note that this will preferentially select systems which have H I 21cm absorption in multiple components covering a broad velocity range. Systems which have only a single narrow-velocity H I 21cm absorption component would not be discovered in samples with this selection criteria. It is important to continue to search for an effective way to find the narrow-line absorbers as well as the broad-line absorbers.

Using the known redshift evolution of the number density of Mg II-absorbers, we estimate $\Omega_{HI}(z)$ for subsamples of our survey defined by Mg II $W_o^{\lambda 2796}$ criteria. For Mg II $W_o^{\lambda 2796} > 0.6$ Å, we find $\Omega_{HI}(z = 0.603) = 0.0015$ for $q_0 = 0$ and $H_o = 75$ km s^{-1} Mpc^{-1}. We compare our value to Ω_{gas} values taken from 21cm surveys at $z = 0$ and DLA surveys at high redshift in Figure 7.1.

Despite the large error bars, the new 21cm result is in close agreement with a recent survey for DLA absorption in Mg II-selected systems at similar redshifts. We find that $\Omega_{H\,I}(z)$ is roughly flat from redshifts of about $z = 3.5$ to the $z = 0.63$ mean redshift of our survey, and must decrease to the well-defined value at $z = 0$ at much more recent times, or lower redshifts, than previously thought (eg. Wolfe et al. 1995).

7.2   Individual Absorber Properties

Chapter4

Chapter 4 presents high velocity resolution spectra for each of the three H I 21cm absorbers discovered in the WSRT survey.

The $z_{abs} = 0.3942$ absorber toward B 0248+430 is a multicomponent absorption system with a peak optical depth $\tau \approx 0.2$ and a total velocity spread of ~ 40 km s^{-1}. The (presumably damped) Lyα line has not been detected for this system at the current time. Using the narrow 21cm line velocity widths to place upper limits on the thermal kinematic temperature T_{k}, we estimate a total column density of $N_{\text{HI}} \leq 3.9 \times 10^{21}$ cm^{-2}.

The $z_{abs} = 0.2212$ absorber toward B 0738+313 consists of a single narrow 21cm absorption line, with a peak optical depth of $\sim 10\%$ and a full width at half maximum velocity width of 5.4 km s^{-1}. Measured from fits to the DLA absorption profile, $N_{\text{HI}} = 7.9 \times 10^{20}$ cm^{-2} (Rao and Turnshek 1998), and we estimate a mean harmonic spin temperature of $< T_{\text{s}} > = 735$ K. The velocity width of the 21cm absorption limits the thermal kinetic temperature of the gas to $T_{\text{k}} \leq 635$.
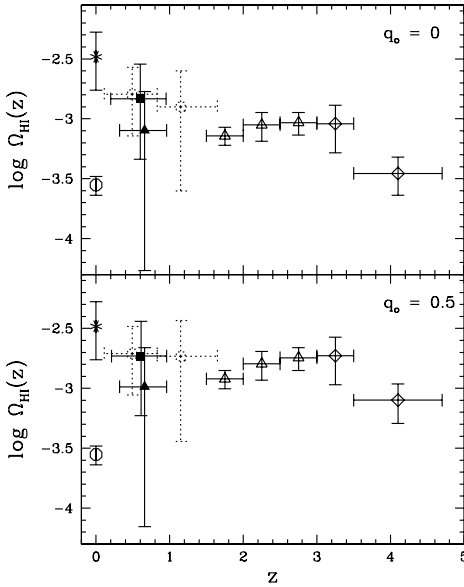
Figure 7.1: $\log \Omega_{HI}(z)$ versus redshift. Vertical bars show 1σ errors, while the horizontal bars indicate bin size. The open diamonds are points from the DLA results of Storrie-Lombardi, et al. (2000), while the open triangles show DLA results from Wolfe et al. (1995). The dotted line open circles are taken from the Rao & Turnshek (2000) low redshift DLA survey, based on Mg II-selected systems with $W_o^{\lambda 2796} > 0.6$ Å. At $z = 0$ the open circle marks Ω_{21cm} measured by Zwaan et al. (1997), and the asterisk is Ω_{stars} as measured by Fukugita, Hogan, & Peebles (1998). The filled square is our 21cm result from the $W_o^{\lambda 2796} > 0.6$ Å sample, while the filled triangle marks the $W_o^{\lambda 2796} > 1.0$ Å result.

The $z_{abs} = 0.3127$ absorber towards B 1127-145 presents a complex, multicomponent absorption profile with a peak optical depth $\tau = 0.11$ and a combined velocity spread of ~ 60 km s^{-1}. The absorption has a so-called "edge-leading" shape, with the deepest absorption component on the high frequency edge of the absorption profile. This is more typically found in metal-line absorption. The column density fit to the DLA absorption is $N_{HI} = 5.1 \times 10^{21}$ cm^{-2} (Rao and Turnshek 2000), and the derived mean harmonic spin temperature $< T_s > = 910$ K. The velocity widths of the individual absorption components to do provide a better temperature constraint for this system.

Chapter 4 concludes with a discussion of the mean harmonic spin temperature $< T_s >$ in redshifted 21cm/DLA absorbers. There is no evidence for redshift evolution over a redshift range $0.1 < z < 3.4$ in this quantity. The roughly inverse relationship between 21cm optical depth and $< T_s >$ seen in Galactic H I clouds is preserved among these high redshift systems, although they have consistently higher $< T_s >$ values than Galactic gas at the same optical depths. The presence of large column densities of warm H I gas, undetected by the cold-gas sensitive 21cm absorption measurements, and/or optical and radio sight line differences could account for this offset.
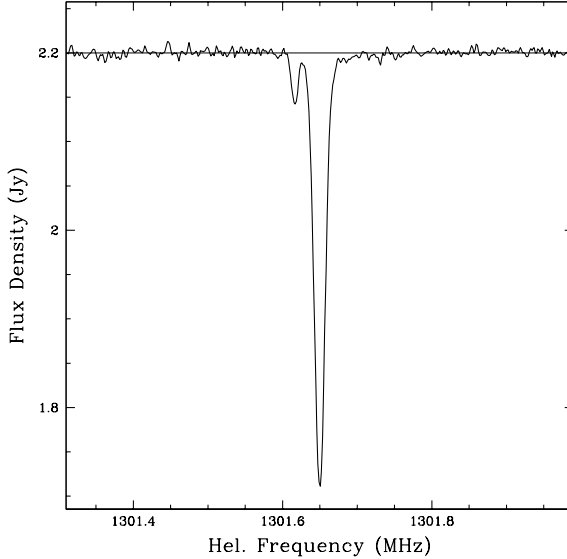
Figure 7.2: An Arecibo spectrum showing the H I 21cm line at $z = 0.0912$ towards the QSO B0738+313. Channel spacing is $0.35 \ \mathrm{km \, s^{-1}}$, allowing this extremely narrow line system to be resolved for the first time. The thin horizontal line marks the continuum level. A second absorption feature is clearly separated from the main line. The shallow feature on the high frequency side of the main absorption is real.

Chapter 5

Chapter 5 contains an in-depth study of the H I gas associated with the DLA absorber at $z = 0.0912$ toward B 0738+313. This is the lowest redshift DLA system for which the Lyα absorption line has been observed. We present VLBA data which shows that the 21cm absorbing gas covers the QSO core, and sensitive WSRT spectra which indicate that it does not cover the very weak radio lobes which extend roughly $30''$ to the north and south. From this we estimate a covering factor of the gas over the radio QSO of $f \leq 0.98$. We also use the WSRT data to place an upper limit on the H I mass in this system of $M_{\mathrm{H \, I}} \leq 2.8 \times 10^9 M_\odot$, which is slightly less than the expected mass of an $L^\star$ galaxy.

Using a very high velocity resolution Arecibo spectrum, shown in Figure 7.2, we are able to resolve three absorption line components in the 21cm profile. Although the harmonic mean spin temperature calculated by comparison of the 21cm lines to the damped Lyα line is $< T_s > = 725 \pm 100$ K, the thermal kinetic temperatures of the two narrow components, calculated from their widths, are much lower: $T_k \leq 297 \pm 3$ and $\leq 103 \pm 10$ K respectively. This is the first case of a redshifted absorption system for which T_k is measured to be significantly *less* than $< T_s >$. We interpret this result in the context of a two-phase gas model, in which the damped Lyα line is sensitive to a significant neutral column density of warm-phase gas as well as the cold-phase gas of the narrow 21cm lines. The third component, visible in Figure 7.2 as a shallow feature on the high frequency side of the main absorption line component, is interpreted as representing the warm-phase gas with with $T_k \leq 5050 \pm 950$ K. The combined column density of the three 21cm components is approximately equal to that derived from fits to the damped Lyα line, $N_{\mathrm{HI}} = 1.5 \times 10^{21} \ \mathrm{cm^{-2}}$.

Chapter 6

Chapter 6 presents near-infrared images of the fields around B 0738+313 and B 1127-145, and discusses the likely host-galaxies for the three DLA/21cm systems on these sight lines. The absorbing gas at $z = 0.2212$ toward B 0738+313 apparently arises in the outskirts of an elliptically shaped galaxy with L≈ 0.1L* in the K-Band. The $z = 0.0912$ absorber on the same sight line is apparently part of a galaxy which falls under the point-spread-function (PSF) of the bright QSO, although there is a faint spiral arm-like structure that extends to a projected separation of $\sim 10\ h_{65}^{-1}$ kpc from the QSO sight line if it has a redshift $z = 0.0912$. The multi-component H I 21 cm absorber at $z = 0.313$ toward B1127-145 most likely arises in interaction gas among a small group of galaxies near the QSO sight line. These three systems add to a growing body of evidence that DLA/21cm absorption does not select a uniform type of galaxy.

7.3   On-going and Future Work

Imaging and Spectroscopy

The near-infrared images presented in Chapter 6 are a small part of an ongoing effort to obtain multi-band colours and spectroscopic redshifts for galaxies in the fields of all QSOs with low- and moderate-redshift DLA/21cm absorbers. The goal is to positively identify the host galaxy for these systems. It was thought that the low-redshift absorbers would be easier to image than their high-redshift counterparts, but in practice the best candidate host-galaxies often lie partially under the PSF of the QSO in our ground-based images. In order to properly image these galaxies it will be necessary to use adaptive optic techniques or obtain *HST* images for these fields.

A Radio-Selected Survey

Optical surveys for QSO absorption lines, and consequently the targeted radio surveys for 21cm absorption such as the WSRT-survey in this thesis, are prone to a number of biases, the effects of which are not completely understood. QSO candidates are selected optically for their point-like appearance in large imaging surveys. This selection criteria can exclude QSOs which lie behind a low-redshift galaxy at very small impact parameter, because the galaxy image will create a fuzzy "halo" around the QSO. These sight lines will then be excluded from the optical QSO absorption line surveys. Because we expect DLA and 21cm absorbers to arise most frequently in the inner parts of their host galaxies, the optical surveys could be biased against these systems at low redshifts. Both the DLA and the metal-line surveys are also limited to the brightest background QSOs, which selects against dusty gas-rich systems.

These biases can be avoided by a blind search for 21cm absorption towards bright background radio sources. The completion of the DZB spectrometer at the WSRT, the recent upgrade to the spectrometer at Arecibo and the planned spectrometer at

the GBT will make it possible to search large ranges of frequency space with good resolution in a time effective manner. The low frequency receivers at the GBT enable an unbroken search from redshift $z = 0$ to $z \approx 4$. A survey can be made for absorption line gas from $z = 0$ to the redshift of each background source (if known, or to the low frequency limits of the receiver if unknown) in a sample defined only by the flux density of the background source. Recent all-sky radio surveys, such as the NVSS Sky Survey, provide a background source catalogue which is complete at the flux density levels for which the absorption experiment will be possible.

Because optical sightlines to quasars are often different from the sightlines to the more extended radio sources, a complete radio survey will provide a unique view of the universe, complementary to that obtained in optical surveys. The 21cm absorption line is weighted by the spin temperature, T_s, of the gas, emphasizing the coldest and lowest velocity dispersion absorbers. Therefore, a 21cm absorption survey would also be complementary to 21cm emission surveys at very low redshifts, and able to detect any extremely low T_s clouds which are hidden from the emission experiments. Furthermore, a radio survey can detect H I-rich absorbers against optically dim background sources, thus facilititating the optical identification and study of their host galaxies.

References

Briggs, F. H. and Wolfe, A. M. 1983, ApJ, 268, 76

Fukugita, M., Hogan, C. J., and Peebles, P. J. E. 1998, ApJ, 503, 518

Peterson, B. M. and Foltz, C. B. 1980, ApJ, 242, 879

Rao, S. and Turnshek, D. 2000, astro-ph/9909164

Rao, S. M. and Turnshek, D. A. 1998, ApJ, 500, L115

Storrie-Lombardi, L. and Wolfe, A. 2000, astro-ph/00060444

Wolfe, A. M., Lanzetta, K. M., Foltz, C. B., and Chaffee, F. H. 1995, ApJ, 454, 698

Zwaan, M. A., Briggs, F. H., Sprayberry, D., and Sorar, E. 1997, ApJ, 490, 173

Nederlandse Samenvatting

Melkwegstelsels

In de jaren twintig van de twintigste eeuw bewees Edwin Hubble overtuigend dat melkwegstelsels, die oorspronkelijk 'nebulae' genoemd werden vanwege hun wolk-achtig uiterlijk, niet alleen buiten onze Melkweg staan, maar ook dat ze erg op onze Melkweg lijken. Al deze melkwegstelsels werden ondergebracht in een classifica-tiesysteem dat gebaseerd was op uiterlijke kenmerken. Stelsels die op draaikolken of spiralen leken, werden spiraalstelsels genoemd. Deze werden verder onderver-deeld in stelsels die een balk in de binnendelen leken te hebben, de balkspiralen, en die zonder balk. Stelsels met weinig zichtbare structuur, en die een ovaal en glad uiterlijk hadden, werden elliptische stelsels genoemd. Alle overige melkwegstelsels werden voor het gemak onregelmatig genoemd. Deze eenvoudige classificatie, hoe-wel niet heel nauwkeurig, bleek nuttig, en wordt, met een paar kleine toevoegingen, nog steeds door sterrenkundigen gebruikt. De belangrijkste toevoegingen zijn de dwergstelsels, die erg klein zijn, de zogeheten lage-oppervlaktehelderheidsstelsels, die erg lichtzwak zijn, en interacterende stelsels met bizarre vormen, die het gevolg zijn van een botsing tussen twee melkwegstelsels.

Melkwegstelsels bestaan uit vier hoofdingredienten: sterren, gas, stof, en don-kere materie. De eerste drie zijn zichtbaar, de vierde, donkere materie, is vereist om de verdeling en de beweging van de zichtbare componenten te verklaren, maar het is nog niet direct waargenomen. Van het gas en de sterren is bekend dat ze hoofdzake-lijk uit waterstof bestaan, terwijl het stof vooral uit silicaten bestaat, maar niemand weet wat de donkere materie nu precies is. Elliptische stelsels hebben doorgaans weinig gas en stof, en bestaan hoofdzakelijk uit sterren. De spiraalstelsels, aan de andere kant, hebben meestal juist veel gas, wellicht ook veel stof, en ook veel ster-ren. De samenstelling van de andere stelsels is minder duidelijk.

De HI 21 cm lijn

In de Melkweg en andere dichtbijstaande melkwegstelsels is de gemakkelijkste ma-nier om het waterstof waar te nemen de HI 21 cm emissielijn te meten. Neutraal ato-mair waterstof, afgekort tot HI, zendt straling uit met een golflengte van 21 cm, maar

het absorbeert het ook. Toen wetenschappers voor het eerst de verdeling van golf-lengten, ook wel een spectrum genoemd, bekeken van het licht dat de verschillende elementen uitzenden, viel het hun op dat het spectrum eruit zag als een verzameling smalle, heldere lijnen tegen een donkere achtergrond. Omgekeerd, straling die ge-absorbeerd werd, zag er uit als een verzameling donkere lijnen tegen een constante, heldere achtergrond. Tegenwoordig meten sterrenkundigen vaak de intensiteit en de golflengte van de uitgezonden of de geabsorbeerde straling, zodat ze de spec-tra kunnen weergeven in grafiek van intensiteit tegen golflengte. Toch zijn de oude termen van emissie- en absorptielijnen in gebruik gebleven.

Door het intensiteitsprofiel van de 21 cm emissielijn waar te nemen met een radi-otelescoop, kunnen sterrenkundigen op een eenvoudige manier de ruimtelijke ver-deling van waterstof in een melkwegstelsel in kaart brengen. Een vergelijking van een optische afbeelding van de sterren met een afbeelding van het gas in een melk-wegstelsel, laat zien dat gas en sterren een tamelijk verschillende verdeling hebben alhoewel de grootste concentraties van gas wel rond gebieden worden gevonden waar sterren gevormd worden. Sterren zijn over het algemeen meer geconcentreerd naar het centrum, waar ze een verdikking vormen die door sterrenkundigen 'bulge' genoemd wordt. De waterstofverdeling heeft daarentegen vaak een klein gat in het midden. Verder strekt de HI verdeling zich vaak verder uit in radius dan die van de sterren, en het kan ook vervormingen en onregelmatigheden hebben die niet zicht-baar zijn in de verdeling van de sterren. Vaak onthullen deze vervormingen dat het melkwegstelsel een interactie ondergaat met naburige stelsels, ondanks dat het optisch geïsoleerd lijkt.

De totale massa van het gas, gebruikelijk uitgedrukt in zonsmassa's, ook wel $M_{\odot}$, kan worden uitgerekend door alle emissie profielen van een heel stelsel bij elkaar op te tellen. Een typisch spiraalstelsel heeft een gasmassa van ongeveer 5×10^9 $M_{\odot}$. Maar astronomen zijn ook geïnteresseerd in het totale aantal atomen langs een be-paalde gezichtslijn, waarvoor een cilinder met een oppervlak van 1 cm^2 genomen wordt. Dit wordt de kolomdichtheid van het gas genoemd, N_{HI}. Een typisch stel-sels heeft zo'n 10^{22} HI atomen per cm^2 in de buurt van het centrum, afnemend tot zo'n 10^{18} HI atomen per cm^2 of zelfs lager aan de randen. Deze twee grootheden, de HI massa en de kolomdichtheid, maken het mogelijk om waterstof in verschillende stelsels op een zinnige manier met elkaar te vergelijken.

Waarnemingen van HI kunnen sterrenkundigen ook wat vertellen over de be-wegingen en de temperatuur van het gas. De golflengte van 21 cm komt overeen met een frequentie van 1420.4 MHz. We noemen dit de rustfrequentie omdat gas dat naar ons toe beweegt, en het gas dat van ons afbeweegt langs de gezichtslijn een net iets andere frequentie lijkt te hebben. Dit wordt het Doppler-effect genoemd. Dit is vergelijkbaar met de verandering in toonhoogte, dat wil zeggen de frequentie die ge-hoord wordt, van een sirene van een brandweerwagen die voorbij raast. Eerst komt de sirene naar de luisteraar toe en de sirene klinkt hoger. Als het voertuig voorbij komt en wegspoedt, klinkt de sirene lager. In de sterrenkunde zeggen we dat de straling van een bron die wegbeweegt van de aarde roodverschoven is omdat het de aarde bereikt met een lagere frequentie, en dus een langere golflengte dan waarop het was uitgezonden. Omgekeerd, straling van een bron die naar de aarde toekomt

is blauwverschoven, en lijkt een hogere frequentie te hebben.

Binnenin een wolk van waterstofgas bewegen alle atomen willekeurig door elkaar heen. Daarom zal, op elk tijdstip, een grote fractie van de atomen geen snelheid langs de gezichtslijn hebben, terwijl de rest snelheden heeft tussen nul en de maximum snelheid binnen de wolk. We zullen dus veel emissie zien op de rustfrequentie, en een deel dat verschoven is door het Doppler-effect. Als we nu in een grafiek de emissie tegen de frequentie uitzetten, ziet het er klokvormig, ofwel Gaussisch, uit. De breedte van deze kromme hangt af van de maximumsnelheid van de atomen, die op zijn beurt weer afhangt van de kinetische temperatuur van het gas. Ruwweg is het zo dat warmer gas sneller beweegt en daarom bredere emissielijnen zal vertonen. Op deze manier kan de 21 cm lijn gebruikt worden om de temperatuur van het gas te meten.

Naast de interne bewegingen hebben de meeste HI wolken ook nog een globale snelheid ten gevolge van hun bewegingen binnen het melkwegstelsel. Dit maakt dat de centrale frequentie van de emissie lijn verschuift, omdat de atomen nu een gemiddelde snelheid langs de gezichtslijn hebben. Door de centrale verschuiving van vele verschillende wolken binnen een melkwegstelsel te meten, en dat te combineren met informatie over waar deze wolken zich bevinden, kan men de grote schaal bewegingen in het melkwegstel in kaart brengen. Bovenop de verschuiving in frequentie door de beweging van elke afzonderlijke wolk, worden de emissielijnen ook nog verschoven door de bewegingen van melkwegstelsels als geheel ten opzichte van onze Melkweg.

Het begrip roodverschuiving

Ons helaal dijt uit. Daarom beweegt alles wat zich buiten onze Melkweg bevindt zich van ons af, op een aantal zeer nabije objecten na. Dit kunnen we begrijpen door eerst te denken aan een ballon met twee stippen erop. Het maakt niet uit waar die stippen staan, als de ballon opgeblazen wordt bewegen de stippen zich van elkaar weg. Het oppervlak van een ballon is echter tweedimensionaal, terwijl het heelal drie dimensies heeft. Denk daarom eens aan het deeg voor een krentenbrood. Als we dit laten rijzen, zet het deeg tussen de krenten uit en de afstand tussen de krenten wordt groter. De uitzetting is gelijk in alle delen van het deeg en heeft geen vast centrum. Het effect van het uitzetten is dus dat alle krenten zich van elkaar weg lijken te bewegen.

In het heelal is de ruimte zelf het rijzende deeg, en de melkwegstelsels en de clusters van melkwegstelsels zijn de krenten. Doordat de ruimte uitzet, wordt de ruimte tussen de stelsels groter. Omdat het moeilijk is de ruimte zelf te zien, maar makkelijk om de stelsels erin te zien, zeggen sterrenkundigen dat stelsels zich van elkaar af bewegen. Net zoals bij de krenten in het rijzende deeg, zo ziet de uitdijing van het heelal er hetzelfde uit vanuit elk gezichtspunt. Omdat wij ons in onze Melkweg bevinden, maken we dat ons referentiekader en zeggen we dat de rest van het heelal zich van ons af beweegt.

Het resultaat van deze uitdijing, dat wil zeggen het feit dat alles van de aarde

weg lijkt te bewegen, is dat de straling van de meeste bronnen buiten onze Melkweg roodverschoven wordt. Sterrenkundigen definiëren de roodverschuiving z van een object op basis van de verschuiving in frequentie van de straling. Voor de 21 cm geeft dat:

$$(1 + z) = \frac{1420.4058 \; MHz}{verschoven \, frequentie \; MHz}.$$

Uit deze vergelijking blijkt dat z eenheidloos en makkelijk uit te rekenen is.

Als we de ruimte zouden opdelen in aparte eenheden, dan zou elke eenheid eenzelfde hoeveelheid uitdijen in dezelfde tijd. Stel je nu drie objecten voor in de ruimte, twee slechts een klein beetje uit elkaar, en een derde veel verder weg. Na een bepaalde tijd is de afstand tussen de twee nabije objecten slechts een klein beetje toegenomen, maar de afstand tot het verre object is veel meer toegenomen. Objecten die verder weg staan, lijken dus sneller van ons af te bewegen dan die die dicht bij staan. Omdat de grootte van de verschuiving in frequentie ten gevolge van het Doppler-effect groter wordt voor een grotere snelheid, hebben objecten op een grotere afstand dus een grotere roodverschuiving z.

Onze Melkweg heeft een roodverschuiving van $z = 0$, en de melkwegstelsels in onze omgeving hebben een roodverschuiving van $z \approx 0$. Het verst bekende object heeft een roodverschuiving van $z \approx 6$. De eenvoudigheid van zijn definitie, en de precisie waarmee het gemeten kan worden, maakt z erg bruikbaar voor sterrenkundigen. Het kan omgerekend worden tot een meer gewone afstand, maar slechts door het te combineren met de uitdijingssnelheid van het heelal, maar helaas is die niet nauwkeurig bekend.

Sterrenkundigen zijn net zo zeer geïnteresseerd in objecten die ver van ons weg zijn, dat wil zeggen die een grote roodverschuiving hebben, als die die dichtbij staan. Licht beweegt met een constante snelheid, dus als een object verder weg staat, doet het licht er langer over om ons te bereiken. Dat betekent dat het licht dat we zien van een verweggelegen melkwegstelsel veel ouder is dan dat van een nabij melkwegstelsel. Net zoals wij op de foto's in een fotoboek jonger zijn in de oudere foto's, zo kunnen we de verweggelegen melkwegstelsels beschouwen als jongere versies van nabije melkwegstelsels. Dus eigenlijk betekent naar een hogere roodverschuiving kijken hetzelfde als naar een jonger heelal kijken. Op deze manier proberen sterrenkundigen zich een beeld te vormen van de globale evolutie van het heelal en de melkwegstelsels die zich erin bevinden

HI 21 cm absorptie

De helderheid van de 21 cm emissie lijn neemt af met het kwadraat van de afstand tot het gas. Als gevolg daarvan kan waterstof op grotere afstanden niet gemeten worden in 21 cm emissie met bestaande radiotelescopen. Om het HI gas toch te kunnen bestuderen in melkwegstelsels die ver weg staan, zijn sterrenkundigen afhankelijk van absorptielijnen. Wanneer licht van een sterke achtergrondbron door een wolk van waterstof heen valt, dan absorberen de atomen straling op dezelfde frequentie

als ze die anders uitzenden. De achtergrondbron werkt als een zaklamp die alles op een lijn tussen ons en zichzelf verlicht. Deze lijn wordt de gezichtslijn genoemd. Absorptielijnen nemen niet af in sterkte als de afstand groter wordt, en zijn daarom dus ideaal voor studies van objecten op grote roodverschuiving.

Elk object dat op een relatief constant niveau straling uitzendt over een groot bereik aan frequenties kan gebruikt worden als achtergrondbron. Een van de beste bronnen is een quasar, ook wel quasi-stellair object (QSO) genoemd. Een quasar ziet er in zichtbaar licht uit als een ster, maar het is in werkelijkheid iets heel anders. Quasars zenden extreem veel straling uit over een groot bereik aan frequenties en komen vrij veel voor op grote roodverschuiving (maar zijn zeldzaam in onze omgeving), en dat maakt ze ideale achtergrondbronnen. Ondanks dat ze er in het optisch als een puntbron uitzien, zijn de meeste quasars uitgebreider op de frequentie van 21 cm absorptie. Door een radiotelescoop te gebruiken met voldoende oplossend vermogen kunnen sterrenkundigen dus soms met één quasar verscheidene gezichtslijnen door het tussenliggende absorberende object, kortweg de absorbeerder genoemd, bestuderen.

Net zoals de emissielijn, geeft de HI 21 cm absorptielijn informatie over de temperatuur, hoeveelheid en snelheidsverdeling van het gas. Maar terwijl de 21 cm emissielijn het HI gas makkelijk kan worden gedetecteerd over een groot bereik aan temperatuur en kolomdichtheid, worden absorptielijnen meestal slechts gevonden in het koudste gas met de hoogste kolomdichtheden. Emissie is zichtbaar op elke positie in een melkstelsel, maar om 21 cm absorptie te zien moet de gezichtslijn naar de quasar vlak langs het centrum van een melkwegstelsel gaan, daar waar er aardig wat koud gas is. Dit beperkt het aantal melkwegstelsels op grote roodverschuiving dat bestudeerd kan worden, en ook beperkt het de informatie over elk stelsel dat 21 cm absorptie veroorzaakt tot één of op zijn best een enkele gezichtslijnen.

Vanwege de noodzaak dat de achtergrondquasar en de absorbeerder op een gezichtslijn moeten staan, is het vinden van 21 cm in absorptie door op een willekeurige manier heldere quasars waar te nemen niet bepaald efficiënt. Dit probleem wordt verergerd door de beperkingen van de meeste radiotelescopen, die effectief slechts één roodverschuiving per meting kunnen bekijken, en die bovendien slechts een relatief beperkt bereik in roodverschuiving kunnen doorzoeken. Daarom zijn er tot nu toe slechts een handvol 21 cm absorbeerders gevonden.

Radiosterrenkundigen die 21 cm in absorptie proberen te vinden hebben dus een manier nodig om van te voren gezichtslijnen door melkwegstelsels die waarschijnlijk veel neutraal waterstof bevatten te selecteren. Het blijkt dat neutraal atomair waterstof ook straalt en absorbeert op een aantal frequenties in het optische en het UV gebied. Een van deze, de Lyman-α lijn genoemd, is uitgesproken sterk en makkelijk te identificeren. Het kan gevonden worden in optische spectra genomen vanaf de grond in objecten met roodverschuivingen groter dan $z > 1.65$, en op lagere roodverschuivingen in UV spectra genomen vanuit de ruimte, zoals met de Hubble ruimtetelescoop. Als de kolomdichtheid van HI erg hoog is, heeft de absorptielijn een een herkenbaar profiel en het object waarin de absorptie plaats vindt wordt dan een gedempte Lyman-α (DLA) absorbeerder genoemd. Zulke systemen zijn ideale kandidaten om 21 cm in absorptie te vinden. Jammer genoeg zijn tot heden ook relatief

weinig (minder dan 100) DLA absorbeerders gevonden, en slechts een derde van deze ligt voor een quasar die ook radiostraling uitzendt. Van deze radiokandidaten liggen er veel in een bereik dat niet met voldoende gevoeligheid met bestaande radiotelescopen kan worden waargenomen om de absorptie te detecteren.

Hoewel het gas in melkwegstelsels bijna alleen uit waterstof bestaat, is dat gelukkig nooit helemaal het geval. Normaal gesproken zijn er kleine hoeveelheden van andere elementen en zelfs moleculen aanwezig. Het viel sterrenkundigen op dat bepaalde elementen zoals magnesium en ijzer in alle systemen met hoge HI kolomdichtheden gevonden werd. Enkelvoudig geïoniseerd magnesium (MgII), wat gewoon magnesium is dat een elektron is kwijtgeraakt, zorgt voor een sterk en makkelijk te vinden paar van absorptielijnen in een optisch spectrum. Het idee om naar 21 cm absorbeerders te zoeken in bekende MgII absorbeerders ontstond voor het eerst laat in de jaren zeventig, en verscheidene nieuwe 21 cm systemen werden met deze techniek gevonden.

Sinds die tijd is er veel gezocht naar MgII absorbeerders over een groot bereik aan roodverschuiving. Statistische analyses van de resultaten maken het voor sterrenkundigen mogelijk om te bestuderen hoe het MgII gas geëvolueerd is van hoge roodverschuiving tot het locale heelal. De gevonden MgII systemen en de statistieken vormen een ideaal gegevensbestand waaruit een verzameling van kandidaatsystemen kan worden geselecteerd dat onderzocht kan worden op HI 21 cm absorptie.

Dit proefschrift

Toen ik mijn proefschrift in 1996 begon, was er een grote lacune in ons begrip van hoe HI evolueert in de loop van de tijd. Waarnemingen vanaf de grond van gedempte Lyman-α absorbeerders maakten een schatting mogelijk van de hoeveelheid HI op roodverschuivingen van $z \geq 1.65$. Op basis van optische afbeeldingen en theoretische modellering kon toen een beeld gevormd worden van de stelsels waarin het HI werd gevonden. Uitgebreide studies van HI emissie in stelsels rond $z = 0$ had al een overvloed aan informatie opgeleverd over de huidige hoeveelheid en plaats van het HI gas. Maar bijna niets was bekend over wat er daartussen gebeurde. Het bereik in roodverschuiving van $z \approx 0$ tot 1.65 bestrijkt echter tussen de helft en twee derde van de leeftijd van het heelal, dus dit was een flinke lacune.

De reden voor de lacune was een gebrek aan telescopen waarmee het HI gas over dat bereik kon worden waargenomen. De situatie voor het vinden van gedempte Lyman-α absorbeerders verbeterde recentelijk door de nieuwe Hubble ruimteteles-scoop, maar het was moeilijk waarneemtijd op dit instrument te verkrijgen, en het zou verscheidene jaren duren voor een groot zoekprogramma compleet zou zijn. In de tussentijd bood een recente verbetering van de Westerbork Synthese Radio Telescoop (WSRT) de mogelijkheid om HI 21 cm absorptie te zoeken in een groot deel van dit bereik aan roodverschuiving.

Het doel van mijn proefschrift is de WSRT te gebruiken om de lacune in onze kennis van het HI gas op te vullen. Het idee was systematisch te zoeken naar 21 cm absorptie in systemen die waren geselecteerd op basis van MgII gehalte, over

het bereik aan roodverschuiving tussen $z = 0.2$ en 1.0. De resultaten van het zoeken konden gebruikt worden om het aantal 21 cm absorbeerders, en de hoeveelheid HI die ze bevatten, te schatten, terwijl de nieuw gevonden systemen gebruikt konden worden om de melkwegstelsels waarin de absorbeerders zich bevinden te identificeren.

In de loop van twee jaar hebben we radio spectra verkregen met de WSRT op de frequenties die overeenkomen met de roodverschuivingen van 62 MgII absorbeerders. We hebben deze spectra gecombineerd met de spectra van 10 MgII absorbeerders die eerder door andere sterrenkundigen waren verkregen, zodat we een totaal aantal van 72 bronnen hadden. Van deze 72, vertoonden er 5 HI 21 cm in absorptie.

Het hoge aantal non-detecties kan ons helpen beter te begrijpen hoe de HI 21 cm absorbeerders verschillen van de MgII absorbeerders. Zo is er bijvoorbeeld een veel hogere kans om 21 cm in absorptie te vinden in systemen met meer MgII. Als de selectiecriteria worden uitgebreid met de eis dat de systemen ook een grote hoeveelheid enkelvoudig geïoniseerd ijzer (FeII) moeten bevatten, dan gaat de detectiekans nog verder omhoog. De 21 cm absorbeerders die veel MgII en FeII bevatten, hebben vaak ook meerdere HI wolken en heel hoge totale kolomdichtheden. Er zijn slechts heel weinig 21 cm absorbeerders die maar een enkele wolk laten zien, en deze systemen hebben niet veel MgII of FeII. Als we er hier meer van willen vinden, moeten we een ander selectiecriterium vinden dat beter werkt dan MgII absorptie.

De oorspronkelijk informatie over HI had gesuggereerd dat het aantal systemen met hoge kolomdichtheden afnam naar lagere roodverschuiving. Onze resultaten stemmen hier mee overeen. Aan de andere kant werd ook gedacht dat de hoeveelheid HI gas zou pieken rond $z = 3$, en dan langzaam zou afnemen naar $z = 0$. Onze resultaten suggereren dat de hoeveelheid HI gas ongeveer constant is tot roodverschuivingen van tenminste zo laag als $z = 0.6$, en pas daarna afnemen tot de waarde bij $z = 0$.

De gedempte Lyman-α absorbeerder met de laagst gevonden roodverschuiving ligt op een roodverschuiving van $z = 0.091$. Een spectrum, genomen met de Arecibo radiotelescoop in Puerto Rico, laat zien dat deze absorbeerder heel uniek is. De meeste 21 cm absorptielijnen zijn verbreed door bewegingen in het gas die niet gerelateerd zijn aan de temperatuur van het gas, en dan is er extra informatie nodig om een waarde voor de temperatuur te vinden. Maar in dit systeem bestaat de 21 cm absorptie uit twee lijnen die extreem nauw zijn, en we waren in staat de temperatuur van het koude HI 21 cm gas te meten. Omdat daarnaast de achtergrondquasar erg helder was, konden we ook een derde, brede en ondiepe absorptiecomponent zien, veroorzaakt door het warme gas. Dit is de eerste keer dat de warme en koude component van het HI gas, reeds goed bekend in onze Melkweg en nabije melkwegstelsels, direct gemeten zijn in een systeem op grotere roodverschuiving. Het toont aan dat de condities in een stelsel op grotere roodverschuiving vergelijkbaar zijn met die in onze eigen Melkweg en in nabije stelsels, en dat is een van de vragen die studies van hoge roodverschuivingen trachten te beantwoorden.

Omdat het merendeel van het HI gas op $z \approx 0$ zich in heldere spiraalstelsels bevindt, werd het aangenomen dat gedempte Lyman-α en HI absorbeerders zich ook in heldere spiraalstelsels bevonden. Maar infraroodafbeeldingen van de nieuwe 21

cm absorbeerders laten zien dat er geen spiraalstelsels zijn in de buurt van de meeste gezichtslijnen naar de quasars. Hoewel de afbeelding van het absorberende stelsel vaak deels overdekt wordt door de afbeelding van de achtergrondquasar, lijkt het waarschijnlijk dat de absorptie tenminste net zo vaak plaats vindt in dwerg- of lage-oppervlaktehelderheidsstelsels, of zelfs in interacterende stelsels, als in traditionele spiraalstelsels. Deze informatie suggereert een verschil tussen de oudere, roodver-schoven populatie en de huidige $z \approx 0$ populatie.

English Summary of Thesis

Galaxies

In the 1920's, Edwin Hubble proved conclusively that galaxies, originally called nebulae because of their cloud-like appearance, are not only exterior to our own Milky Way, but are in fact the same general class of object. A classification system, based on physical appearance was devised. Simply put, galaxies which looked like whirlpools or spirals were called spiral galaxies. These were subdivided into systems which appeared to have a bar at the center, called barred spirals, and those which didn't. Galaxies which appeared to have little internal structure but had a generally rounded smooth appearance were called ellipticals. Anything else was conveniently called an irregular galaxy. Although somewhat imprecise, this very simple classification has proven useful and is still used by astronomers with a few additions. Most important are the dwarf galaxies which are very small, the low surface brightness galaxies which are very faint optically, and the bizarrely shaped interacting galaxies which are the result of two galaxies colliding.

Galaxies are composed of four basic materials: stars, gas, dust, and dark-matter. The first three can be seen. The dark matter is required to explain the distribution and movement of the visible components, but has not been directly observed. Both the stars and the gas are composed mainly of Hydrogen, while the dust is mostly silicates, and nobody knows exactly what the dark matter is. Elliptical galaxies usually have little gas or dust, and appear to be mostly stars. Spiral galaxies, on the other hand, tend to have lots of gas, and may have quite a bit of dust, as well as the visible stars. The situation is less clear for the other types of galaxies.

The HI 21cm Line

In the Milky Way and other nearby galaxies, the easiest way to study the Hydrogen gas is by measuring the *HI 21cm emission line*. Neutral atomic Hydrogen, which is called HI, emits and absorbs radiation at a wavelength of 21cm. When scientists first measured the wavelength distribution or spectrum of light emitted by various elements, any emission feature would literally look like a narrow bright line against

a dark background. Similarly, absorbed radiation appeared as dark lines against a constant bright background. Astronomers today are usually interested in precisely measuring the intensity as well as the wavelength of the emitted or absorbed radiation, so they depict spectra as plots of intensity versus wavelength. Nevertheless the old terminology of emission and absorption lines remains in use.

By observing the intensity profile of the 21cm emission line with a radio telescope, astronomers can easily map out the spatial distribution of the gas over an entire galaxy. Comparing an optical image of the stars to an image of the gas in a galaxy shows that although the highest concentrations of Hydrogen are found near regions where stars are forming, the gas and the stars are actually quite different in distribution. Stars tend to be concentrated at the center of the galaxy, making a bulge, while Hydrogen often has a small hole in its distribution at the center of the galaxy. Further the HI usually extends to greater radii than the stars, and can have distortions and irregularities in its distribution which are not visible in the stars. Often these distortions reveal that the galaxy is interacting with neighbouring galaxies despite an isolated optical appearance.

The total mass of the gas, usually measured in units of solar Mass, or $M_\odot$ can be calculated by adding up emission profiles from an entire galaxy. A typical spiral galaxy might have a mass of roughly 5×10^9 $M_\odot$. However, astronomers are also interested in the total number of Hydrogen atoms on a generic sightline, which is taken to be a cylinder with a 1 cm^2 base. This is called the column density, N_{HI}, of the gas. A typical galaxy might have 10^{22} HI atoms per cm^2 near its center, decreasing to as little as 10^{18} HI atoms per cm^2 or less at the edges. These two quantities allow the Hydrogen in different galaxies to be compared in a sensible fashion.

HI observations can also tell astronomers about the movements and temperature of the gas. The wavelength of 21cm corresponds to a frequency of 1420.4 MHz. We call this the rest frequency because gas which is moving either towards or away from us along the line of sight will appear to emit at a slightly different frequency. This is called the Doppler effect. It is comparable to the change in the pitch, or heard frequency, of a siren as a fire engine passes. At first, the siren is moving towards the listener and it sounds higher. As the vehicle passes and moves away the siren sounds lower. In astronomy, we say that emission from a source moving away from earth is redshifted because it reaches the astronomer at a lower frequency and therefore a longer wavelength than that at which it was emitted. Conversely, emission from a source moving towards us is blueshifted, and appears at a higher frequency.

Inside a cloud of Hydrogen gas, all of the individual atoms are moving around at random, so at any given moment, a large percentage of the atoms will have no line of sight velocity, while the rest will have some velocity between zero and the maximum within the cloud. Thus we see a lot of emission at the rest frequency, and some which is slightly Doppler shifted. If we plot the amount of emission versus frequency, it looks like a bell-shaped, or Gaussian curve. The width of the curve depends on the maximum velocity of the atoms, which in turn depends largely on the kinetic temperature of the gas. Roughly speaking, warmer gas moves faster and creates broader emission lines. In this way the 21cm emission line can be used to measure temperature.

In addition to interior motions, most HI clouds have a bulk velocity at which they are moving within the galaxy. This causes the central frequency of the emission curve to shift, because now the atoms do have an average motion along the line of sight. By measuring the central shift for many different clouds in a galaxy, and combining that with knowledge of where those clouds lie, one can build up a picture of how the gas within the galaxy is moving. In addition to the frequency shift caused by individual cloud motion, emission lines from external galaxies are also shifted due to the motion of their galaxies towards or away from the Milky Way.

The concept of Redshifts

Our universe is expanding, so, with the exception of a few very nearby objects, everything we study outside of our own galaxy is moving away from us. This can be understood by first thinking about a balloon which is marked with two dots. No matter where those dots are placed, when you blow up the balloon the dots move away from each other. The surface of a balloon, however, is two-dimensional, and our universe has three-dimensions. Picture instead a loaf of unbaked raisin bread. As the bread rises, the dough between the raisins expands, creating a greater separation between them. The expansion happens equally in all parts of the bread and does not have a fixed center. The effect of the expansion, is that any two raisins will appear to move away from each other.

In the universe, space itself is the expanding dough, and the galaxies and galaxy clusters are the raisins. As space expands, the distance between any two galaxies increases. However it is hard to see space and easy to see the galaxies, so astronomers say that the galaxies are moving away from each other. As with the raisins in the bread, the expansion looks the same from any vantage point. Since we happen to be in the Milky Way galaxy, we make that our reference point and claim that everything else is moving away from us.

The effect of this expansion, of everything appearing to move away from earth, is a redshifting of the radiation from most extra-galactic sources. Astronomers define the redshift, z, of an object based on how much its radiation is shifted in frequency. For the HI 21cm line:

$$(1 + z) = \frac{1420.4058\,\mathrm{M}Hz}{shifted frequency\ MHz}$$

From this equation you can see that z is a unitless number and is very easy to calculate.

If we were to divide space up into discrete units, then each unit would expand by the same amount over the same time. Imagine three objects in space, the first two separated by only a small distance, and the third at a much larger separation. After a certain amount of time, the distance between the close pair would have increased by a little bit, but the distance between them and the third object would have increased by much more. Thus objects at greater distances appear to move away from us more quickly than those nearby. Because the size of the frequency shift caused by

the Doppler effect increases with increasing velocity, objects at greater distances are assigned larger redshifts z.

The Milky Way lies at a redshift of $z = 0$, and galaxies in its immediate neighbourhood have redshifts of $z \approx 0$. The most distant object in our universe has a redshift of $z \approx 6$. The simplicity of its definition, and the precision with which it can be measured make z very useful to astronomers. It can be converted to a more conventional distance measurement, but only by combining it with the expansion rate of the universe, which is not known with much precision.

Astronomers are very interested in objects which are far away from us, or at high redshift, as well as those nearby. Light travels at a constant velocity, so when an object is farther away, it takes longer for its light to reach us. This means that the light we see from a distant galaxy is much older than that from a nearby galaxy. And just as when we look at photos in a scrapbook, we are younger in the older pictures, so we can consider distant galaxies as younger versions of nearby galaxies. In effect, looking at a higher redshift implies looking at a younger universe. In this way, astronomers try to piece together the general evolution of our universe and the galaxies within it.

HI 21cm Absorption

The strength of the 21cm emission line decreases with the square of the distance to the emitting gas. As a result Hydrogen cannot be measured in HI 21cm emission at any great distance using existing radio telescopes. In order to study the HI gas in distant galaxies, astronomers have to rely on absorption lines. When light from a strong background source passes through a hydrogen cloud, the atoms absorb radiation at the same frequency they normally emit radiation. The background source acts like a flashlight, illuminating everything on the line between us and it, which is called the sightline. Absorption lines do not diminish in strength over distance, so they are ideal for high redshift studies.

Any object which emits continuum radiation over a wide range of frequencies at a relatively constant level can be used as the background source. One of the best is an object called a quasar, or a quasi-stellar object (QSO), which looks like a star at optical wavelengths, but is actually very different. Quasars are extremely powerful emitters at a wide range of frequencies and are fairly numerous at high redshift (although rarer locally), making them ideal background sources. Despite their point-like optical appearance, most quasars have a more extended appearance at the frequency of HI 21cm absorption. By using a radio telescope with sufficient resolution astronomers can sometimes use one quasar to study several sightlines through the intervening absorber.

Like the emission line, the HI 21cm absorption line provides information on the temperature, amount, and velocity distribution of the gas. But while 21cm emission lines from gas at a wide range of temperatures and column densities are easily detected, absorption lines are rarely detected from any but the coldest, highest column density gas. Emission can be seen at any position across the galaxy, but in order to

detect HI 21cm absorption, the sightline to the background quasar must pass fairly close to the center of a galaxy where there is quite a bit of cold gas. This limits the number of high redshift galaxies that can be studied, as well as limiting the available information on a galaxy which does have 21cm absorption to a single or at best a few sightlines.

Because of the necessity of a good alignment between the background quasar and the absorbing galaxy, finding 21cm absorption by randomly observing bright quasars is not particularly efficient. This problem is made worse by the limitations of most radio telescopes, which can only observe at what is effectively a single redshift in one measurement, and can only search a relatively limited range of redshifts in total. In fact only a small handful of 21cm absorbers have ever been identified.

Radio astronomers trying to find 21cm absorption lines need a way to pre-select sightlines through galaxies which would be likely to have lots of neutral Hydrogen. As it turns out, neutral atomic Hydrogen also radiates and absorbs at a number of optical and UV frequencies. One of these, called the Lyman-α line, is particularly strong and easily identified. It can be seen in ground-based optical spectra at redshifts $z > 1.65$ and in UV spectra taken with space-based telescopes such as the Hubble Space Telescope at lower redshifts. When the column density of HI is very high, the absorption line has a distinctive profile and the gas in which it arises is called a Damped Lyman-α (DLA) absorber. Such systems are ideal candidates for finding 21cm absorption. Unfortunately, relatively few (less than 100 in total) DLA absorbers have been identified to date, and only about a third of those lie in front of quasars which are bright radio sources. Of the radio candidates, many lie at redshifts not able to be observed with sufficient sensitivity to detect the 21cm absorption using existing radio telescopes.

Luckily, the gas in galaxies, while mostly neutral Hydrogen, is never pure neutral Hydrogen. There are typically small amounts of many elements and even molecules present as well. Astronomers noticed that certain elements such as Magnesium and Iron were found in all high-column density HI systems. Singly ionized Magnesium (MgII), which is just Magnesium that has lost an electron, creates a strong and easily identified pair of absorption lines in an optical spectrum. The idea to look for 21cm absorption in known MgII absorbers first arose in the late 1970's, and several new 21cm systems were identified using this technique.

Since that time, many large surveys to identify MgII-absorbers over a wide range of redshifts have been made. Statistics from these surveys allow astronomers to study how the MgII gas has evolved from high redshift to the local universe. These surveys and statistics provide an ideal database from which to draw a sample of candidate systems which can be searched for HI 21cm absorption.

This Thesis

When I began my thesis in 1996, there was a large gap in our understanding of how HI evolved over time. Groundbased observations of Damped Lyman-α absorbers provided an estimate of the amount of HI at redshifts of $z \geq 1.65$. Optical imaging

and theoretical modelling had begun to build up a picture of the galaxies in which the HI was found. Extensive HI emission studies near $z = 0$ had provided a wealth of information on the current amount and location of HI gas. However almost nothing was known about what happened in between. The redshift range from $0 < z < 1.65$ spans between a half and two-thirds of the history of our universe, so this was a considerable gap.

The reason for the gap was quite simply a lack of telescopes which could observe the HI gas over that redshift range. The situation for searching out Damped Lyman-α absorbers had recently improved thanks to the new Hubble Space Telescope, but time on the instrument was hard to get, and it would be several years before a large survey was completed. Meanwhile, a recent upgrade to the Westerbork Synthesis Radio Telescope (WSRT) provided an opportunity to search for HI 21cm absorption over a large portion of this redshift range.

The purpose of my thesis is to use the WSRT to address the gap in our knowledge of HI gas. The idea was to make a large systematic search for HI 21cm absorption in MgII-selected systems over the redshift range $0.2 < z < 1.0$. The results of the survey could be used to estimate the numbers of 21cm absorbers and the amount of HI they contained, while the new systems identified could be studied to identify typical host galaxies.

Over the course of two years we obtained radio spectra from the WSRT at frequencies corresponding to the redshifts for 62 MgII absorbers. We combined these with spectra for 10 MgII absorbers taken previously by other astronomers to create a total sample of 72 sources. Of these, 5 showed HI 21cm absorption.

The high number of non-detections can be used to help us better understand how the HI 21cm absorbers differ from the MgII absorbers. For example,there is a much higher probability of finding HI 21cm absorption in systems which have more MgII. If the selection criteria is expanded to require that the systems also have a lot of singly ionized iron (FeII) then the detection probability increases even more. The 21cm absorbers which do have a lot of MgII and FeII also usually have multiple HI clouds and very high total column densities. There are a very few 21cm absorbers which show just a single cloud, and these systems actually do not have a lot of MgII or FeII. If we wish to detect more of them we need to find some other selection criteria which will work better than MgII absorption.

The previously known HI information had suggested that the number of high column density HI systems decreased with decreasing redshift. Our results agree with this prediction. On the other hand, it was also thought that the amount of HI gas peaked near $z = 3$ and then decreased smoothly to $z = 0$. The 21cm survey, however, suggests that the amount of HI gas is roughly constant down to redshifts of at least $z = 0.6$, and must decrease to the $z = 0$ value after that.

The lowest redshift Damped Lyman-α/21cm absorber which has been found lies at a redshift of $z = 0.091$. A spectrum taken with the Arecibo radio telescope in Puerto Rico reveals that this absorber is very unique. Most 21cm absorption lines are broadened by motions in the gas which are unrelated to the gas' temperature, and extra information is needed to derive a value for the temperature. However, in this system, the 21cm absorption has two lines which are extremely narrow, and

we are able to measure the temperature of the cold HI 21cm gas. In addition, because the background quasar is particularly bright, we are able to see a third broad shallow absorption feature caused by warm HI as well. This is the first time the well-known warm and cold temperatures of HI gas in our own and nearby galaxies have been directly measured in a redshifted system. It shows that conditions in the redshifted galaxy are similar to those in our own and local galaxies, which is one of the questions high redshift studies seeks to answer.

Because most of the HI gas at $z \approx 0$ is found in bright spiral galaxies, it was assumed that Damped Lyman-α and HI 21cm absorbers probably arose in bright spiral galaxies as well. Infrared imaging of the new 21cm absorbers reveals that there are no spiral galaxies near many of the quasar sightlines. Although the image of the absorbing galaxy often appears partially obscured by the image of the background quasar, it seems likely that the absorption is occurring in either compact, low surface brightness, or even interacting galaxies at least as often as it occurs in spiral galaxies. This information suggests a difference between the older, redshifted gas-rich galaxy population, and the current $z \approx 0$ population of gas-rich spirals.

Acknowledgements

Nobody lives in complete isolation, and we accomplish nothing without the input and encouragement of those around us. This thesis is no exception.

To start at the beginning, I would like to thank Chris Carilli for introducing me to radio astronomy and encouraging me to do my thesis work here in Groningen.

My advisor, Frank Briggs, has constantly challenged me to expand my point of view and see the bigger picture. He has been amazingly patient with my tendency to do everything at the last possible minute. Along the way he told me how to make my own spaghetti sauce. His support and guidance have been critical to this thesis.

Chris Moore was a huge source of help during the first few years of this thesis. I must offer him my somewhat uncertain thanks for teaching me everything I know about running AIPS. Alain Smette has also been a great help, particularly as regards spectroscopy. His dedication to precision has been much appreciated.

I would like to thank the students and postdocs at the Kapteyn Institute and particularly my officemates from the past 4 years for their conversation, advice, and general help with *all things dutch*. I am especially grateful to Rob Swaters for his ready friendship and for the translation he did for my Nederlandse Samenvatting.

This thesis was greatly enriched by several months spent at the University of Pittsburgh. I owe thanks to my collaborators Sandhya Rao and Dave Turnshek who made my stay possible and encouraged me constantly, and to Dan Nestor for his unending good humor.

My parents and brother have been unfailing in their belief in my ability to do a good job at anything I try. Their love and patience have been invaluable. My parents deserve a special thanks for giving me a completely Linux-compatible laptop, without which I might have never finished this thesis. This is especially commendable given that they had never heard of Linux at the time.

The "Engelse Kring" has been a source of comradeship and support, as has the International Church of Assen. The latter has provided me with a spiritual haven, a piano and plenty of conversation.

My friends in the US, particularly Judi, Shami, Dena and Judson have all been more than generous with phone calls, emails and visits. I must also thank Brett, whose boundless support, humor, belief and love have gotten me through many of the most difficult days. Best of all he helped me find my inner 8-year-old whenever she went missing.

I am grateful to much of the support staff at the Kapteyn Institute, particularly to Jantina, Hennie and Greta for helping me through the intricacies of dutch bureaucracy, and to Kor and Wim for their help with all things computer-related. I would like to thank the Ubbo Emmius Scholarship program at the Rijks*universiteit* Groningen (R*u*G) and the Kapteyn Institute for their financial support during my study. In addition, I must acknowledge the Leids Kerkhoven Bosscha Fonds (LKBF) which has provided funding for so many of my travels.